1 One-Dimensional Magnetism

Hans-Jürgen Mikeska[1] and Alexei K. Kolezhuk[1,2]

[1] Institut für Theoretische Physik, Universität Hannover, Appelstaße 2, 30167 Hannover, Germany, mikeska@itp.uni-hannover.de
[2] Institute of Magnetism, National Academy of Sciences and Ministry of Education of Ukraine, Vernadskii prosp. 36(B), Kiev 03142, Ukraine

Abstract. We present an up-to-date survey of theoretical concepts and results in the field of one-dimensional magnetism and of their relevance to experiments and real materials. Main emphasis of the chapter is on quantum phenomena in models of localized spins with isotropic exchange and additional interactions from anisotropy and external magnetic fields.

Three sections deal with the main classes of model systems for 1D quantum magnetism: $S = 1/2$ chains, spin chains with $S > 1/2$, and $S = 1/2$ Heisenberg ladders. We discuss the variation of physical properties and elementary excitation spectra with a large number of model parameters such as magnetic field, anisotropy, alternation, next-nearest neighbour exchange etc. We describe the related quantum phase diagrams, which include some exotic phases of frustrated chains discovered during the last decade.

A section on modified spin chains and ladders deals in particular with models including higher-order exchange interactions (ring exchange for S=1/2 and biquadratic exchange for S=1 systems), with spin-orbital models and mixed spin (ferrimagnetic) chains.

The final section is devoted to gapped one-dimensional spin systems in high magnetic field. It describes such phenomena as magnetization plateaus and cusp singularities, the emergence of a critical phase when the excitation gap is closed by the applied field, and field-induced ordering due to weak three-dimensional coupling or anisotropy. We discuss peculiarities of the dynamical spin response in the critical and ordered phases.

1.1 Introduction

The field of low-dimensional magnetism can be traced back some 75 years ago: In 1925 Ernst Ising followed a suggestion of his academic teacher Lenz and investigated the one-dimensional (1D) version of the model which is now well known under his name [1] in an effort to provide a microscopic justification for Weiss' molecular field theory of cooperative behavior in magnets; in 1931 Hans Bethe wrote his famous paper entitled 'Zur Theorie der Metalle. I. Eigenwerte und Eigenfunktionen der linearen Atomkette' [2] describing the 'Bethe ansatz' method to find the exact quantum mechanical ground state of the antiferromagnetic Heisenberg model [3], for the 1D case. Both papers were actually not to the complete satisfaction of their authors: The 1D Ising model failed to show any spontaneous order whereas Bethe did not live up to

H.-J. Mikeska and A.K. Kolezhuk, One-Dimensional Magnetism, Lect. Notes Phys. **645**, 1–83 (2004)
http://www.springerlink.com/

the expectation expressed in the last sentence of his text: 'In einer folgenden Arbeit soll die Methode auf räumliche Gitter ausgedehnt ... werden' ('in a subsequent publication the method is to be extended to cover 3D lattices').

In spite of this not very promising beginning, the field of low-dimensional magnetism developed into one of the most active areas of today's solid state physics. For the first 40 years this was an exclusively theoretical field. Theorists were attracted by the chance to find interesting exact results without having to deal with the hopelessly complicated case of models in 3D. They succeeded in extending the solution of Ising's (classical) model to 2D (which, as Onsager showed, *did* exhibit spontaneous order) and in calculating excitation energies, correlation functions and thermal properties for the quantum mechanical 1D Heisenberg model and (some of) its anisotropic generalizations. In another line of research theorists established the intimate connection between classical models in 2D and quantum mechanical models in 1D [4, 5]. An important characteristic of low-dimensional magnets is the absence of long range order in models with a continuous symmetry at any finite temperature as stated in the theorem of Mermin and Wagner [6], and sometimes even the absence of long range order in the ground state [7].

It was only around 1970 when it became clear that the one- and two-dimensional models of interest to theoretical physicists might also be relevant for real materials which could be found in nature or synthesized by ingenious crystal growers. One of the classical examples are the early neutron scattering experiments on TMMC [8]. Actually, magnets in restricted dimensions have a natural realization since they exist as real bulk crystals with, however, exchange interactions which lead to magnetic coupling much stronger in one or two spatial directions than in the remaining ones. Thus, in contrast to 2D lattices (on surfaces) and 2D electron gases (in quantum wells) low D magnets often have all the advantages of bulk materials in providing sufficient intensity for experiments investigating thermal properties (e.g. specific heat), as well as dynamic properties (in particular quantum excitations) by e.g. neutron scattering.

The interest in low-dimensional, in particular one-dimensional magnets developed into a field of its own because these materials provide a unique possibility to study ground and excited states of quantum models, possible new phases of matter and the interplay of quantum fluctuations and thermal fluctuations. In the course of three decades interest developed from classical to quantum mechanics, from linear to nonlinear excitations. From the theoretical point of view the field is extremely broad and provides a playground for a large variety of methods including exact solutions (using the Bethe ansatz and the mapping to fermion systems), quantum field theoretic approaches (conformal invariance, bosonization and the semiclassical nonlinear $\sigma-$model (NLSM)), methods of many-body theory (using e.g. Schwinger bosons and hard core bosons), perturbational approaches (in particular high order series expansions) and finally a large variety of numerical methods such as exact diagonalization (mainly using the Lanczos algorithm for the lowest eigen-

values but also full diagonalization), density matrix renormalization group (DMRG) and Quantum Monte Carlo (QMC) calculations.

The field of one-dimensional magnets is characterized by strong interactions between theoretical and experimental research: In the early eighties, the seminal papers of Faddeev and Takhtajan [9] who revealed the spinon nature of the excitation spectrum of the spin-$\frac{1}{2}$ antiferromagnetic chain, and Haldane [10] who discovered the principal difference between chains of integer and half-integer spins caused an upsurge of interest in new quasi-1D magnetic materials, which substantially advanced the corresponding technology. On the other hand, in the mid eighties, when the interest in the field seemed to go down, a new boost came from the discovery of high temperature superconductors which turned out to be intimately connected to the strong magnetic fluctuations which are possible in low D materials. At about the same time a new boost for experimental investigations came from the new energy range opened up for neutron scattering experiments by spallation sources. Further progress of material science triggered interest in spin ladders, objects staying "in between" one and two dimensions [11]. At present many of the phenomena which turned up in the last decade remain unexplained and it seems safe to say that low-dimensional magnetism will be an active area of research good for surprises in many years to come.

It is thus clear that the field of 1D magnetism is vast and developing rapidly. New phenomena are found and new materials appear at a rate which makes difficult to deliver a survey which would be to any extent complete. Our aim in this chapter will be to give the reader a proper mixture of standard results and of developing topics which could serve as an advanced introduction and stimulate further reading. We try to avoid the overlap with already existing excellent textbooks on the subject [12–14], which we recommend as complementary reading. In this chapter we will therefore review a number of issues which are characteristic for new phenomena specific for one-dimensional magnets, concentrating more on principles and a unifying picture than on details.

Although classical models played an important role in the early stage of 1D magnetism, emphasis today is (and will be in this chapter) on models where quantum effects are essential. This is also reflected on the material side: Most investigations concentrate on compounds with either Cu^{2+}-ions which realize spin-$\frac{1}{2}$ or Ni^{2+}-ions which realize spin 1. Among the spin-$\frac{1}{2}$ chain-like materials, $CuCl_2{\cdot}2NC_5H_5$ (Copperpyridinchloride = CPC) is important as the first quantum chain which was investigated experimentally [15]. Among today's best realizations of the spin-$\frac{1}{2}$ antiferromagnetic Heisenberg model we mention $KCuF_3$ and Sr_2CuO_3. Another quasi-1D spin-$\frac{1}{2}$ antiferromagnet which is widely investigated is $CuGeO_3$ since it was identified in 1992 as the first inorganic spin-Peierls material [16]. The prototype of ladder materials with spin-$\frac{1}{2}$ is $SrCu_2O_3$; generally, the SrCuO materials realize not only chains and two-leg ladders but also chains with competing interactions and ladders with more than two legs. Of particular interest is the material

$Sr_{14}Cu_{24}O_{41}$ which can be easily synthesized and consists of both CuO_2 zigzag chains and Cu_2O_3 ladders. A different way to realize spin-$\frac{1}{2}$ is in chains with Co^{++}-ions which are well described by a pseudospin $\frac{1}{2}$: The free Co-ion has spin $\frac{3}{2}$, but the splitting in the crystal surrounding is so large that for the interest of 1D magnetism only the low-lying doublet has to be taken into account (and then has a strong tendency to Ising-like anisotropy, e.g. in $CsCoCl_3$). Among the spin-1 chain-like materials, $CsNiF_3$ was important in the classical era as a ferromagnetic xy-like chain which allowed to demonstrate magnetic solitons; for the quantum S=1 chain and in particular the Haldane gap first ($Ni(C_2H_8N_2)_2NO_2(ClO_4)$ = NENP) and more recently ($Ni(C_5H_{14}N_2)_2N_3(PF_6)$ = NDMAP) are the most important compounds. It should be realized that the anisotropy is usually very small in spin-$\frac{1}{2}$ chain materials with Cu^{2+}-ions whereas S=1 chains with Ni^{2+}-ions, due to spin-orbit effects, so far are typically anisotropic in spin space. An increasing number of theoretical approaches and some materials exist for alternating spin-1 and $\frac{1}{2}$ ferrimagnetic chains and for chains with $V^{2+}-$ions with spin $\frac{3}{2}$ and Fe^{2+}-ions with spin 2, however, to a large degree this is a field for the future. Tables listing compounds which may serve as 1D magnets can be found in earlier reviews [17,18]; for a discussion of the current experimental situation, see the Chapter by Lemmens and Millet in this book.

We will limit ourselves mostly to models of localized spins $\boldsymbol{S}_n$ with an exchange interaction energy between pairs, $J_{n,m}$ $(\boldsymbol{S}_n \cdot \boldsymbol{S}_m)$ (Heisenberg model), to be supplemented by terms describing (spin and lattice) anisotropies, external fields etc., when necessary. Whereas for real materials the coupling between the chains forming the 1D system and in particular the transition from 1D to 2D systems with increasing interchain coupling is of considerable interest, we will in this chapter consider only the weak coupling limit and exclude phase transitions into phases beyond a strictly 1D character. With this aim in mind, the most important single model probably is the $S = 1/2$ ($S^\alpha = \frac{1}{2}\sigma^\alpha$) XXZ model in 1D

$$\mathcal{H} = J \sum_n \left\{ \frac{1}{2} \left(S_n^+ S_{n+1}^- + S_n^- S_{n+1}^+ \right) + \Delta S_n^z S_{n+1}^z \right\}. \tag{1.1}$$

We have decomposed the scalar product into longitudinal and transverse terms

$$\boldsymbol{S}_1 \cdot \boldsymbol{S}_2 \;=\; S_1^z S_2^z \;+\; \frac{1}{2} \left(S_1^+ S_2^- \;+\; S_1^- S_2^+ \right) \tag{1.2}$$

($S^\pm = S^x \pm iS^y$) and we note that the effect of the transverse part for $S = 1/2$ is nothing but to interchange up and down spins, $|\uparrow\downarrow\rangle \quad \longleftrightarrow \quad |\downarrow\uparrow\rangle$ (apart from a factor of $\frac{1}{2}$). The Hamiltonian of (1.1), in particular for antiferromagnetic coupling, is one of the important paradigms of both many-body solid state physics and field theory. Important for the discussion of its properties is the presence of symmetries leading to good quantum numbers

such as wave vector $\boldsymbol{q}$ (translation), $S^z_{\rm tot}$ (rotation about z-axis), $S_{\rm tot}$ (general rotations, for $|\Delta| = 1$) and parity (spin inversion).

This chapter will present theoretical concepts and results, which, however, are intimately related to experimental results. The most important link between theory and experiment are the spin correlation functions or resp. dynamical structure factors which for a spin chain are defined as follows:

$$S^{\alpha,\alpha}(q,\omega) \;=\; \sum_n \int dt e^{i(qn-\omega t)} \langle S^\alpha_n(t) S^\alpha_0(t=0)\rangle \tag{1.3}$$

$$S^{\alpha,\alpha}(q) \;=\; \sum_n e^{iqn} \langle S^\alpha_n S^\alpha_0\rangle \;=\; \frac{1}{2\pi} \int d\omega S^{\alpha,\alpha}(q,\omega). \tag{1.4}$$

$S(q,\omega)$ determines the cross section for scattering experiments as well as line shapes in NMR and ESR experiments. A useful sum rule is the total intensity, obtained by integrating $S(q,\omega)$ over frequency and wave vector,

$$\frac{1}{4\pi^2} \int d\omega S^{\alpha,\alpha}(q,\omega) \;=\; \frac{1}{2\pi} \int dq S^{\alpha,\alpha}(q) \;=\; \langle (S^\alpha_0)^2\rangle \tag{1.5}$$

which is simply equal to $\frac{1}{3}S(S+1)$ in the isotropic case.

1.2 $S = \frac{1}{2}$ Heisenberg Chain

The $S = \frac{1}{2}$ XXZ Heisenberg chain as defined in (1.1) (XXZ model) is both an important model to describe real materials and at the same time the most important paradigm of low-dimensional quantum magnetism: it allows to introduce many of the scenarios which will reappear later in this chapter: broken symmetry, the gapless Luttinger liquid, the Kosterlitz-Thouless phase transition, gapped and gapless excitation continua. The XXZ model has played an essential role in the development of exact solutions in 1D magnetism, in particular of the Bethe ansatz technique. Whereas more details on exact solutions can be found in the chapter by Klümper, we will adopt in this section a more phenomenological point of view and present a short survey of the basic properties of the XXZ model, supplemented by an external magnetic field and by some remarks for the more general XYZ model,

$$\begin{aligned}\mathcal{H} = J \sum_n \left\{ (1+\gamma)\, S^x_n S^x_{n+1} + (1-\gamma)\, S^y_n S^y_{n+1} + \Delta S^z_n S^z_{n+1} \right\} \\ -g\mu_B \boldsymbol{H} \sum_n \boldsymbol{S}_n \end{aligned} \tag{1.6}$$

as well as by further typical additional terms such as next-nearest neighbor (NNN) interactions, alternation etc. We will use a representation with positive exchange constant $J > 0$ and we will frequently set J to unity, using it as the energy scale.

1.2.1 Ferromagnetic Phase

For $\Delta < -1$ the XXZ chain is in the ferromagnetic Ising phase: the ground state is the saturated state with all spins aligned in either z or $-z$ direction, i.e., the classical ground state with magnetization $S^z_{tot} = \pm\frac{1}{2}N$, where N is the number of sites. This is thus a phase with broken symmetry: the ground state does not exhibit the discrete symmetry of spin reflection $S^z \to -S^z$, under which the Hamiltonian is invariant. In the limit $\Delta = -1$ this symmetry is enlarged to the full rotational symmetry of the isotropic ferromagnet.

When an external magnetic field in z-direction is considered, the Zeeman term as included in (1.6), $\mathcal{H}_Z = -g\mu_B H \sum_n S^z_n$, has to be added to the Hamiltonian. Since $\mathcal{H}_{XXZ}$ commutes with the total spin component $S^z_{\rm tot}$, the external magnetic field results in an additional energy contribution $-g\mu_B H S^z_{\rm tot}$ without affecting the wave functions. The symmetry under spin reflection is lifted and the saturated ground state is stabilized.

The low-lying excited states in the ferromagnetic phase are magnons with the total spin quantum number $S^z_{tot} = \frac{1}{2}N - 1$ and the dispersion law (valid for general spin S)

$$\epsilon(q) = 2JS\,(1 - \cos q - (\Delta + 1)) + 2g\mu_B HS. \tag{1.7}$$

These states are *exact* eigenstates of the XXZ Hamiltonian. In zero field the excitation spectrum has a gap at $q = 0$ of magnitude $|\Delta| - 1$ for $\Delta < -1$. At $\Delta = -1$ the discrete symmetry of spin reflection generalizes to the continuous rotational symmetry and the spectrum becomes gapless. This is a consequence of Goldstone's theorem: the breaking of a continuous symmetry in the ground state results in the emergence of a gapless excitation mode. Whereas the ground state exhibits long range order, the large phase space available to the low-lying excitations in 1D leads to exponential decay of correlations at arbitrarily small finite temperatures following the theorem of Mermin and Wagner [6].

Eigenstates in the subspace with two spin deviations, $S^z_{\rm tot} = N - 2$ can be found exactly by solving the scattering problem of two magnons. This results in the existence of bound states below the two magnon continuum (for a review see [19]) which are related to the concept of domain walls: In general two spin deviations correspond to 4 domains walls (4 broken bonds). However, two spin deviations on neighboring sites correspond to 2 domain walls and require intermediate states with a larger number of walls, i.e. higher energy, to propagate. They therefore have lower energy and survive as a bound state. General ferromagnetic domain wall states are formed for smaller values of $S^z_{\rm tot}$ The ferromagnetic one-domain-wall states can be stabilized by boundary fields opposite to each other. They contain admixtures of states with a larger number of walls, but for $\Delta < -1$ they remain localized owing to conservation of $S^z_{\rm tot}$ [20]. A remarkable exact result is that the lowest magnon energy is not affected by the presence of a domain wall [21]: the excitation energy is $|\Delta| - 1$ both for the uniform ground state and for the one domain wall states.

We mention two trivial, but interesting consequences of (1.7) which can be generalized to any XXZ-type Hamiltonian conserving $S^z_{\rm tot}$:
(i) For sufficiently strong external magnetic field the classical saturated state is forced to be the ground state for arbitrary value of Δ and the lowest excitations are exactly known. If the necessary magnetic fields are within experimentally accessible range, this can be used for an experimental determination of the exchange constants from the magnon dispersion (an example in 2D are recent neutron scattering experiments on Cs_2CuCl_4 [22]).
(ii) The ferromagnetic ground state becomes unstable when the lowest spin wave frequency becomes negative. This allows to determine e.g. the boundary of the ferromagnetic phase for $\Delta > -1$ in an external field as $H = H_c$ with $g\mu_B H_c = \Delta + 1$.

1.2.2 Néel Phase

For $\Delta > +1$ the XXZ chain is in the antiferromagnetic Ising or Néel phase with, in the thermodynamic limit, broken symmetry and one from 2 degenerate ground states, the $S = 1/2$ remnants of the classical Néel states. The spatial period is $2a$, and states are described in the reduced Brillouin zone with wave vectors $0 \le q \le \pi/a$. The ground states have $S^z_{tot} = 0$, but finite sublattice magnetization

$$N^z = \sum_n (-1)^n \, S^z_n. \tag{1.8}$$

and long range order in the corresponding correlation function. In contrast to the ferromagnet, however, quantum fluctuations prevent the order from being complete since the sublattice magnetization does not commute with the XXZ Hamiltonian. For periodic boundary conditions and large but finite N (as is the situation in numerical approaches), the two ground states mix with energy separation $\propto \exp(-\text{const} \times N)$ (for $N \to \infty$). Then invariance under translation by the original lattice constant a is restored and the original Brillouin zone, $0 \le q \le 2\pi/a$, can be used.

The elementary excitations in the antiferromagnetic Ising phase are described most clearly close to the Ising limit $\Delta \to \infty$ starting from one of the two ideal Néel states: Turning around one spin breaks two bonds and leads to a state with energy Δ, degenerate with all states resulting from turning around an arbitrary number of subsequent spins. These states have $S^z_{\rm tot} = \pm 1$, resp. 0 for an odd, resp. even number of turned spins. They are appropriately called two-domain wall states since each of the two broken bonds mediates between two different Néel states. The total number of these states is $N(N-1)$: there are $N^2/4$ states with $S^z_{tot} = +1$ and $S^z_{tot} = -1$ (number of turned spins odd) and $N^2/2 - N$ states with $S^z_{tot} = 0$ (number of turned spins even). These states are no more eigenstates when Δ^{-1} is finite, but for $\Delta^{-1} \ll 1$ they can be dealt with in perturbation theory, leading to the excitation spectrum in the first order in $1/\Delta$ [23]

$$\omega(q,k) = \Delta + 2\,\cos q \cos 2\Phi \tag{1.9}$$

$$= \epsilon(\frac{q}{2} + \Phi) + \epsilon(\frac{q}{2} - \Phi) \tag{1.10}$$

with

$$\epsilon(k) = \frac{1}{2}\Delta + \cos 2k. \tag{1.11}$$

q is the total momentum and takes the values $q = 2\pi l/N$ with $l = 1, 2 \ldots N/2$, Φ is the wave vector related to the superposition of domain walls with different distances and for $S^z_{\rm tot} = \pm 1$ takes values $\Phi = m\pi/(N+2)$ with $m = 1, 2 \ldots N/2$. Φ is essentially a relative momentum, however, the precise values reflect the fact that the two domain walls cannot penetrate each other upon propagation. The formulation of (1.10) makes clear that the excitation spectrum is composed of two entities, domain walls with dispersion given by (1.11) which propagate independently with momenta k_1, k_2. These propagating domain walls were described first by Villain [24], marking the first emergence of magnetic (quantum) solitons. A single domain wall is obtained as eigenstate for an odd number of sites, requiring a minimum of one domain wall, and therefore has spin projection $S^z_{\rm tot} = \pm\frac{1}{2}$. A domain wall can hop by two sites due to the transverse interaction whence the argument $2k$ in the dispersion.

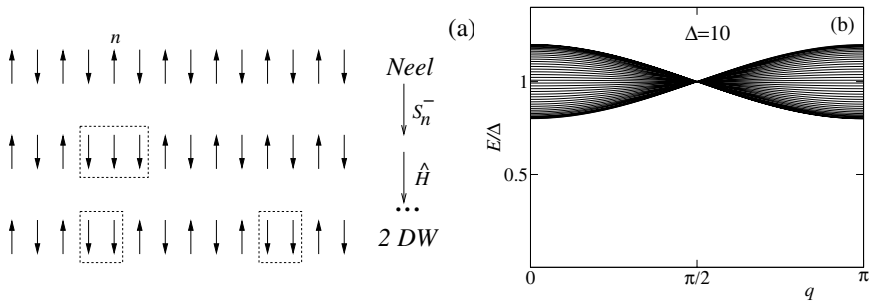

Fig. 1.1. Domain wall picture of elementary excitations in the Néel phase of the XXZ $S = \frac{1}{2}$ chain: (a) acting with S_n^- on the Néel state, one obtains a "magnon" which decays into two domain walls (DW) under repeated action of the Hamiltonian; (b) the two-DW continuum in the first order in Δ, according to (1.9)

Figure 1.1 shows the basic states of this picture and the related dispersions. The two domain wall dispersion of (1.9) is shown in the reduced Brillouin zone; the full BZ can, however, also be used since the corresponding wave functions (for periodic boundary conditions) are also eigenstates of the translation by one site. The elementary excitations in the antiferromagnetic Ising phase thus form a continuum with the relative momentum of the two domain walls serving as an internal degree of freedom.

1.2.3 XY Phase

For $-1 < \Delta < +1$ and zero external field the XXZ chain is in the XY phase, characterized by uniaxial symmetry of the easy-plane type and a gapless excitation continuum. Whereas the full analysis of this phase for general Δ requires the use of powerful methods such as Bethe ansatz and bosonization, to be discussed in later chapters, an approach in somewhat simpler terms is based on the mapping of $S = \frac{1}{2}$ spin operators in 1D to spinless fermions via the nonlocal Jordan-Wigner transformation [25, 26]:

$$S_n^+ = c_n^\dagger \, e^{i\pi \sum_{p=1}^{n-1} c_p^\dagger c_p}, \qquad S_n^z = c_n^\dagger c_n - \frac{1}{2}. \tag{1.12}$$

When a fermion is present (not present) at a site n, the spin projection is $S_n^z = +\frac{1}{2}$ $(-\frac{1}{2})$. In fermion language the XXZ Hamiltonian reads

$$\begin{aligned} \mathcal{H}_{\mathrm{XXZ}} = J \sum_n \Big\{ \frac{1}{2}\big(c_n^\dagger c_{n+1} + c_{n+1}^\dagger c_n\big) + \Delta\big(c_n^\dagger c_n - \frac{1}{2}\big)\big(c_{n+1}^\dagger c_{n+1} - \frac{1}{2}\big) \Big\} \\ - g\mu_B H \sum_n \Big(c_n^\dagger c_n - \frac{1}{2} \Big) \end{aligned} \tag{1.13}$$

For general Δ the XXZ chain is thus equivalent to an interacting 1D fermion system. We discuss here mainly the simplest case $\Delta = 0$ (XX model), when the fermion chain becomes noninteracting and is amenable to an exact analysis in simple terms to a rather large extent: For periodic boundary conditions the assembly of free fermions is fully described by the dispersion law in wave vector space

$$\epsilon(k) = J \cos k - g\mu_B H. \tag{1.14}$$

Each of the fermion states can be either occupied or vacant, corresponding to the dimension 2^N of the Hilbert space for N spins with $S = \frac{1}{2}$. The ground state as the state with the lowest energy has all levels with $\epsilon(k) \leq 0$ occupied: For $g\mu_B H > J$ all fermion levels are occupied (maximum positive magnetization), for $g\mu_B H < -J$ all fermion levels are vacant (maximum negative magnetization) whereas for intermediate H two Fermi points $k = \pm k_F$ exist, separating occupied and vacant levels. This is the regime of the XY phase with a ground state which is a simple Slater determinant. For $H = 0$, as assumed in this subsection, the Fermi wave vector is $k_F = \pi/2$ and the total ground state magnetization vanishes. Magnetic field effects will be discussed in Sect. 1.2.7.

We note that periodic boundary conditions in spin space are modified by the transformation to fermions: the boundary term in the Hamiltonian depends explicitly on the fermion number N_f and leads to different Hamiltonians for the two subspaces of even, resp. odd fermion number. For fixed fermion number this reduces to different sets of allowed fermion momenta

k: If the total number of spins N is even, the allowed values of fermion momenta are given by $k_n = 2\pi I_n/N$, where the numbers I_n are integer (half-odd-integer) if the number of fermions $N_f = S^z_{\rm tot} + \frac{N}{2}$ is odd (even). The total momentum of the ground state is thus $P = N_f\pi$. The same two sets of k-values are found in the Bethe ansatz solution of the XXZ chain. The complication of two different Hilbert spaces is avoided with free boundary conditions, giving up translational symmetry.

Static correlation functions for the XX model can be calculated for the discrete system (without going to the continuum limit) [26]. The longitudinal correlation function in the ground state is obtained as

$$\langle 0|S^z_n S^z_0|0\rangle = -\frac{1}{4}\left(\frac{2}{\pi n}\right)^2 \tag{1.15}$$

for n odd, whereas it vanishes for even $n \neq 0$. The transverse correlation function is expressed as a product of two $n/2 \times n/2$ determinants; an explicit expression is available only for the asymptotic behavior [27]

$$\langle 0|S^x_n S^x_0|0\rangle = \langle 0|S^y_n S^y_0|0\rangle \sim C\,\frac{1}{\sqrt{n}}, \qquad C \approx 0.5884\ldots \tag{1.16}$$

A discussion of these correlation functions for finite temperature has been given by Tonegawa [28]. Static correlation functions can also be given exactly for the open chain, thus accounting for boundary effects, see e.g. [29]. Dynamic correlation functions cannot be obtained at the same level of rigor as static ones since they involve transitions between states in different Hilbert spaces (with even resp. odd fermion number). Nevertheless, detailed results for the asymptotic behavior have been obtained [30] and the approach to correlation functions of integrable models using the determinant representation to obtain differential equations [31] has emerged as a powerful new method.

Quantities of experimental relevance can be easily calculated from the exact expression for the free energy in terms of the basic fermion dispersion, (1.14),

$$F \;=\; -N\,k_{\rm B}\,T\,\left[\ln 2 + \frac{2}{\pi}\int_0^{\frac{\pi}{2}} dk \ln\cosh\left(\frac{\epsilon(k)}{2k_{\rm B}T}\right)\right]. \tag{1.17}$$

An important quantity is the specific heat whose low-temperature behavior is linear in T:

$$C(T) \simeq \frac{\pi T}{6v_F}, \tag{1.18}$$

where $v_F = (\partial\epsilon/\partial k)|_{k=k_F} = J$ is the Fermi velocity.

Low-lying excitations are also simply described in the fermion picture: They are either obtained by adding or removing fermions, thus changing the total spin projection S^z_{tot} by one unity and adding or removing the energy

$\epsilon(k)$, or particle-hole excitations which do not change $S^z_{\rm tot}$. Creating a general particle-hole excitation involves moving a fermion with momentum k_i inside the Fermi sea to some momentum k_f outside the Fermi sea. It is clear that moving a fermion just across the Fermi point costs arbitrarily low energy: the excitation spectrum is gapless. It is easily seen that for a given total momentum $q = k_f - k_i$ a finite range of excitation energies is possible, thus the spectrum of particle-hole excitations is a continuum with the initial momentum $k = k_i$ as internal degree of freedom:

$$\omega(q,k) = \epsilon(k+q) - \epsilon(k). \tag{1.19}$$

The resulting continuum for $S^z_{tot} = 0$ is shown in Fig. 1.2.$S^z_{tot} = \pm 1$ excitations result from the one-fermion dispersion, but develop a continuum as well by adding particle-hole excitations with appropriate momentum; those excitations involve changing the number of fermions by one which implies a change of the total momentum by π, and thus the $S^z_{tot} = \pm 1$ spectrum is the same as in Fig. 1.2 up to the shift by π along the q axis.

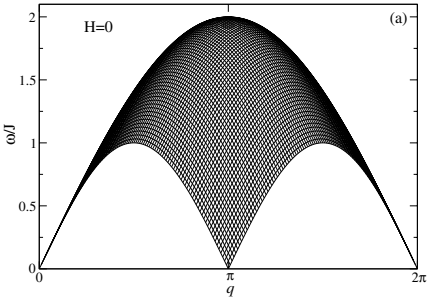

Fig. 1.2. Excitation spectrum of the spin-$\frac{1}{2}$ XY chain in the $S^z_{\rm tot} = 0$ subspace

For $\Delta \neq 0$ the interacting fermion Hamiltonian can be treated in perturbation theory [32]; from this approach and more generally from the Bethe ansatz and field-theoretical methods it is established that the behavior for $-1 < \Delta < +1$ is qualitatively the same as the free fermion limit $\Delta = 0$ considered so far: the excitation spectrum is gapless, a Fermi point exists and correlation functions show power-law behavior. The Heisenberg chain in the XY regime thus is in a critical phase. This phase is equivalent to the so-called Tomonaga-Luttinger liquid [33]. The fermion dispersion to first order in Δ is obtained by direct perturbation theory starting from the free fermion limit [34] (in units of J),

$$\begin{aligned}\epsilon(k) &= \Delta - \lambda + \cos q \\ &\quad -(2\Delta/\pi)\,\theta(1-\lambda)\left\{\arccos\lambda - (1-\lambda^2)^{1/2}\cos q\right\}, \end{aligned} \tag{1.20}$$

where $\lambda = g\mu_B H/J$, and θ is the Heaviside function.

Finally we indicate how these results generalize for $\gamma > 0$, i.e. (see (1.6)) when the rotational symmetry in the xy-plane is broken and a unique preferred direction in spin space exists: $\Delta = 0$ continues to result in a free fermion system, but the basic fermion dispersion acquires a gap and the ground state correlation function $\langle 0|S_n^x S_0^x|0\rangle$ develops long range order [26].

1.2.4 The Isotropic Heisenberg Antiferromagnet and Its Vicinity

The most interesting regime of the $S = 1/2$ XXZ chain is $\Delta \approx 1$, i.e. the vicinity of the isotropic Heisenberg antiferromagnet (HAF). This important limit will be the subject of a detailed presentation in the chapters by Cabra and Pujol, and Klümper, with the use of powerful mathematical methods of Bethe ansatz and field theory. Here we restrict ourselves to a short discussion of important results.

The ground state energy of the HAF is given by

$$E_0 = -NJ \ln 2 \tag{1.21}$$

The asymptotic behavior of the static correlation function at the isotropic point is [35–37]

$$\langle 0|\boldsymbol{S}_n \cdot \boldsymbol{S}_0|0\rangle \propto (-1)^n \frac{1}{(2\pi)^{\frac{3}{2}}} \frac{\sqrt{\ln n}}{n}. \tag{1.22}$$

This translates to a weakly diverging static structure factor at $q \approx \pi$,

$$S(q) \propto \frac{1}{(2\pi)^{\frac{3}{2}}} \, |\ln|q-\pi|\,|^{\frac{3}{2}}. \tag{1.23}$$

The uniform susceptibility at the HAF point shows the logarithmic corrections in the temperature dependence [38]

$$\chi(T) = \frac{1}{\pi^2 J}\left(1 + \frac{1}{2\,\ln(T_0/T)} + \dots\right); \tag{1.24}$$

this singular behavior at $T \to 0$ was experimentally observed in Sr_2CuO_3 and $SrCuO_2$ [39]. The elementary excitations form a particle-hole continuum $\omega(q,k) = \epsilon(q+k) - \epsilon(k)$, obtained from fundamental excitations with dispersion law

$$\epsilon(k) = \frac{\pi}{2} \, J \, |\sin k| \tag{1.25}$$

which are usually called spinons. This dispersion law was obtained by des-Cloizeaux and Pearson [40], however, the role of $\epsilon(k)$ as dispersion for the basic constituents of a particle-hole continuum was first described by Faddeev and Takhtajan [9].

When the HAF point is crossed, a phase transition from the gapless XY-regime to the gapped antiferromagnetic Ising regime takes place which is of the Kosterlitz-Thouless type: the Néel gap opens up with nonanalytic dependence on $\Delta - 1$ corresponding to a correlation length

$$\xi \propto e^{\pi/\sqrt{\Delta-1}} \tag{1.26}$$

The divergence of the transverse and the longitudinal structure factors differs when the HAF is approached from the Ising side in spite of the isotropy at the HAF point itself [37].

In contrast to the behavior of the isotropic HAF, the correlation functions for $\Delta < 1$ do not exhibit logarithmic corrections and the asymptotic behavior in the ground state is given by

$$\langle 0|S_n^x \cdot S_0^x|0\rangle = (-1)^n A_x \frac{1}{n^{\eta_x}}, \quad \langle 0|S_n^z \cdot S_0^z|0\rangle = (-1)^n A_z \frac{1}{n^{\eta_z}}, \tag{1.27}$$

where

$$\eta_x = \eta_z^{-1} = 1 - \frac{\arccos \Delta}{\pi}. \tag{1.28}$$

For $|\Delta| < 1$ presumably exact expressions for the amplitudes A_x, A_z have been given in [41, 42].

1.2.5 The Dynamical Structure Factor of the XXZ Chain

Two-Domain Wall Picture of the Excitation Continua

The dynamical structure factor $S(q, \omega)$ of the XXZ chain for low frequencies is dominated by the elementary excitations for the HAF as well as in the Ising and XY phases. The common feature is the presence of an excitation continuum as was made explicit in the Néel phase and for the free fermion limit above and stated to be true for the HAF.

In the Néel phase a one-domain wall state was seen to have $S_{\text{tot}}^z = \pm 1/2$. The only good quantum number is S_{tot}^z and two domain walls can combine into two states with $S_{\text{tot}}^z = 0$ and two states with $S_{\text{tot}}^z = \pm 1$ with equal energies (in the thermodynamic limit) but different contributions to the DSF. When the isotropic point is approached these four states form one triplet and one singlet to give the fourfold degenerate spinon continuum.

For all phases the excitation continuum emerges from the presence of two dynamically independent constituents. The spinons of the isotropic HAF can be considered as the isotropic limit of the Néel phase domain walls. The domain wall picture applies also to the XY phase: A XY-phase fermion can be shown to turn into a domain wall after a nonlocal transformation [43] and adding a fermion at a given site corresponds to reversing all spins beyond that site. Thus the domain wall concept of the antiferromagnetic Ising regime is in

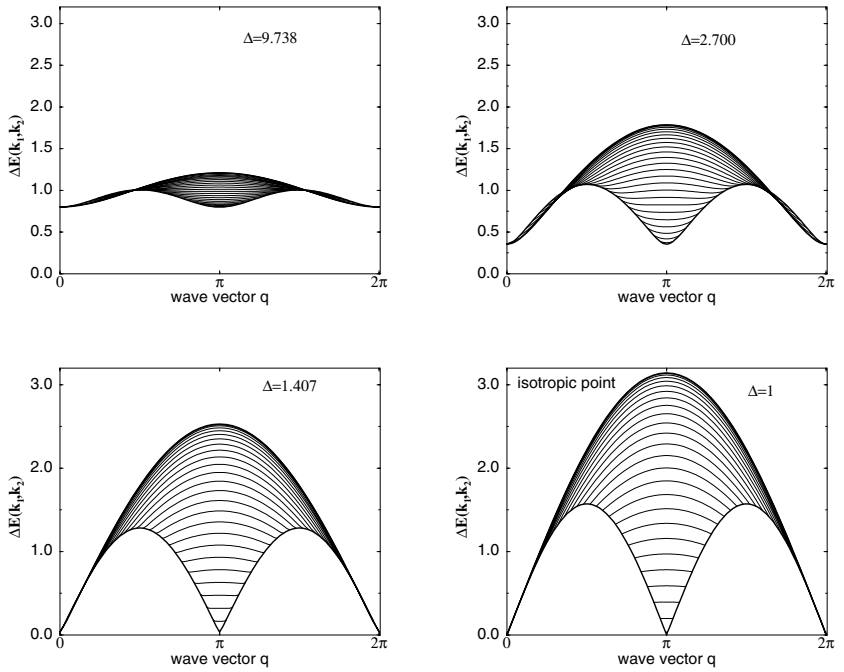

Fig. 1.3. Spinon continuum for various anisotropies Δ (reproduced from [46])

fact a general concept unifying the dynamics in the regime $+\infty > \Delta > -1$, i.e. up to the transition to the ferromagnetic regime.

The one-DW dispersion as well as the appearance of a continuum with an energy gap for $\Delta > 1$ agrees with the results obtained from Bethe ansatz calculations [44, 45] taken in lowest order in $1/\Delta$. We make use of the full Bethe ansatz results for finite values of $1/\Delta$ to show a a numerical evaluation of these results. Figure 1.3 demonstrates that the gapped, anisotropic two spinon continuum develops continuously from the antiferromagnetic Ising phase into the gapless spinon continuum of the isotropic Heisenberg antiferromagnet. To make contact with the isotropic limit, in Fig. 1.3 spectra in the Néel phase are presented using the extended Brillouin zone (the Bethe ansatz excitations can be chosen as eigenfunctions under translation by one site). Although these graphs are suggestive the precise relation between the Bethe ansatz excitation wave functions and the lowest order domain wall ones (cf. Fig. 1.1) is difficult to establish.

Frequency Dependence of $S(q, \omega)$

In the XY regime (including the limit of the HAF) the asymptotic spatial dependence of the static correlation function is generalized to the time-

dependent case by replacing n^2 by $(n-vt)(n+vt)$ (v is the spin wave velocity). This leads immediately to the most important property of the dynamic structure factor, namely the appearance (at $T = 0$) of an edge singularity at the lower threshold of the continuum:

$$S^{\alpha,\alpha}(q,\omega) \propto \frac{1}{(\omega^2-\omega(q)^2)^{1-\frac{\eta_\alpha}{2}}}\theta(\omega^2-\omega(q)^2) \tag{1.29}$$

(obtained by bosonization for $S = 1/2$ in the zero temperature and long wavelength limit, by Schulz [47]) with exponents η_α depending on the anisotropy Δ as given in (1.28) above. This expression is consistent with the exact result obtained for the longitudinal DSF of the XX model using the free fermion approach [48, 49]:

$$S^{zz}(q,\omega) = 2\frac{1}{\sqrt{4J^2\sin^2\left(\frac{q}{2}\right)-\omega^2}}\Theta(\omega - J\sin q)\Theta(2J\sin\frac{q}{2}-\omega); \tag{1.30}$$

the XX model is however peculiar since there is no divergence in S^{zz} at the lower continuum boundary.

This edge singularity is of essential relevance for experiments probing the dynamics of spin chains in the XY phase including the antiferromagnetic point and we therefore give a short survey of the phenomenological, more physical approaches in order to provide an understanding beyond the formal results.

The singularity is already obtained on the semiclassical level in an expansion in $1/S$. This approach served to interpret the first experimental verification of the infrared singularity by neutron scattering experiments on the material CPC [15]. In this approach the exponent to first order in $1/S$ is $\eta = 2/(\pi\hat{S}), \hat{S} = \sqrt{S(S+1)}$ for $\Delta = 1$ [50] and has also been obtained to second order in $1/S$ for chains with XY like exchange and single-ion anisotropy [51].

The semiclassical approach clearly shows the essence of this singularity: Many low-lying modes which are harmonic in simple angular variables ϕ_n, θ_n add up to produce the singularity in the spin variable $S_n \propto \exp i\phi_n$, whose correlations are actually measured in $S(q,\omega)$. The finite temperature result for $S(q,\omega)$ in this approach is identical to the result of bosonization [32] which was then generalized to the exact Bethe ansatz result with exact values $\eta = 1$ for $\Delta = 1$ (HAF) and $\eta = \frac{1}{2}$ for $\Delta = 0$ (XY). The physical understanding of the excitation continuum as domain wall continuum was finally established by Faddeev and Takhtajan [9].

The singular behavior of the dynamic structure factor was supported by numerical calculations using complete diagonalization. Combined with exact results, this lead to the formulation of the so-called Müller ansatz [49, 52] for the isotropic $S = \frac{1}{2}$ chain:

$$S(q,\omega) = \frac{A}{\sqrt{\omega_1^2-\omega(q)^2}}\Theta(\omega-\omega_1(q))\Theta(\omega_2(q)-\omega), \tag{1.31}$$

with $\omega_1(q) = (\pi/2)J|\sin q|$ and $\omega_2(q) = \pi J|\sin(q/2)|$. This ansatz parametrizes the dynamic structure factor as in (1.29) and adds an upper limit corresponding to the maximum two spinon energy (note that for the isotropic chain there is no divergence at the upper continuum boundary). This ansatz is now frequently used for an interpretation of experimental data, neglecting the presence of small but finite excitation strength above the upper threshold frequency $\omega_2(q)$ as confirmed by detailed numerical investigations (the total intensity of the two spinon continuum has been determined as 72.89 % of the value 1/4, given by the sum rule (1.5) [53]). Experimental investigations of the excitation continuum include the Heisenberg antiferromagnet $CuCl_2{\cdot}2NC_5H_5$ (CPC) [15] and recent work on the HAF $KCuF_3$ [54]. Beautiful pictures of the spinon continuum are also available for the spin-Peierls material $CuGeO_3$ [55].

Temperature dependence and lineshapes of the dynamic structure factor for $q \approx \pi$ have been investigated by bosonization techniques [47], conformal field theory [13] and numerical approaches [56]. Numerical calculations of all eigenvalues for chains with 16 spins [57] have shown the full picture of the spinon continuum and its variation with temperature. The functional form of the Müller ansatz found strong support when the dynamical structure factor for the Haldane-Shastry chain (Heisenberg chain on a ring geometry with long range interactions propertional to the inverse square of the distance [58]) was calculated exactly [59] and was shown to take exactly the form of (1.31).

For XXZ chains close to the Ising limit with their spectrum determined by gapped solitons the dynamic response is different: At $T = 0$ both $S^{xx}(q,\omega)$ and $S^{zz}(q,\omega)$ are dominated by the two-domain wall or spin wave continuum in the finite frequency range determined from (1.9) with no singularity at the edges [23] (there is just an asymmetry with a steepening at the lower frequency threshold). Upon approach to the isotropic limit the infrared singularity develops gradually starting from wave vector $\pi/2$. At finite temperature an additional central peak develops from energy transfer to a single domain wall [24]. These continua have been observed in the material $CsCoCl_3$ [60–62]. The two-domain wall continuum has been shown to shift its excitation strength towards the lower edge in frequency when a (ferromagnetic) NNN interaction is added to the Hamiltonian [63].

1.2.6 Modified S=1/2 Chains

In this subsection we shortly discuss a number of modifications to the ideal $S = 1/2$ XXZ chain which add interesting aspects to the theoretical picture and are also relevant for some real materials.

A theoretically particularly important model is the isotropic Heisenberg chain with nearest and next-nearest exchange

$$\mathcal{H} = J \sum_n (\boldsymbol{S}_n \cdot \boldsymbol{S}_{n+1} + \alpha \boldsymbol{S}_n \cdot \boldsymbol{S}_{n+2}) \tag{1.32}$$

which for $\alpha > 0$ exhibits the effects of frustration from competing interactions. In the classical limit the system develops spiral order in the ground state for $\alpha > 1/4$ whereas for $S = 1/2$ a phase transition to a dimerized state occurs at $\alpha = \alpha_c \approx 0.2411....$ This dimerized state is characterized by a singlet ground state with doubled lattice constant and twofold degeneracy and an excitation gap to the first excited states, a band of triplets. It is thus one of the simple examples for the emergence of an energy gap in a 1D system with rotational symmetry by dynamical symmetry breaking. This quantum phase transition was first found at $\alpha \approx 1/6$ from the bosonization approach [64]. The phase transition has been located with high numerical accuracy by Okamoto and Nomura [65] considering the crossover between the singlet-singlet and singlet-triplet gaps, a criterion which has proven rather effective also in related cases later.

For $\alpha = 1/2$, one arrives at the Majumdar-Ghosh limit [66], where the exact form of these singlet ground states $|0\rangle_{I,II}$ is known to be a product of singlets (dimers):

$$|0\rangle_I = |[1,2]\ \cdots\ [2p+1,2p+2]\ \cdots\rangle \qquad |0\rangle_{II} = |[2,3]\ \cdots\ [2p,2p+1]\ \cdots\rangle \tag{1.33}$$

with the representation of a singlet as

$$|\,[2p,2p+1]\rangle = \frac{1}{\sqrt{2}} \sum_{s,s'} \chi_{2p}(s)\ \epsilon^{s,s'}\ \chi_{2p+1}(s') \tag{1.34}$$

where $\chi_m(s)$ is the spin state at site m and $\boldsymbol{\epsilon}$ is the antisymmetric tensor

$$\epsilon = \begin{pmatrix} 0 & 1 \\ -1 & 0 \end{pmatrix}. \tag{1.35}$$

in spin space $s = (\uparrow, \downarrow)$. This becomes easily clear by considering the following Hamiltonian

$$\widetilde{\mathcal{H}}_{MG} = \frac{1}{4}(\boldsymbol{S}_1 + \boldsymbol{S}_2 + \boldsymbol{S}_3)^2 + \frac{1}{4}(\boldsymbol{S}_2 + \boldsymbol{S}_3 + \boldsymbol{S}_4)^2 + \frac{1}{4}(\boldsymbol{S}_3 + \boldsymbol{S}_4 + \boldsymbol{S}_5)^2 + \ldots$$

for N spins and periodic boundary conditions. $\widetilde{\mathcal{H}}_{MG}$ is identical to $\mathcal{H}_{MG}$ apart from a constant:

$$\widetilde{\mathcal{H}}_{MG} = \sum_n \boldsymbol{S}_n \cdot \boldsymbol{S}_{n+1} + \frac{1}{2} \sum_n \boldsymbol{S}_n \cdot \boldsymbol{S}_{n+2} + \frac{3}{4} \sum_n \boldsymbol{S}_n^2 = \mathcal{H}_{MG} + \frac{9}{16} N$$

Using

$$(\boldsymbol{S}_n + \boldsymbol{S}_{n+1} + \boldsymbol{S}_{n+2})^2 \geq S(S+1)|_{S=\frac{1}{2}} = \frac{3}{4}$$

we obtain

$$\widetilde{E}_0 \geq \frac{3}{16}N.$$

The two ground states obtained by covering the chain completely with singlets formed of two spins 1/2 have energy equal to this lower bound since each contribution of the type $(\boldsymbol{S}_n + \boldsymbol{S}_{n+1} + \boldsymbol{S}_{n+2})^2$ contains two spins which are coupled to a singlet and therefore reduces to $\boldsymbol{S}^2 = \frac{3}{4}$. The dimer product states are therefore ground states of the Majumdar-Ghosh Hamiltonian with energy per spin $E_0/N = -3/8$. It is evident that this ground state is completely disordered, i.e. all two-spin correlation functions vanish identically. There is however, perfect order of the singlets, expressed in the statement that the Majumdar-Ghosh ground state forms a *dimer crystal*. Quantitatively this is expressed in a finite value of the dimer-dimer (four spin) correlation function

$$_I\langle 0|(\boldsymbol{S}_1 \cdot \boldsymbol{S}_2)(\boldsymbol{S}_{2p+1} \cdot \boldsymbol{S}_{2p+2})|0\rangle_I. \tag{1.36}$$

for arbitrary n (and the equivalent relation for $|0\rangle_{II}$).

Another variant of the Heisenberg chain is obtained by adding dimerization explicitly to the Hamiltonian, giving the alternating chain

$$\mathcal{H} = J \sum_n (1 + (-1)^n \delta)\, (\boldsymbol{S}_n \cdot \boldsymbol{S}_{n+1}) \tag{1.37}$$

This model was first investigated by Cross and Fisher [67]; with explicit dimerization the ground state is unique and a gap opens up immediately, $E_g \propto \delta^{2/3}$ (apart from logarithmic corrections). The ground state prefers to have singlets at the strong bonds and the lowest excitations are propagating one-triplet states. These can be considered as bound domain wall states since two domain walls of the type described above with singlets on the 'wrong' sites between them feel an attractive interaction growing with distance. The model with both NNN exchange and alternation is equivalent to a spin ladder and will be discussed in more detail in Sect. 1.4.

Models with explicit or spontaneous dimerization are now frequently used to describe spin-Peierls chains, i.e. spin chains which dimerize due to the spin phonon interaction. This field was stimulated in particular by the discovery of the inorganic spin-Peierls material $CuGeO_3$ [16]. Whereas the adiabatic limit when phonons follow spins without relaxation is not appropriate for this material, the flow equation approach has been used to reduce the general spin-phonon model to a spin only Hamiltonian [68, 69] and the spin Peierls gap then results from the combined action of alternation and frustration. Phonons, however, do introduce some features not covered by this simplification [70] and it is not clear at the moment whether the simplified spin model captures the physics of real spin Peierls materials, in particular of the inorganic compound $CuGeO_3$ (for a review see [71]).

Another variant of the simple 1D chain are decorated chains, where more complicated units are inserted in the 1D arrangement. As an example we

mention the orthogonal-dimer spin chain with frustrated plaquettes inserted in the chain [72,73], see Fig. 1.4. Depending on the strength of the competing interactions, this chain can be in a dimer phase or in a plaquette phase with interesting dynamic properties. Interest in this model is motivated by its relation to the 2D orthogonal-dimer model which is realized in the compound $SrCu_2(BO_3)_2$.

Fig. 1.4. An example of decorated chains: orthogonal-dimer spin chain [72]

Interesting aspects are found in $S = 1/2$ chains with random couplings. Using the real space renormalization group it has been shown that the ground state of the random antiferromagnetic Heisenberg chain is the random singlet state, i.e. spins form singlets randomly with distant partners [74]. Hida has extended these studies to dimerized chains [75]. Heisenberg chains with a random distribution of ferro- and antiferromagnetic exchange constants have been shown to have a different type of ground state called the large spin state [76, 77], characterized by a fixed point distribution not only of bond strength, but also of spin magnitudes.

1.2.7 The XXZ Chain in an External Magnetic Field

An external magnetic field leads to qualitatively new phenomena in spin chains when the Zeeman energy becomes comparable to the scale set by the exchange energies. Contrary to other parameters in the Hamiltonian (e.g. chemical composition, exchange integrals) an external field is relatively easy to vary experimentally. Therefore these effects deserve particular attention; actually experimental and theoretical investigations involving high magnetic fields have developed into one of the most interesting topics in the field of low-dimensional magnetism in the last few years.

The phase diagram of the XXZ model in an external magnetic field in z-direction is shown in Fig. 1.5: The boundary between the ferromagnetic phase and the XY phase is given by $H_c = \pm J(1 + \Delta)$. For $\Delta < 1$ (XY symmetry) the XY phase extends down to $H = 0$. In the fermion representation the external field acts as chemical potential, and the fermion occupation number changes from zero to saturation when the XY phase is crossed at constant Δ. For $\Delta > 1$ (Ising symmetry) there is a transition from the Néel phase to the XY phase at $H = H_{c1} = E_g(\Delta)$, where $E_g(\Delta)$ is the triplet gap. In the $S = \frac{1}{2}$ chain this transition is of the second order [78] and the magnetization appears continuously as $m \propto (H - H_c)^{1/2}$, whereas for $S > \frac{1}{2}$ it acquires the features of the classical first-order spin-flop transition with a jump in m at $H = H_{c1}$ [79].

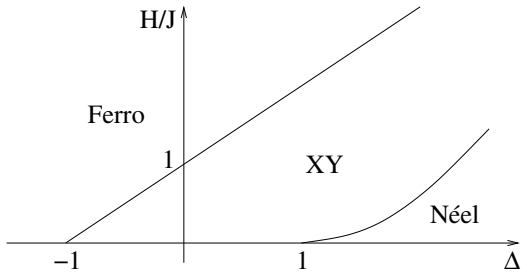

Fig. 1.5. Phase diagram of a XXZ Heisenberg $S = \frac{1}{2}$ chain in magnetic field

The effect of the external field on the excitation spectrum is calculated exactly for the XX model, i.e. in the free fermion case, with the result shown in Fig. 1.6: The Fermi points shift from $k_F = \pm\pi/2$ to $\pm(\pi/2+\delta k)$ and gapless excitations are found for wave vectors $q = \pi \pm 2\delta k$, where δk is determined by $J\cos(\pi/2+\delta k)+H = 0$ and implies incommensurability in the ground state. This result is representative for the XY-phase and the isotropic Heisenberg antiferromagnet. It has been confirmed in neutron scattering experiments on the $S = \frac{1}{2}$ chain material Cu-Benzoate [80]. On the theoretical side, e.g., line shapes for finite external field have been calculated from the Bethe ansatz [81].

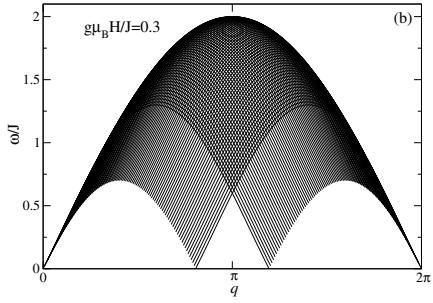

Fig. 1.6. Excitation spectrum of the spin-$\frac{1}{2}$ XY chain in the $S^z_{\rm tot} = 0$ subspace for finite external field, $g\mu_B H/J = 0.3$

For the Heisenberg antiferromagnet with general anisotropies a remarkable curiosity has been found by Kurmann et al [82]: For any combination of couplings and any field direction there exists a field strength H_N which renders the ground state very simple, namely factorizable, i.e. it essentially becomes identical to the classical ground state. Simple examples are the XXZ model with external field in z- resp. x-direction, where the corresponding field values are

$$H_N^{(z)} = J(1+\Delta), \quad H_N^{(x)} = J\sqrt{2(1+\Delta)}. \tag{1.38}$$

An interesting situation can develop when a uniform external field via a staggered g-factor and possibly a Dzyaloshinkii-Moriya interaction induces a staggered field such as in Cu-Benzoate [80] and materials of related symmetry [83,84]: Then a staggered field is induced which is proportional to the external field and a gap opens up which for small fields behaves as [85, 86]

$$E_g \propto \left(\frac{H}{J}\right)^{2/3} \ln^{1/6}\left(\frac{J}{H}\right). \tag{1.39}$$

The magnetic chain in this situation is equivalent to a quantum sine-Gordon chain carrying solitons and breathers (soliton-antisoliton bound states) as excitations; these were identified in neutron scattering and ESR experiments [87] and their contributions to the dynamical structure factor were calculated from sine-Gordon field theory [88, 89].

For an external *transverse* field the Ising model in a transverse field is the best known example. It is solved as free fermion model [90] and serves as one of the standard models of a quantum phase transition [91]. More interesting and much more difficult is the case of an XY chain where a transverse field breaks the rotational symmetry since in this case a simple free fermion limit does not exist and also bosonization does not go beyond establishing the existence of a gap. Such a system is of interest as the quantum analog of the standard example for classical soliton bearing magnetic chains like $CsNiF_3$ [18]. The phase diagram for the Heisenberg chain in a transverse field has been discussed already in [82] and recently again for the XX model [56] and for the XXZ model in mean-field approximation (MFA) [92] and MFA with additional field theoretic input [93]. Recent experiments on the XY spin chain Cs_2CoCl_4 in a transverse magnetic field [94] show an interesting phase diagram including a quantum spin liquid phase which extends to zero temperature and are presently stimulating theoretical investigations in this field.

1.2.8 Effects of 3D Coupling

Since the isotropic spin-$\frac{1}{2}$ chain is gapless, even a weak 3D coupling between the chains $J' \ll J$ will lead to the emergence of the long-range staggered order. The magnitude of this order as a function of J' can be calculated within the mean-field or RPA approximation [95–98]: solving the problem of an isolated chain in an external staggered field $h_{\rm st}$, one obtains for the staggered magnetization $m_{\rm st}$ the expression [86]

$$m_{\rm st} = c\,[(h_{\rm st}/J)\ln(J/h_{\rm st})]^{1/3}, \quad c \simeq 0.387. \tag{1.40}$$

This is then treated as a self-consistency equation for $m_{\rm st}$ after assuming the mean-field relation $h_{\rm st} = \widetilde{J}'(\boldsymbol{q}_B)m_{\rm st}$, where $\widetilde{J}'(\boldsymbol{q})$ is the Fourier transform of the interchain interaction and $\boldsymbol{q}_B$ is the magnetic Bragg wave vector. This yields $m_{\rm st} \simeq 0.29\,[(J'/J)\ln(J/J')]^{1/2}$ [98], where $J' \equiv \widetilde{J}'(\boldsymbol{q}_B)$.

The dynamical susceptibilities of an isolated chain in a staggered field were calculated in [97]. Both the longitudinal and transverse (with respect to the ordered moment) polarization channels contain quasiparticle and continuum contributions. The transverse single mode has the gap $\Delta \simeq 0.842J' \ln^{1/2}(J/J')$ [98], and the gap of the longitudinal mode is $\Delta\sqrt{3}$, while the continuum in both channels starts at 2Δ. The 3D dynamical susceptibility $\chi_{3D}(\boldsymbol{q},\omega)$ can be obtained with the help of the RPA formula

$$\chi^{\alpha}_{3D}(\boldsymbol{q},\omega) = \frac{\chi^{\alpha}_{1D}(q_{\parallel},\omega)}{1-\widetilde{J'}(\boldsymbol{q})\chi^{\alpha}_{1D}(q_{\parallel},\omega)}, \tag{1.41}$$

where $\alpha = \parallel, \perp$ denotes the longitudinal or transverse direction with respect to the ordered moment. This expression follows from the usual susceptibility definition $m(\boldsymbol{q},\omega) = \chi(\boldsymbol{q},\omega)h(\boldsymbol{q},\omega)$ if one replaces h with the effective mean field $h_{\text{eff}} = h(\boldsymbol{q},\omega) + \widetilde{J'}(\boldsymbol{q})m(\boldsymbol{q},\omega)$. Physical excitation frequencies are determined as poles of the χ_{3D}. An intrinsic flaw of this approach is that both the transverse and longitudinal modes come out gapped, while it is physically clear that there should be gapless Goldstone modes in the transverse channel at $\boldsymbol{q} = \boldsymbol{q}_B$. This can be fixed [96] by the renormalization $\chi^{\perp}_{1D} \mapsto Z\chi^{\perp}_{1D}$, where the renormalization factor Z is determined from the condition $Z\widetilde{J'}(\boldsymbol{q}_B)\chi^{\perp}_{1D}(\boldsymbol{q}_B,0) = 1$. Within this approach, the longitudinal mode remains a well-defined gapped excitation. Such a mode was successfully observed in $KCuF_3$ [99], but it was argued it cannot be distinguished from the continuum in another $S = \frac{1}{2}$-chain material $BaCu_2Si_2O_7$ [98, 100]. Those results indicate that the lifetime of the longitudinal mode can be limited by the processes of decay into a pair of transverse modes with nearly zero frequency [98], which cannot be analyzed in framework of the RPA approach.

1.3 Spin Chains with $S > 1/2$

Antiferromagnetic Heisenberg spin chains with integer and half-integer value of spin S behave in a very different way, as was discovered by Haldane twenty years ago [10]. He has shown that the ground state of an integer-S Heisenberg AF chain should have a finite spectral gap, though exponentially small in the large-S limit. This special disordered state of isotropic integer-S chains with only short-range, exponentially decaying AF spin correlations has received the name of *the Haldane phase*. The most thoroughly studied example is the $S = 1$ chain.

1.3.1 $S = 1$ Haldane Chain

The isotropic $S = 1$ Heisenberg antiferromagnetic chain is the simplest example of a system with the Haldane phase and is thus often called *the Haldane*

chain. Following Haldane's conjecture it was the subject of numerous investigations and although an exact solution of the proper $S = 1$ HAF has not been found, many approximate and numerical approaches have established a coherent picture characterized by the following properties [101, 102]: The Haldane chain has the ground state energy per spin $E \simeq -1.40$ and short-range AF spin correlations $\langle S_0^\alpha S_n^\beta \rangle \propto (-1)^n \delta_{\alpha\beta} n^{-1/2} e^{-n/\xi}$ characterized by the correlation length $\xi \simeq 6.0$. Its lowest excitations form a massive magnon triplet, the excitation spectrum has a gap $\Delta \simeq 0.41J$ at wave vector $q = \pi$, and the dispersion of the low-lying excitations with q close to π is well described by the "relativistic" law $\varepsilon(q) = \sqrt{\Delta^2 + v^2(q-\pi)^2}$, with the spin wave velocity $v \simeq 2.46J$. The single-particle energy grows fast as q moves away from π, so that the spectrum around $q = 0$ is dominated by the two-particle continuum whose lower boundary starts at approximately 2Δ. The second lowest excitation at $q = \pi$ belongs to the three-soliton continuum and has the energy $\approx 3\Delta$, as shown in Fig. 1.7. The gap in the spectrum translates into an activated behavior of magnetic specific heat and susceptibility, the fingerprints of gapped systems in macroscopic properties.

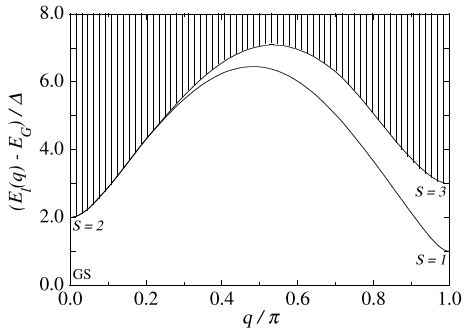

Fig. 1.7. Spectrum of low-lying excitations in $S = 1$ Haldane chain, from the QMC calculation of [103]

An important property of the $S = 1$ Haldane chain is the so-called string order *string order* which is a nonlocal quantity defined as the limiting value of the correlator

$$\mathcal{O}_1^\alpha(n, n') = \left\langle -S_n^\alpha \, e^{i\pi \sum_{j=n+1}^{n'-1} S_j^\alpha} \, S_{n'}^\alpha \right\rangle, \qquad \alpha = x, y, z. \tag{1.42}$$

at $|n - n'| \to \infty$. Presence of this order means that the ground state of the chain favors such spin states where the $|+\rangle$ and $|-\rangle$ spin-1 states alternate, "diluted" with strings of $|0\rangle$ of arbitrary length. One speaks about a "diluted AF order". This "diluted AF order" reaches its maximal value, 1, in the Néel state. In the Haldane phase, however, the Néel order vanishes, while the string order persists, its value for a *rotational invariant* state being limited

by 4/9 from above. For the Haldane chain the value of the string order is somewhat lower, $\mathcal{O}_1^{\mathrm{Hald}} \simeq 0.37$ [104, 105].

Hidden order was originally introduced in constructing an analogy to surface phase transitions in *solid-on-solid (SOS)* models [106] and to the fractional quantum Hall effect [107]. This leads to a very visual interpretation of the hidden order: If we define a correspondence between $|+\rangle$ sites and a positive $\Delta h = +1$ step of the interface position, and respectively between $|-\rangle$ sites and a $\Delta h = -1$ step, then hidden order corresponds to the so-called "disordered flat" (or "fluid flat") phase. This *preroughening* phase is characterized by a flat surface with a *finite* average fluctuation of the surface height, but no order in the *position* of the $\Delta h = \pm 1$ steps. As shown by Kennedy and Tasaki [108], the hidden symmetry breaking by the string order parameter can be transformed into an explicit breaking of a $Z_2 \times Z_2$ symmetry by a nonlocal unitary transformation which characterizes the Haldane chain.

Importance of the string order is even more stressed by the fact that the lowest excitations of the $S = 1$ Haldane chain can be interpreted as *solitons in the string order* [109–112].

Experimentally the Haldane chain was most comprehensively studied via inelastic neutron scattering in $S = 1$ chain material $\mathrm{Ni}(\mathrm{C_2H_8N_2})_2\mathrm{NO_2}(\mathrm{ClO_4})$ (NENP), confirming the theoretical predictions. For higher S the experiments are scarce; the Haldane phase was reported to be found in the $S = 2$ AF chain material $\mathrm{MnCl_3}(2, 2' - \text{bipyridine})$ on the basis of the magnetization measurements [113]: under application of an external magnetic field, the magnetization remained zero in a finite field range, indicating presence of a gapped phase. We postpone to Sect. 1.6 the discussion of interesting physics which arises if one succeeds to close the gap by the magnetic field, and concentrate here on the properties of the Haldane phase itself.

Anisotropic $S = 1$ Haldane Chain

An interesting phase diagram emerges if one considers a $S = 1$ chain with anisotropies as described by the Hamiltonian

$$\mathcal{H} = \sum_n (S_n^x S_{n+1}^x + S_n^y S_{n+1}^y) + J^z S_n^z S_{n+1}^z + D(S_n^z)^2 \tag{1.43}$$

The effects of exchange anisotropy J_z and single-ion anisotropy D are very different, and the system exhibits a rich phase diagram [47, 106] shown in Fig. 1.8. To visualize the characteristic features of different phases, it is sometimes convenient to resort to the language of "solid-on-solid" models of surface phase transitions [106]. One identifies $|\pm\rangle$ spin-1 states with $\Delta h = \pm 1$ steps of the interface (domain walls), and treats those domain walls as particles with an internal degree of freedom –"spin" $\pm\frac{1}{2}$. Then one can interpret the Néel phase as a "solid flat," or "AF spin-ordered solid" one, i.e., a phase where there is a long-range correlation of particle positions, and their "spins" exhibit a long-range AF order. The gapped Haldane phase corresponds to the

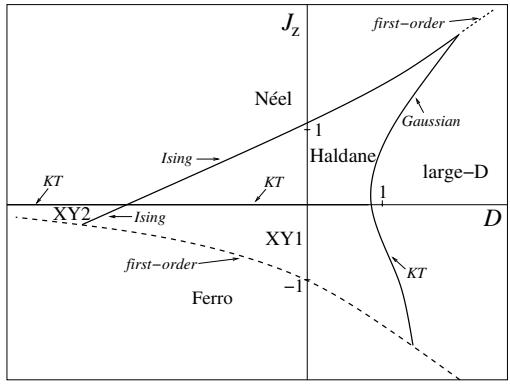

Fig. 1.8. Phase diagram of the $S = 1$ Heisenberg chain with exchange anisotropy J_z and single-ion anisotropy D

"AF spin-ordered fluid" phase, characterized by the AF order in "spin" but with no order in the position of particles. The AF order disappears along the transition to the gapless $XY1$ phase which is a "spin-disordered fluid". Another gapless phase, the $XY2$ phase, can be described as a "spin-disordered solid" with the restored order in the particle positions. The so-called large-D phase *large-D* phase, which is achieved at sufficiently large values of the single-ion anisotropy, can be characterized as a gas of bound pairs of particles with opposite "spin". Those pairs unbind when D is decreased, and this transition is of the first order if it is to the ferromagnetic or to the Néel phase, of the Kosterlitz-Thouless (KT) type on the boundary to the XY1 phase, and Gaussian along the boundary to the Haldane phase.

The phase diagram of the anisotropic $S = 1$ chain was studied numerically [114, 115]. For purely exchange anisotropy ($D = 0$) the Haldane phase was found to exist in the interval from $J_z \approx 0$ $J_z \approx 1.2$, while for purely single-ion anisotropy ($J_z = 1$) it persists from $D \approx -0.2$ to $D \approx 1$.

The role of anisotropy was also investigated for a $S = \frac{1}{2}$ chain with alternating ferro- and antiferromagnetic exchange, and a rich phase diagram was found [105]. In the limit of strong ferromagnetic bonds this system may be viewed as another physical model of the $S = 1$ Haldane chain, with the ferro exchange playing the role of the Hund coupling.

The phase diagram in the (D, J_z) space was analyzed by Schulz [47] for general S in the bosonization approach, which is able to capture the topology of the phase diagram. According to his results, the diagram of Fig. 1.8 should be generic for integer S, while for half-integer S the Haldane and large-D phases disappear, being replaced by the $XY1$ phase. Numerical studies [116] revealed that for $S = 2$ the $XY1$ phase creeps in between the Haldane phase and large-D one, squeezing the Haldane phase to a narrow region near the boundary to the Néel phase.

1.3.2 Integer vs Half-Odd-Integer S

The emergence of an energy gap in spite of rotational invariance comes as a surprise, especially because the classical Heisenberg chain, as well as the only exactly solvable quantum model of a Heisenberg spin chain, namely the $S = \frac{1}{2}$ one, are gapless. Classical intuition expects that a state arbitrarily close in energy to the ground state can be created by infinitesimally changing the angles between neighboring spins. For a quantum system whose ground state is a global singlet (the total spin $S_{\rm tot} = 0$), however, this operation may just reproduce the initial state and thus fail to demonstrate the existence of gapless excitations.

Nonlinear σ-Model Description

Haldane's prediction, which created a surge of interest to one-dimensional magnets, was based on a large-S mapping to the continuum field theory, the so-called nonlinear sigma model (NLSM) (see e.g. [117]) which we will briefly review (for details, see the chapter by Cabra and Pujol).

Consider a spin-S antiferromagnetic Heisenberg chain described by the Hamiltonian

$$\mathcal{H} = J \sum \boldsymbol{S}_j \cdot \boldsymbol{S}_{j+1} - \boldsymbol{H} \cdot \sum_j \boldsymbol{S}_j, \tag{1.44}$$

where we have included the external magnetic field $\boldsymbol{H}$ for the sake of generality. In the quasiclassical NLSM description one starts with introducing the set of coherent states

$$|\boldsymbol{n}\rangle = e^{iS^z\varphi} e^{iS^y\theta} |S^z = S\rangle, \tag{1.45}$$

where $\boldsymbol{n}$ is the unit vector parameterizing the state and having the meaning of the spin direction. The partition function $Z = \mathrm{Tr}(e^{-\beta\mathcal{H}})$, where $\beta = 1/T$ is the inverse temperature, can be rewritten as a coherent state path integral $Z = \int \mathcal{D}\boldsymbol{n} e^{-\mathcal{A}_E/\hbar}$, where $\mathcal{A}_E = \int_0^{\beta\hbar} d\tau L_E$ is the Euclidean action and $\tau = it$ is the imaginary time.

Breaking the spin variable $\boldsymbol{n}$ into the smooth and staggered parts, $\boldsymbol{n}_j = \boldsymbol{m}_j + (-1)^j \boldsymbol{l}_j$, one can pass from discrete variables to the continuum fields $\boldsymbol{m}$, $\boldsymbol{l}$ subject to the constraints $\boldsymbol{ml} = 0$, $\boldsymbol{l}^2 + \boldsymbol{m}^2 = 1$. We assume that the magnetization for the low-energy states of the antiferromagnet is small, $|\boldsymbol{m}| \ll |\boldsymbol{l}|$, and therefore neglect higher than quadratic terms in $\boldsymbol{m}$. Then one can show that on the mean-field level $\boldsymbol{m}$ is a slave variable, which can be excluded from the action,

$$\boldsymbol{m} = \frac{1}{4JS}\big\{ i\hbar(\boldsymbol{l} \times \partial_\tau \boldsymbol{l}) + \boldsymbol{H} - \boldsymbol{l}(\boldsymbol{H} \cdot \boldsymbol{l}) \big\}. \tag{1.46}$$

In weak fields and at low energies $\boldsymbol{m}^2$ may be neglected in the constraint, so that $\boldsymbol{l}$ can be regarded as a unit vector and one arrives at the following effective Euclidean action depending on the unit vector $\boldsymbol{l}$ only:

$$\mathcal{A}_E = \mathcal{A}_B + \frac{\hbar}{2g}\int_0^{\beta\hbar c} dx_0 \int dx_1 \Big\{ (\partial_0 \boldsymbol{l} + \frac{i}{\hbar c}\, \boldsymbol{l} \times \boldsymbol{B})^2 + (\partial_1 \boldsymbol{l})^2 \Big\}, \qquad (1.47)$$

where $x_0 = c\tau$, $x_1 = x$, $c = \frac{2JSa}{\hbar}$, and $g = 2/S$. In absence of the magnetic field the model is Lorentz invariant (c plays the role of the limiting velocity) and is known as the $O(3)$ NLSM with topological term. The so-called topological, or *Berry term* $\mathcal{A}_B$ is given by

$$\mathcal{A}_B = i2\pi\hbar S Q, \qquad Q = \frac{1}{4\pi}\int d^2x\, \boldsymbol{l} \cdot (\partial_0 \boldsymbol{l} \times \partial_1 \boldsymbol{l}), \qquad (1.48)$$

The integer-valued quantity Q is the so-called *Pontryagin index* indicating how many times the vector $\boldsymbol{l}$ sweeps the unit sphere when x sweeps the two-dimensional space-time.

Without the topological term, the $T = 0$ partition function of the quantum AF spin-S chain is equivalent to that of a classical 2D ferromagnet at the effective temperature $T_{\text{eff}} = g$ in the continuum approximation. For integer spin S the topological term is ineffective since $\mathcal{A}_B$ is always a multiple of $2\pi\hbar$, and the properties of the 1D quantum antiferromagnet can be taken over from the 2D classical ferromagnet. (This correspondence is in fact quite general, connecting the behavior of a *Lorentz invariant* quantum system in dimension d to that of its classical counterpart in dimension $D = d + 1$, and is often referred to as the *quantum-classical correspondence*).

At finite temperature the 2D classical ferromagnet is known [118, 119] to have a finite correlation length $\xi \propto e^{2\pi/T_{\text{eff}}}$, which, in view of the Lorentz invariance, corresponds in the original spin chain to a finite *Haldane gap*

$$\Delta_{\text{Hald}} \propto \hbar c/\xi = JSe^{-\pi S}.$$

Thus, the $T = 0$ ground state of the integer-S isotropic Heisenberg one-dimensional ($D = 1 + 1$) antiferromagnet is disordered, and the spectrum of elementary excitations has a gap. The degeneracy of the lowest excitations is threefold (in contrast to only double degeneracy obtained in spin wave approximation which is absent on the Néel state with broken symmetry). Spin correlations in real space are given by the so-called *Ornstein-Zernike correlation function*

$$\langle \boldsymbol{l}(x)\boldsymbol{l}(0)\rangle \propto \frac{e^{-|x|/\xi}}{|x|^{(D-1)/2}}, \quad |x| \to \infty. \qquad (1.49)$$

For half-odd-integer spins, the contribution of any field configuration into the partition function carries a nontrivial phase factor $e^{-i2\pi SQ}$, which leads to the interference of configurations with different Q, and at the end to the absence of a gap in Heisenberg spin-S chains with half-odd-integer S. There is an argument due to Affleck [117] which connects this effect to the contribution of *merons* – objects with the topological charge $Q = \pm\frac{1}{2}$ which may be

thought of as elementary entities constituting a $Q = 1$ solution known as the Belavin-Polyakov soliton [120].

Although in the NLSM formulation the presence of the topological term renders the half-odd integer spin chain theoretically more complicated than the integer-S one, the emergence of an energy gap in the latter in spite of rotational invariance calls for a simple physical explanation. It is instructive to see where the intuition goes wrong; this can be seen from the statement known as the Lieb-Schultz-Mattis theorem [26] for spins $\frac{1}{2}$, *generalized* later by Affleck and Lieb [121] to arbitrary half-odd-integer S and by Oshikawa et al. to finite magnetization [122]:

Generalized Lieb-Schultz-Mattis Theorem

Assume that (i) we have a spin-S chain with *short-range* exchange interaction, (ii) the Hamiltonian $\mathcal{H}$ is invariant with respect to a *translation by l lattice constants* and (iii) $\mathcal{H}$ is invariant with respect to arbitrary rotation around the z axis, so that the ground state has a definite $S^z_{\rm tot} = LM$, where L is the number of spins in the chain.

Then, *if $l(S - M)$ is a half-odd-integer,* there system is *either gapless* in the thermodynamic limit $L \to \infty$, *or the ground state is degenerate, with spontaneously broken translational symmetry.*

The proof runs as follows: let $|\psi_0\rangle$ be the ground state with certain magnetization M per spin. Consider the unitary *twist operator*

$$\widehat{U} = \exp\{i\frac{2\pi}{L}\sum_{j=1}^{L} j S^z_j\}$$

and construct a new state $|\psi_1\rangle = \widehat{U}|\psi_0\rangle$. Assume for definiteness that

$$\mathcal{H} = \sum_{nm}\Big\{\frac{1}{2}J_{nm}(S^+_n S^-_{n+m} + S^-_n S^+_{n+m}) + J^z_{nm} S^z_n S^z_{n+m}\Big\};$$

this exact form is not essential, the same course of derivation can be performed assuming presence of any powers $(S^+_n S^-_{n+m})^k$. Operator S^z remains invariant under the unitary transformation, and $U^\dagger S^+_n U = e^{i2\pi n/L} S^+_n$, so that the energy difference between $|\psi_0\rangle$ and $|\psi_1\rangle$ is

$$\Delta E = \sum_{nm} J_{nm} e_{nm}(\cos\frac{2\pi m}{L} - 1), \qquad e_{nm} \equiv \langle\psi_0|S^+_n S^-_{n+m}|\psi_0\rangle.$$

Denoting $\sum_{n=1}^{L} J_{nm} e_{nm} = L f_m$ and taking the thermodynamic limit $L \to \infty$, one obtains

$$\Delta E = E_1 - E_0 \propto \frac{1}{L}\sum_m m^2 f_m,$$

and, if the last sum is finite (which is true for J_{nm} being a reasonably fast decaying function of the distance m), we come to the conclusion that the energy E_1 of the state $|\psi_1\rangle$ tends to the ground state energy E_0 in the thermodynamic limit.

Now consider the overlap of $|\psi_0\rangle$ and $|\psi_1\rangle$: if they are orthogonal, one can be sure that E_1 gives a variational upper bound of the energy of the true eigenstate, otherwise no statement can be made.

Assume that the original translational symmetry of the Hamiltonian is not broken, i.e. that $T_l|\psi_0\rangle = |\psi_0\rangle$, where T_l is the operator of translation by l lattice sites, $T_l S_n T_l^{-1} = S_{n+l}$. Then the overlap

$$z_1 = \langle\psi_0|\psi_1\rangle = \langle\psi_0|T_l U T_l^{-1}|\psi_0\rangle.$$

The transformed twist operator can be rewritten as

$$T_l U T_l^{-1} = \exp\{i\frac{2\pi}{L}\sum_{j=1}^{L} jS_{j+l}^z\} = \exp\Big\{i\frac{2\pi}{L}\sum_{j=1}^{L}(j-l)S_j^z + i2\pi\sum_{k=1}^{l} S_k^z\Big\},$$

where we have used periodic boundary conditions $S_{L+n}^z = S_n^z$. It is easy to see that $e^{i2\pi S_n^z}|\psi\rangle = e^{i2\pi S}|\psi\rangle$, since $|\psi\rangle$ contains only spin-S states, and $e^{i2\pi S^z}$ yields ± 1 depending on whether S is integer or half-integer. Thus, the equation for the overlap takes the form

$$z_1 = e^{i2\pi l(S-M)} z_1. \tag{1.50}$$

From that equation it is clear that $l(S-M) =$ integer is a necessary condition for the overlap z_1 to be nonzero. Thus, for $l(S-M) =$ half-odd-integer the system is either gapless, or our assumption that $T_l|\psi_0\rangle = |\psi_0\rangle$ is wrong.

The spin-S Heisenberg chain in its ground state corresponds to $l = 1$ and $M = 0$. From the above theorem it follows that, if a spontaneous breaking of the translational symmetry is excluded, a spin-S Heisenberg chain can only be gapped if S is integer. We will come back to this result later in Sect. 1.6 since it establishes also a connection to the phenomenon known as *magnetization plateau*; actually, the integer spin chain ground state with the Haldane gap is the simplest example of a magnetization plateau at $M = 0$.

1.3.3 The AKLT Model and Valence Bond Solid States

Although the large-S NLSM description allows one to get some basic understanding for the $S = 1$ chain, chains with low integer S exhibit several important features which go beyond the large-S limit. These deficiencies are to some extent filled by the additional insight obtained from the so-called *valence bond solid* (VBS) models. The prototype of these models was proposed by Affleck, Kennedy, Lieb, and Tasaki [123] and is thus known as the *AKLT model*. In the following we introduce this model and use it as a starting point

to discuss the matrix product representation and an approximate treatment of excitations in the Haldane chain.

Let us introduce the *projector* operator $P_{12}^{J=2}$ which projects the states of two $S = 1$ spins $\boldsymbol{S}_1$, $\boldsymbol{S}_2$ onto the subspace with the total spin $J = 2$. Consider the Hamiltonian defined in terms of this projector:

$$\mathcal{H} = \frac{1}{12}\sum_i \{P_{i,i+1}^{(J=2)} - 8\} = \sum_i \boldsymbol{S}_i\boldsymbol{S}_{i+1} + \frac{1}{3}(\boldsymbol{S}_i\boldsymbol{S}_{i+1})^2. \tag{1.51}$$

Obviously, the minimum energy is obtained for a state with the property that the total spin of any two neighboring spins is never equal to 2. Such a state can be constructed by regarding every $S = 1$ as a composite object consisting of two symmetrized $S = \frac{1}{2}$ spins, and linking each $S = \frac{1}{2}$ spin to its neighbor from the nearest site with a singlet bond, see Fig. 1.9a. Remarkably, uniform VBS states can be constructed in the same way for any integer S (Fig. 1.9b), while for half-integer S only dimerized VBS states are possible. For periodic boundary conditions the ground state is unique and is a global singlet, while for open boundary conditions there are two free $\frac{1}{2}$ spins at the open ends of the chain, so that the ground state is fourfold degenerate and consists of a singlet and of the so-called *Kennedy triplet* [124].

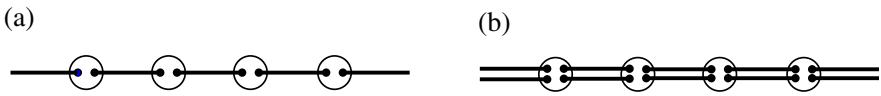

Fig. 1.9. Valence bond solid (VBS) wave functions: (a) the ground state (1.52) of the $S = 1$ AKLT model (1.51); (b) $S = 2$ VBS state

The AKLT model (1.51), which can be obviously generalized for higher S, serves as a good example visualizing the nature of the Haldane phase.

The $S = 1$ VBS state, taken as a variational trial wave function, yields for the Haldane chain the ground state energy per spin $E = -\frac{4}{3}$, rather close to the numerically obtained value $E \simeq -1.40$ [102].

Though the construction looks simple, it seems to be rather a nontrivial task to write down the VBS wave function in terms of the original spin states. There exists, however, a simple and elegant representation of VBS wavefunctions in the language of *matrix product states* [125,126]. The AKLT wave function can be presented in the following form:

$$|\Psi\rangle = \mathrm{Tr}(g_1 g_2 \cdots g_N), \qquad g_n^{AKLT} = \frac{1}{\sqrt{3}} \begin{pmatrix} -|0\rangle_n & -\sqrt{2}|-\rangle_n \\ \sqrt{2}|+\rangle_n & |0\rangle_n \end{pmatrix}, \tag{1.52}$$

where $|\mu\rangle_n$ denotes the state of the spin $S = 1$ at site n with $S^z = \mu$.

Indeed, it is easy to show that a product of any two matrices $g_1 g_2$ does not contain states with the total spin $J = 2$, which is exactly the property

of the AKLT wave function. The trace corresponds to periodic boundary conditions, and the four matrix elements of $\Omega = g_1 g_2 \cdots g_N$ are nothing but the four degenerate ground states of the open chain. A similar representation exists for higher-S VBS states [127].

The matrix product (MP) formulation is remarkable since it allows to write complicated states in a factorized (product) form. Technically, averages over VBS states can be easily calculated using the transfer matrix technique [127], e.g., for any operator $\widehat{L}_{12}$ involving two neighboring spins one has

$$\begin{aligned} \langle \Psi | \widehat{L}_{12} | \Psi \rangle &= Tr(G^{N-2} M_{12}) \,, \\ G = g_i^* \otimes g_i, \quad M_{12} &= (g_1 g_2)^* \otimes \widehat{L}_{12} (g_1 g_2) \,, \end{aligned} \tag{1.53}$$

where $\otimes$ denotes the direct (tensor) product of matrices.

The correlation function of the AKLT model for an infinite chain is explicitly given by

$$\langle S_n^\alpha S_{n'}^\beta \rangle = (-1)^{|n-n'|} (4/3)\, e^{-|n-n'| \ln 3} \delta_{\alpha\beta}; \tag{1.54}$$

for finite chains the free spins at the edges give an additional contribution which also decays exponentially when moving away from the boundary [128]. All correlations decay purely exponentially, which is a peculiarity of the AKLT model connected to the fact that it is a special *disorder point* where the so-called *dimensional reduction* of the generic $D = 2$ Ornstein-Zernike behavior (1.49) takes place [129]. The correlation length of the AKLT model $\xi = 1/\ln 3$ is very short in comparison with $\xi \simeq 6.0$ in the Haldane chain, [102]. This means, that despite the qualitative similarity to the ground state of the $S = 1$ Haldane chain, quantitatively the AKLT state is rather far from it. However, one may say that $S = 1$ Haldane chain and the AKLT model are in the same phase, i.e., in any reasonable phase space the points corresponding to those two models can be connected by a line which does not cross any phase boundary. Respectively, those two models can be said to belong to the same *universality class* in the sense that corresponding quantum phase transitions caused by changing some parameter in the general phase space occur at the same phase boundary and thus have the same universal behavior.

The MP representation makes it easy to see the presence of the string order in the VBS wave function. Since the elementary matrix g_i can be rewritten through the Pauli matrices σ^μ as

$$g_i^{AKLT} = 1/\sqrt{3} (\sigma^+ |-\rangle_i + \sigma^- |+\rangle_i - \sigma^0 |0\rangle_i) \,, \tag{1.55}$$

it is clear that, since $(\sigma^\pm)^2 = 0$ and $\sigma^+ \sigma^0 = -\sigma^+$, the ground state contains *only* such spin states where the $|+\rangle$ must be followed by a $|-\rangle$, with an arbitrary number of $|0\rangle$ in between. The "diluted AF order" is thus perfect in the AKLT model. The AKLT state is rotationally invariant, and states $|0\rangle$, $|+\rangle$ and $|-\rangle$ appear with the equal probability of 1/3. Nonzero contribution

to the correlator (1.42) comes only from states with no $|0\rangle$ at sites n and n', so that the value $\mathcal{O}_1^{AKLT} = 4/9$, which is the *maximal value for a rotational invariant state*, to be compared with $\mathcal{O}_1^{\mathrm{Hald}} \simeq 0.37$ for the Haldane chain [104].

The hidden order, together with the fourfold degeneracy of the ground state for open chain, is a characteristic feature of the Haldane phase for $S = 1$ chains. This provides an elegant way of detecting the Haldane state [130]: doping a $S = 1$ Haldane chain with Cu^{2+} ions having spin $\frac{1}{2}$, one breaks it effectively into finite pieces, and effectively free $S = \frac{1}{2}$ spins are created at the edges adjacent to the impurity site. The resulting three spins $\frac{1}{2}$ are bound together by a weak host-impurity interaction, forming a loose cluster practically decoupled from the bulk of the chain. In applied magnetic field, resonant transitions between the cluster levels should be visible inside the Haldane gap. Such a response was successfully observed in the ESR experiment on Cu-doped NENP [130], confirming that the system is in the Haldane phase.

Excitations in the AKLT Chain

The lowest excitation above the singlet ground state of the Haldane chain is known to be a massive triplet with the total spin equal to 1. Creating such an excitation may be visualized as replacing one of the singlet links in the AKLT state by a triplet one. The resulting trial wave function for a triplet excitation with $S^z = \mu$ at site n can be written down as follows:

$$|\mu, n\rangle = \mathrm{Tr}\{g_1^{AKLT} g_2^{AKLT} \dots g_{n-1}^{AKLT} (g_n^{1\mu}) g_{n+1}^{AKLT} \dots g_N^{AKLT}\}, \tag{1.56}$$

where $g^{(1\mu)}$ is in the most general case defined as

$$g^{(1\mu)} = a\sigma^\mu \cdot g^{AKLT} + b g^{AKLT} \cdot \sigma^\mu, \tag{1.57}$$

the ratio a/b being a free parameter. States $|\mu, n\rangle$ with different n are generally not orthogonal. However, one may achieve such an orthogonality by setting $a/b = 3$ [131].

Those states are in fact *solitons in the string order* [109–112]. One can straightforwardly check that in the soliton state $|r, n\rangle$ the string order correlators $\mathcal{O}_1^{r'}(l, l')$ with $r' \neq r$ change sign when n gets inside the (l, l') interval, while $\mathcal{O}_1^{r}(l, l')$ remains insensitive to the presence of the soliton.The variational dispersion relation for such a soliton takes an especially simple form for the AKLT model [132]:

$$\varepsilon(k) = \frac{10}{27}(5 + 3\cos k). \tag{1.58}$$

The one-particle gap $\Delta = \varepsilon(k = \pi)$ is at $k = \pi$, and the overall structure of excitation spectrum is qualitatively very similar to that of the Haldane chain. Numerical analysis [103, 112] confirms that the above picture of excitations,

constructed for the AKLT model, remains qualitatively correct in case of the $S = 1$ Haldane chain as well, also in anisotropic case [133].

The difference between the ground states of the Haldane chain and of the AKLT model may be visualized as follows: the Haldane chain contains a finite number of bound pairs of solitons with opposite spin, which reduce the hidden order and renormalize the excitation energy [134].

1.3.4 Spin Chains with Alternating and Frustrated Exchange

If the exchange integral is allowed to alternate along the chain, i.e., $J_n = J[1 + (-1)^n\delta]$, the NLSM analysis shows [135] that the topological term (1.48) gets multiplied by $(1 - \delta)$. The theory is gapless if $2\pi S(1 - \delta) = \pi \mod(2\pi)$, which yields $2S$ critical points if $\delta \in [-1; 1]$. The same conclusion is supported by the VBS approach which allows exactly $2S + 1$ different dimerized VBS states for a given S, so that there are $2S$ transitions between them. Numerically, such transitions were observed in chains with S up to 2 [136].

Recently, a dimerized $S = 1$ VBS state was detected in the ESR experiment on Zn-doped NTENP [137]. The idea of the experiment was similar to that of detecting the Haldane state: due to the dimerized nature of the ground state, effective free $S = 1$ spins emerge on doping at the edges adjacent to the impurities, and the corresponding resonance response can be measured.

If one adds a small frustrating next-nearest-neighbor interaction j, the $2S$ critical points can be expected to continue as critical lines in the (j, δ) plane. In the strong frustration region, however, little is known, except for the cases $S = \frac{1}{2}$ and $S = 1$.

In the $S = \frac{1}{2}$ case there is a single critical line $\delta_c = 0$ extending up to the point $j \simeq 0.24$, and continuing till $j = \infty$ as a first-order line [65]. For $S = 1$ there are two symmetrical lines $\delta = \pm\delta_c(j)$, with $\delta_c(0) \simeq 0.25$ [136], which, according to the numerical results [138, 139], extend up to about $j \simeq 0.2$ as second-order transition lines, continue afterwards as first-order ones and cross the symmetry line $\delta = 0$ at a finite $j \simeq 0.75$. The symmetry line (i.e., a frustrated chain without alternation) was studied in [131, 140] and the point $j_c \simeq 0.75$ was identified as that of the first-order "connectivity transition" from the Haldane phase to the so-called "double Haldane" phase. The string order (1.42) disappears discontinuously at $j > j_c$ [140], signaling a breakdown of the Haldane phase (Fig. 1.10b).

The "double Haldane" phase at $j > j_c$ can be visualized (see Fig. 1.10a) as a VBS state consisting of two interconnected AKLT chains [131]; the corresponding order parameter can be written as

$$\mathcal{O}_2^\alpha(n, n') = \left\langle -S_{n-1}^\alpha S_n^\alpha \, e^{i\pi \sum_{l=n+1}^{n'-1} S_l^\alpha} \, S_{n'}^\alpha S_{n'+1}^\alpha \right\rangle, \qquad \alpha = x, y, z, \quad (1.59)$$

and turns out to emerge discontinuously at $j > j_c$ (Fig. 1.10b). It is, however, not clear at present how the "double Haldane" phase is connected to the

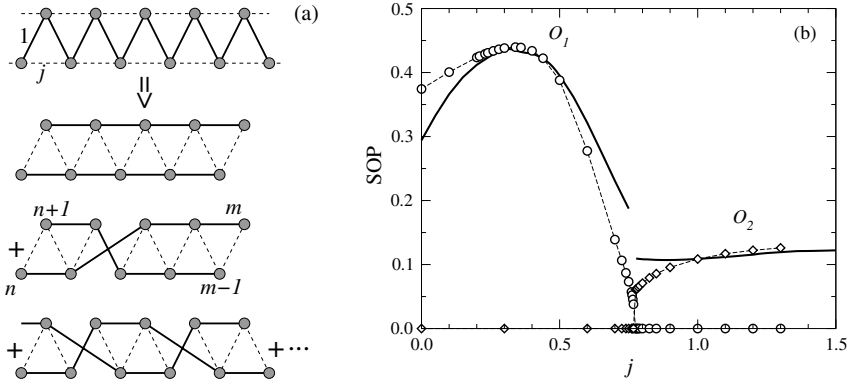

Fig. 1.10. (a) visual interpretation of the "double-Haldane" phase; (b) behavior of string order parameters (1.42) and (1.59) on the frustration j [131]

dimerized phase: the string order (1.59) was found to survive in the dimerized phase as well [141].

1.3.5 Frustrated Chains with Anisotropy: Quantum Chiral Phases

In recent few years, the problem of possible nontrivial ordering in frustrated quantum spin chains with easy-plane anisotropy has attracted considerable attention [142–146]. The simplest model of this type is described by the Hamiltonian:

$$\mathcal{H} = J \sum_n \{(\boldsymbol{S}_n \boldsymbol{S}_{n+1})_\Delta + j(\boldsymbol{S}_n \boldsymbol{S}_{n+2})_\Delta\}\,, \tag{1.60}$$

where $(\boldsymbol{S}_1 \boldsymbol{S}_2)_\Delta \equiv S_1^x S_2^x + S_1^y S_2^y + \Delta S_1^z S_2^z$, and $0 < \Delta < 1$ is the anisotropy parameter.

In the classical ground state of (1.60) spins always lie in the easy plane (xy), i.e. in terms of angular variables θ, φ for the classical spins ($S_n^x + iS_n^y = S \sin\theta_n e^{i\varphi_n}$, $S_n^z = \cos\theta_n$) one has $\theta = \frac{\pi}{2}$. For $j < \frac{1}{4}$ the alignment of spins is antiferromagnetic, $\varphi_n = \varphi_0 + \pi n$, and for $j > \frac{1}{4}$ one obtains an incommensurate helical structure with $\varphi_n = \varphi_0 \pm (\pi - \lambda_0)n$, where $\lambda_0 = \arccos(1/4j)$, and the $\pm$ signs above correspond to the two possible chiralities of the helix.

The classical *isotropic* ($\Delta = 1$) system has for $j > \frac{1}{4}$ three massless modes with wave vectors $q = 0$, $q = \pm\delta$, where $\delta \equiv \pi - \lambda_0$ is the pitch of the helix. The effective field theory for the isotropic case is the so-called $SO(3)$ nonlinear sigma model, with the order parameter described by the local rotation matrix [148, 149].

Quantum fluctuations make the long-range helical order impossible in one dimension, since it would imply a spontaneous breaking of the continuous in-

plane symmetry; in contrast to that, the existence of the finite *vector chirality*

$$\boldsymbol{\kappa}_n = \langle (\boldsymbol{S}_n \times \boldsymbol{S}_{n+1}) \rangle \tag{1.61}$$

is not prohibited by the Coleman theorem, as first noticed by Villain [151]. Positive (negative) chirality means, that spins on average prefer to rotate to the left (right), respectively, thus the discrete symmetry between left and right is spontaneously broken in the chiral phase. Nersesyan *et al.* [142] predicted the existence of a gapless *chiral phase* for $S = \frac{1}{2}$ in the $j \gg 1$ limit, using the bosonization technique combined with a subsequent mean-field-type decoupling procedure. Except having the chiral order, this phase is characterized by the power-law decaying incommensurate in-plane spin correlations of the form $\langle S_0^+ S_n^- \rangle \propto n^{-\eta} e^{iQn}$, where Q is very close to π in the limit $j \gg 1$, and $\eta = \frac{1}{4}$ for $S = \frac{1}{2}$ [142].

Early attempts [143, 145] to find this *chiral gapless* phase in numerical calculations for $S = \frac{1}{2}$ were unsuccessful. At the same time, to much of surprise, DMRG studies for frustrated $S = 1$ chain [145, 146] have shown the presence of *two* different types of chiral phases, *gapped* and *gapless*.

The model (1.60) was studied analytically in the large-S limit and for j close to the classical Lifshitz point $\frac{1}{4}$ by mapping it to a planar helimagnet [147, 152]. This mapping is based on the fact that in presence of anisotropy the modes with $q = \pm\delta$ acquire a finite mass and can be integrated out. It was shown that the existence of two types of chiral phases is not specific for $S = 1$, but is a generic large-S feature for integer S [147]. The predicted large-S phase diagram for integer S is shown in Fig. 1.11. Later large-S study [152] has shown that the chiral gapped phase should be absent for half-integer S, due to the effect of the topological term.

In subsequent works, chiral phases were numerically found for $S = \frac{1}{2}$, [150, 153] as well as for $S = \frac{3}{2}$ and $S = 2$ [150]; the resulting phase diagrams

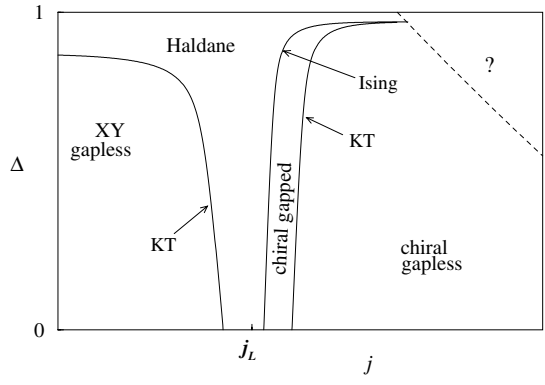

Fig. 1.11. Predicted phase diagram of frustrated anisotropic chains with integer S in the large-S approximation, according to [147]

are shown in Fig. 1.12 and one can see that there is a qualitative agreement with the predictions of the large-S theory. The predicted dependence of the critical exponent η on j in the vicinity of the transition into a chiral phase, $\eta \propto \frac{1}{S\sqrt{j-1/4}} \to \frac{1}{4}$ at $j \to j_c$, also agrees qualitatively with the numerical results of [150]. However, the large-S theory is unable to describe the transition into the dimerized phase for half-integer S.

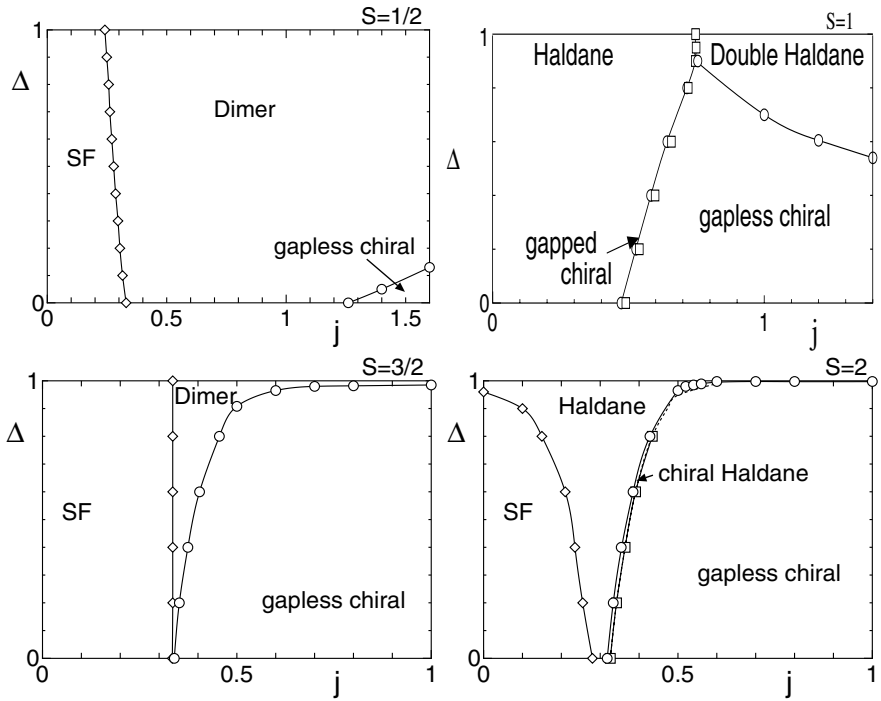

Fig. 1.12. Phase diagrams of frustrated anisotropic chains with $S = \frac{1}{2}$, 1, $\frac{3}{2}$ and 2, obtained by means of DMRG [150]

Another theoretical approach using bosonization [154] suggests that the phase diagram for integer and half-integer S should be very similar, with the only difference that the Haldane phase gets replaced by the dimerized phase in the case of half-integer S. This is in contradiction with the recent numerical results [150] indicating that the chiral gapped phase is absent for half-integer S. On the other hand, the bosonization prediction of the asymptotic value of the critical exponent, $\eta \to 1/(8S)$ at $j \to \infty$, agrees well with the numerical data.

There are indications [155] that chiral order may have been found experimentally in the 1D molecular magnet $Gd(hfac)_3NITiPr$.

1.4 $S = \frac{1}{2}$ Heisenberg Ladders

Spin ladders consist of two or more coupled spin chains and thus represent an intermediate position between one- and two-dimensional systems. The prototype of a spin ladder is shown in Fig. 1.13a and consists of two spin chains (legs) with an additional exchange coupling between spins on equivalent positions on the upper and lower leg (i.e. on rungs). The interest in spin ladders started with the observation that this ladder with standard geometry and antiferromagnetic couplings is a spin liquid with a singlet ground state and a Haldane type energy gap even for $S = 1/2$ [156]. More generally, spin ladders with an arbitrary number of antiferromagnetically coupled chains and arbitrary spin value S extend the class of spin liquids: For half-odd-integer spin and an odd number of legs they are gapless, whereas they exhibit a Haldane type energy gap otherwise (for a review of the early phase of spin ladder research see [11] and for a review of experiments and materials see [157]). Spin ladders are realized in a number of compounds and interest in these materials was in particular stimulated by the hope to find a new class of high temperature superconductors. However, so far only two SrCuO spin ladder materials were found which become superconducting under high pressure: T_c is about 10 K for $Sr_{0.4}Ca_{13.6}Cu_{24}O_{41}$ at 3 GPa pressure [158]. Nevertheless, theoretical interest continued to be strong since generalized spin ladder models cover a wide range of interesting phenomena in quantum spin systems and on the other hand allow to study in a reduced geometry interacting plaquettes of quantum spins identical to the CuO_2 plaquettes which are the basic building blocks of HTSC's. In this section we will concentrate on reviewing the properties of spin ladder models which connect seemingly disjunct quantum spin models.

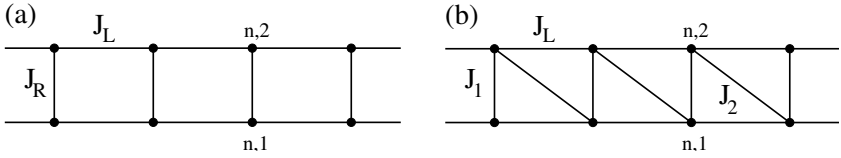

Fig. 1.13. (a) generic spin ladder with only "leg" and "rung" exchange interactions J_L, J_R; (b) zigzag spin ladder

1.4.1 Quantum Phases of Two-Leg $S = 1/2$ Ladders

The prototype of quantum spin ladders has the geometry shown in Fig. 1.13a and is defined by the Hamiltonian

$$\mathcal{H} = \sum_n \sum_{\alpha=1,2} J_{\mathrm{L}} \boldsymbol{S}_{n,\alpha} \cdot \boldsymbol{S}_{n+1,\alpha} + \sum_n J_{\mathrm{R}}\, \boldsymbol{S}_{n,1} \cdot \boldsymbol{S}_{n,2} \tag{1.62}$$

with exchange energies J_{L} along the legs and J_{R} on rungs. The 'standard' ladder results for equal antiferromagnetic exchange $J_{\mathrm{L}} = J_{\mathrm{R}} = J > 0$. Whereas the corresponding classical system has an ordered ground state of the Néel type the quantum system is a spin liquid with short range spin correlations, $\xi \approx 3.2$ (in units of the spacing between rungs) and an energy gap $\Delta \approx 0.5 J_{\mathrm{R}}$ [159,160] at wave vector π. Regarding the similarity to the Haldane chain indicated by these properties it was therefore tempting to speculate that the ladder gap is nothing but the Haldane gap of a microscopically somewhat more complicated system. In order to discuss this speculation we consider the system of (1.62) with varying ratio $J_{\mathrm{R}}/J_{\mathrm{L}}$. In the strong coupling limit with $J_{\mathrm{R}}/J_{\mathrm{L}}$ positive and large, the ladder reduces to a system of noninteracting dimers with the dimer excitation gap $\Delta_{\mathrm{dimer}} = J_{\mathrm{R}}$. With increasing J_{L} the gap decreases to become $\Delta \approx 0.4 J_{\mathrm{R}}$ in the weak coupling limit [161,162]. On the other hand, for large negative values, the formation of $S = 1$ units on rungs is favored and the system approaches an antiferromagnetic $S = 1$ chain (with effective exchange $\frac{1}{2} J_{\mathrm{L}}$). However, these two simple and apparently similar limiting cases are separated by the origin, $J_{\mathrm{R}} = 0$, corresponding to the gapless case of two independent $S = 1/2$ chains. The relation between ladder gap and Haldane gap therefore does not become clear by this simple procedure (see the early discussion by Hida [163]).

Before we approach this point in more detail, we shortly consider the ladder Hamiltonian (1.62) for the alternative case of ferromagnetically interacting legs, $J_{\mathrm{L}} < 0$: The classical ground state then is the state of two chains with long range ferromagnetic order, oriented antiparallel to each other. One would speculate that this ferromagnetic counterpart of the standard ladder is less susceptible to quantum fluctuations since without rung interactions the ground state for $S = 1/2$ is identical to the classical ground state. This is, however, not the case: An arbitrarily small amount of (antiferromagnetic) rung exchange leads to the opening up of a gap as shown by analytical [164–166] and numerical [167] methods. The situation is somewhat more involved (and interesting) when the exchange interactions are anisotropic: up to some finite rung coupling the classical ground state survives for an anisotropy of the Ising-type in the leg interactions and a spin liquid ground state of the Luttinger liquid type appears for leg anisotropy of the XY type [165,166].

The relation between Haldane and ladder gap can be clarified when the somewhat generalized model for a $S = 1/2$ ladder shown in Fig. 1.13b, with the Hamiltonian

$$\mathcal{H} = \sum_n \sum_{\alpha=1,2} J_L \boldsymbol{S}_{n,\alpha} \cdot \boldsymbol{S}_{n+1,\alpha} + \sum_n \left(J_1 \, \boldsymbol{S}_{n,1} \cdot \boldsymbol{S}_{n,2} + J_2 \, \boldsymbol{S}_{n,2} \cdot \boldsymbol{S}_{n+1,1} \right) \tag{1.63}$$

is studied. This model is mostly known under the name of zigzag ladder, i.e. two Heisenberg chains with zigzag interactions, but it can be viewed alternatively as a chain with alternating exchange J_1, J_2 and NNN interactions J_L. If either J_1 or J_2 vanishes the Hamiltonian reduces to the ladder geometry with

two legs and rungs. For $J_1 = J_2$, the model reduces to the Heisenberg chain with NNN interactions already discussed in Sect. 1.2, including the quantum phase transition from the Heisenberg chain universality class to the (twofold degenerate and gapped) dimer crystal ground state at $J_1 = J_2 = \alpha_c^{-1} J_\mathrm{L}$ (with $\alpha_c \simeq 0.2411$) and the Majumdar-Ghosh point $J_1 = J_2 = 2J_\mathrm{L}$ with two degenerate ground states, see Sect. 1.2.6 above. Upon including alternation, $J_1 \neq J_2$, the Majumdar-Ghosh point extends into two Shastry-Sutherland lines [168], $J_2 = \frac{1}{2}$ for $J_1 > \frac{1}{2}$ and $J_1 = \frac{1}{2}$ for $J_2 > \frac{1}{2}$: If the exchange coupling along the chain alternates between J_1 on even bonds and $J_2 < J_1$ on odd bonds, $|0_I\rangle$ continues to be the ground state for $J_2 = \frac{1}{2}$ as long as $J_2 > -1$.

It is instructive to study this more general model introduced by White [169], for several reasons: The ground state phase diagram for various combinations of the variables J_1, J_2, J_L allows to discuss the relations between a number of seemingly different models by continuous deformation of the interaction parameters [169–171] and it serves as an instructive example for quantum phase transitions depending on the parameters in interaction space. Moreover it allows to make contact to real quasi 1D materials by showing the position in this diagram in rough correspondence to their interaction parameters.

In the following we present and discuss three ground state phase diagrams, in order to cover (partly overlapping) the full phase space in the variables J_1, J_2, J_L. Evidently the phase diagrams are symmetric under exchange of J_1 and J_2 and we will discuss only one of the two possible cases.

(a) Figure 1.14a shows the phase diagram J_2 vs J_1, assuming a finite value of $J_\mathrm{L} > 0$ as energy unit. It has been established by various methods that the only phase transition lines occur at $J_2 = -2J_1/(2+J_1)$ (transition to the ferromagnetically ordered ground state) and along the line $J_1 = J_2 > -4$. This line is a line of first order quantum phase transitions for $0 < J_1 = J_2 < \alpha_c^{-1}$ and of second order quantum phase transitions for $J_1 = J_2 > \alpha_c^{-1}$ (in the following we use finite value of $J_\mathrm{L} > 0$ as energy unit and restrict to the $J_1 > J_2$ half of the plane).

The origin $J_1 = J_2 = 0$ corresponds to the gapless case of *two* noninteracting Heisenberg chains, whereas on the line $J_1 = J_2 > 0$ one has *one* $S = 1/2$ Heisenberg chain with NNN interaction. This line separates two distinct gapped regimes, each containing the limit of noninteracting dimers $J_1 \to \infty$ resp. $J_2 \to \infty$, the standard ladder, an effective $S = 1$ chain and the Shastry-Sutherland (SS) line.

The concept of string order can be extended to ladders [172, 173] introducing two complementary string order parameters in the $J_1 - J_2$ phase diagram:

$$\mathcal{O}^\alpha_{\mathrm{lad},1}(n,m) = \left\langle -(S^\alpha_{n,1} + S^\alpha_{n,2})\, e^{i\pi \sum_{j=n}^{m-1}(S^\alpha_{j,1}+S^\alpha_{j,2})}\, (S^\alpha_{m,1} + S^\alpha_{m,2}) \right\rangle, \quad (1.64)$$

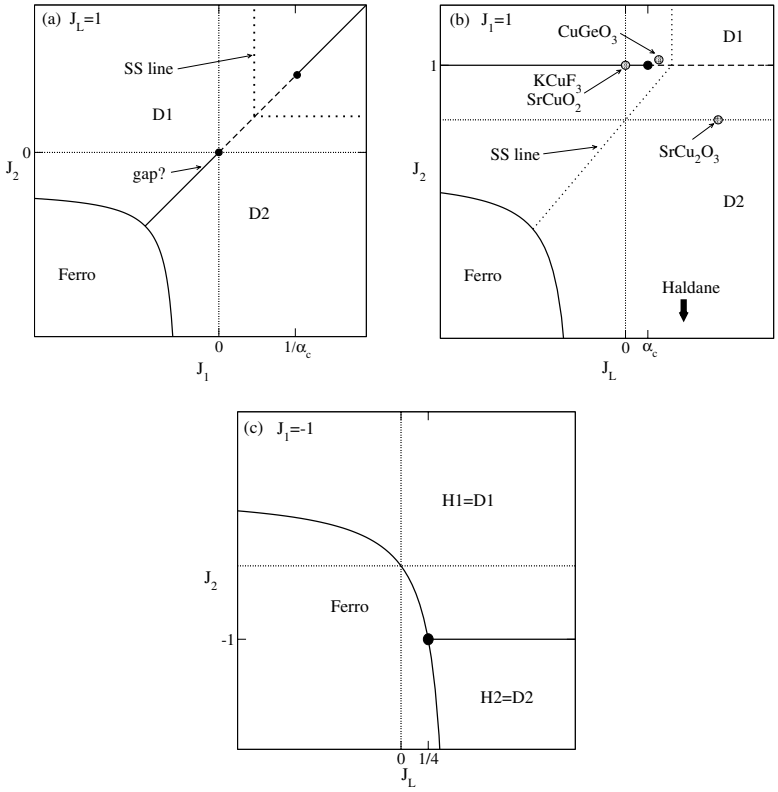

Fig. 1.14. Phase diagrams of the $S = \frac{1}{2}$ zigzag ladder: (a) $\mathrm{J_L} = 1$, (b) $\mathrm{J_1} = 1$, (c) $\mathrm{J_1} = -1$. *Solid (dashed) lines* correspond to the second (first) order transitions, respectively

$$\mathcal{O}^{\alpha}_{\mathrm{lad},2}(n,m) = \left\langle -(S^{\alpha}_{n,1} + S^{\alpha}_{n+1,2})\, e^{i\pi \sum_{j=n}^{m-1}(S^{\alpha}_{j,1}+S^{\alpha}_{j+1,2})}\, (S^{\alpha}_{m,1} + S^{\alpha}_{m+1,2}) \right\rangle. \quad (1.65)$$

For $J_1 > J_2$ (phase D2) singlets are found preferably on the rungs and the remaining antiferromagnetic leg exchange then leads to a tendency towards triplets, i.e. $S = 1$ units on diagonals. This implies a vanishing value for $\mathcal{O}_{\mathrm{lad},1}$ whereas a finite string order parameter $\mathcal{O}_{\mathrm{lad},2}$ develops. This type of string order characterizes the standard ladder ($J_1 = 1, J_2 = 0$) and becomes identical with the $S = 1$ chain string order parameter for $J_2 \to -\infty$. The complementary situation is true for $J_1 < J_2$: rungs and diagonals as well as $\mathcal{O}_{\mathrm{lad},1}$ and $\mathcal{O}_{\mathrm{lad},2}$ exchange their roles. In the field theoretic representation of the generalized ladder [13,174,175] $\mathcal{O}_{\mathrm{lad},1}$ and $\mathcal{O}_{\mathrm{lad},2}$ correspond to Ising order resp. disorder parameters. Both order parameters become zero on the line $J_1 = J_2$ for $J_1 = J_2 > \alpha_c^{-1}$ (gapless line) whereas they change discontinuously

following the discontinuous change in ground state when the line $J_1 = J_2$ for $J_1 = J_2 < \alpha_c^{-1}$ (line with two degenerate ground states) is crossed.

Thus it is possible to deform various gapped models, noninteracting dimers, the standard ladder and the $S = 1$ Haldane chain, continuously into each other without closing the gap if one stays on the same side of the line $J_1 = J_2$. Then the ladder gap evolves into the dimer gap when the rung coupling increases to infinity and the dimer gap evolves into the Haldane gap when two dimers on neighboring rungs interact ferromagnetically via J_2, forming $S = 1$ units on diagonals. However, when the standard ladder is deformed into a $S = 1$ chain by changing rung dimers from antiferromagnetic to strongly ferromagnetic, one moves to a different symmetry class since the line $J_1 = J_2$ is crossed.

For ferromagnetic couplings $J_1, J_2 < 0$ there is a regime of disorder due to competing interactions before ferromagnetic order sets in. This applies in particular to the limit $-4 < J_1 = J_2 < 0$, a ferromagnetic chain with AF NNN exchange. It is usually taken for granted that the corresponding ground state of this frustrated chain is in an incommensurate phase and gapless; however, a recent interesting speculation [176] suggests the presence of a tiny but finite gap on some part of this line.

(b) In Fig. 1.14b the phase diagram in the variables J_2 vs J_L is presented, assuming a finite value of $J_1 > 0$ as energy unit. This choice of variables displays most clearly the neighborhood of the dimer point (the origin in this presentation) and the situation when ferromagnetic coupling is considered on the legs and on one type of inter-leg connections. The dividing line between the two dimer/Haldane phases D1 and D2 appears now as the line $J_2 = 1$ with the end of the gapless phase at $J_L = \alpha_c$ and the Majumdar-Ghosh point at $J_L = \frac{1}{2}$. The gap on this line starts exponentially small from zero at the Kosterlitz Thouless transition at $J_L = \alpha_c$, goes through a maximum at $J_L \approx 0.6$ and drops to zero exponentially for $J_L \to \infty$ (two decoupled chains) [149, 177].

The Shastry-Sutherland (SS) lines $J_L = \frac{1}{2}J_2$ (in D2) resp. $J_L = \frac{1}{2}$ in D1 are to be considered as disorder lines where spin-spin correlations in real space become incommensurate [178, 179]. The precise properties in the incommensurate regime beyond these lines have not been fully investigated up to now. The SS line extends into the range of ferromagnetic couplings and (in D2) ends at $J_L = \frac{1}{2}J_2 = -1$. This point lies on the boundary of the ferromagnetic phase, $J_2 = -2J_L/(1 + 2J_L)$. This boundary is obtained from the instability of the ferromagnetic state against spin wave formation. There are indications that ground states on this line are highly degenerate: states with energies identical to the ferromagnetic ground state are explicitly known for $J_1 = J_L = -1$ (end of the SS line, dimers on J_1 bonds), for $J_1 = J_L = -\frac{3}{2}$ (a matrix product ground state, see Sect. 1.4.2) and for a family of states which exhibit double chiral order as studied in ref. [180].

As mentioned before, the ladder is gapless on the line $J_2 = 1, J_L < 0$ (antiferromagnetic Heisenberg chain with ferromagnetic NNN exchange), but

an infinitesimal alternation, $J_2 \neq 1$ drives it into the gapless phase, smoothly connected to the Haldane/dimer phase. At strongly negative values of J_1 the phase diagram of Fig. 1.14b shows the second order phase transition from the ferromagnetic to the antiferromagnetic $S = 1$ chain at $J_L = -\frac{1}{2}$.

(c) In Fig. 1.14c the phase diagram in the same variables J_2 vs J_L is shown, but assuming a finite *ferromagnetic* value of $|J_1| = -J_1 > 0$ as energy unit. This choice of variables allows to discuss the situation for two ferromagnetic couplings. The origin is identified as the limit of noninteracting spins 1 and the neighborhood of the origin covers both the ferro- as the antiferromagnetic $S = 1$ chain, depending on the direction in parameter space.

1.4.2 Matrix Product Representation for the Two Leg S = 1/2 Ladder

The matrix product representation introduced for the $S = 1$ chain above can be extended to ladders and is found to be a powerful approach to describe spin ladder ground states in the regime covered by the J_1-J_2 phase space of the model of (1.63). It formulates possible singlet ground states as a product of matrices g_n referring to a single rung n, $|..\rangle = \prod_n g_n$. Matrices g_n as used in Sect. 1.3.3 are generalized to include the possibility of singlets on a rung and read [170]:

$$\begin{aligned} g_n(u) &= u\widehat{1}\,|s\rangle_n + v\Big(\frac{1}{\sqrt{2}}\sigma^-|t_-\rangle_n - \frac{1}{\sqrt{2}}\sigma^+|t_+\rangle_n + \sigma^z|t_0\rangle_n\Big) \\ &= \begin{pmatrix} u|s\rangle + v|t_0\rangle & -\sqrt{2}v|t_+\rangle \\ \sqrt{2}v|t_-\rangle & u|s\rangle - v|t_0\rangle \end{pmatrix}. \end{aligned} \tag{1.66}$$

(Note that the triplet part of (1.66) is equivalent to (1.55) up to a unitary transformation; here we keep the original nonation of [170].) We now show that the ground states of the Majumdar-Ghosh chain can be written in the form of a matrix product. This is trivially true for $|0\rangle_{II}$ which is obtained for $u = 1, v = 0$. It is also true for the state $|0\rangle_I$ if it is formulated in terms of the complementary spin pairs $[2,3],[4,5]\ldots$ used in $|0_{II}\rangle$: We start from the representation of a singlet as in (1.34, 1.35) and write

$$\begin{aligned} |0\rangle_I = \frac{1}{2^{N/2}} \sum_{\{..s,s',t,..\}} & \cdots \chi_{2p-1}(s)\ \epsilon^{s,s'}\ \chi_{2p}(s') \\ \times\ \chi_{2p+1}(t)\ \epsilon^{t,t'}\ \chi_{2p+2}(t')\ \chi_{2p+3}(r)\ \epsilon^{r,r'}\ \chi_{2p+4}(r') \cdots &= \mathrm{Tr}\Big(\prod_p g_p\Big) \end{aligned}$$

after defining the matrix with state valued elements

$$g_p(s,t) := \frac{1}{\sqrt{2}} \sum_{s'} \chi_{2p}(s)\ \chi_{2p+1}(s')\ \epsilon^{s',t}$$

to replace the singlet, (1.34) as new unit. The explicit form for g is

$$\frac{1}{\sqrt{2}}\begin{pmatrix} |\uparrow,\downarrow\rangle & -|\uparrow,\uparrow\rangle \\ |\downarrow,\downarrow\rangle & -|\downarrow,\uparrow\rangle \end{pmatrix}$$

which is identical to (1.66) with $u = v = 1/\sqrt{2}$.

1.4.3 Matrix Product States: General Formulation

The above construction of the matrix product ansatz for $S = \frac{1}{2}$ ladders can be generalized for arbitrary 1D spin systems [181]. Let $\{|\gamma S\mu\rangle\}$ be the complete set of the spin states of the elementary cell of a given 1D spin system, classified according to the total spin S, its z-projection μ and an (arbitrary) additional quantum number γ. Define the object g as follows:

$$g^{(jm)} = \sum_{\lambda q, S\mu} c_\gamma \langle jm|\lambda q, S\mu\rangle \, \widehat{T}^{\lambda q}|\gamma S\mu\rangle \,, \tag{1.67}$$

where $\langle jm|\lambda q, S\mu\rangle$ are the standard Clebsch-Gordan coefficients, c_γ are free c-number parameters, and $\widehat{T}^{\lambda q}$ are irreducible tensor operators acting in some auxiliary space, which transform under rotations according to the $\mathcal{D}^\lambda$ representation. Then it is clear that g transforms according to $\mathcal{D}^j$ and thus can be assigned "hyperspin" quantum numbers jm. Then, building on those elementary objects g_i (where i denotes the i-th unit cell) one can construct wave functions with certain total spin almost in the same way as from usual spin states. For instance, for a quantum 1D ferrimagnet with the excess spin j per unit cell the state with the total spin and its z-projection both equal to Nj would have the form

$$|\Psi^{Nj,Nj}\rangle = \mathrm{Tr}_{\mathcal{M}}(\Omega_N), \quad \Omega_N = g_1^{(jj)} \cdot g_2^{(jj)} \cdots g_N^{(jj)} \,, \tag{1.68}$$

where the trace sign denotes an appropriate trace taken over the auxiliary space. The choice of the auxiliary space $\mathcal{M}$ determines the specific *matrix representation* of the operators $T^{\lambda q}$; the space $\mathcal{M}$ can be always chosen in a form of a suitable decomposition into multiplets $\mathcal{M} = \sum_{\alpha J} \oplus \mathcal{M}^{\alpha J}$, and then the structure of the matrix representation is dictated by the Wigner-Eckart theorem:

$$\langle \alpha JM|T^{\lambda q}|\alpha' J' M'\rangle = \widetilde{T}_{\lambda,\alpha J,\alpha' J'} \langle JM|\lambda q, J' M'\rangle \,. \tag{1.69}$$

The reduced matrix elements $\widetilde{T}_{\lambda,\alpha J,\alpha' J'}$ and the coefficients c_γ are free parameters.

Matrix product states (MPS) are particularly remarkable because the matrices $g_1 g_2$, $g_1 g_2 g_3$, etc. all have the same structure (1.67) if they are constructed from the "highest weight" components $g^{(j,m=j)}$. This self-similarity is actually an indication of the deep connection of singlet MPS and the density-matrix renormalization group technique, as first pointed out by Ostlund and Römmer [182] and developed later in works of Sierra *et al.* [183–185].

A Few Examples

In the simplest case of a two-dimensional $\mathcal{M} = \{|J = \frac{1}{2}, M\rangle\}$, the allowed values of λ are 0 and 1, and T^{1q} are just proportional to the usual Pauli matrices σ^q, and T^{00} is proportional to the unit matrix. If one wants the wavefunction to be a global singlet, the simplest way to achieve that is to have the construction (1.68) with $j = 0$. Then, for the case of $S = 1$ chain with one spin in a unit cell, one obtains exactly the formula (1.55), with no free parameters.

Higher-S AKLT-type VBS states can be also easily represented in the matrix product form. In this case one has to choose $\mathcal{M} = \{|S/2, M\rangle\}$, then the only possible value of λ is S, and, taking into account that $\langle 00|Sq, S\mu\rangle = \delta_{q,-\mu}(-1)^{S-\mu}$, we obtain

$$g_S = \sum_{\mu} (-1)^{S-\mu} T^{S,-\mu} |S, \mu\rangle.$$

For a generic *quantum ferrimagnet,* i.e., a chain of alternating spins 1 and $\frac{1}{2}$, coupled by antiferromagnetic nearest-neighbor exchange, the elementary unit contains now two spins. The ground state has the total spin $\frac{1}{2}$ per unit cell, then one would want to construct the elementary matrix $g^{1/2,1/2}$. If $\mathcal{M}$ is still two-dimensional, the elementary matrix has according to (1.67) the following form:

$$g = \begin{pmatrix} (u-v)|\uparrow\rangle - |\frac{1}{2}\rangle & \sqrt{3}|\frac{3}{2}\rangle \\ -2v|\downarrow\rangle - |-\frac{1}{2}\rangle & (u+v)|\uparrow\rangle + |\frac{1}{2}\rangle \end{pmatrix}, \tag{1.70}$$

where $|\uparrow\rangle$, $|\downarrow\rangle$ and $|\pm\frac{1}{2}\rangle$, $|\pm\frac{3}{2}\rangle$ are the cell states with the total spin $\lambda = \frac{1}{2}$ and $\lambda = \frac{3}{2}$, respectively.

1.4.4 Excitations in Two-Leg S=1/2 Ladders

The excitation spectrum in this simplest ladder type spin liquid is similar to that of a Haldane chain: The lowest excitation is a triplet band with minimum energy at $q = \pi$ and a continuum at $q = 0$. Since the ground state is a disordered singlet, a spin wave approach (which would result in a gapless spectrum) is inappropriate. In different regimes of the space of coupling constants, different methods have been developed to deal approximately with the low-lying excitations:

Weak Coupling Regime

In the *weak coupling regime*, close to two independent chains, the bosonization approach can be applied to decide whether the excitation is gapless or

gapped. The standard situation is that the coupling between legs is relevant and a gap develops for arbitrarily small coupling. Some examples are: antiferromagnetic interactions in the standard rung geometry [177] (the gap is linear in $J_{\rm R}$, the numerical result is $\Delta \approx 0.4 J_{\rm R}$ [162]), antiferromagnetic interactions in the zigzag geometry [186], and antiferromagnetic interactions for isotropic ferromagnetic legs [165]. The gapless (Luttinger liquid) regime of the decoupled chains can survive, e.g. for ferromagnetic legs with XY-type anisotropy and antiferromagnetic coupling [166].

Strong Coupling Regime

In the *strong coupling regime*, close to the dimer limit the lowest elementary excitation develops from the excited triplet state of a dimer localized on one of the rungs which starts propagating due to the residual interactions. For the Hamiltonian of (1.63) the dispersion to first order is (we choose $J_1 \gg J_2$ to be the strong dimer interaction)

$$\omega(q) = J_1 + \Big(J_L - \frac{1}{2}J_2\Big)\cos q \; + \; J_1\Big(\frac{3}{4}(\alpha_L - \frac{1}{2}\alpha_2)^2 + -\frac{1}{4}\alpha_2^2(1+\cos q) - \frac{1}{4}(\alpha_L - \frac{1}{2}\alpha_2)^2\cos 2q \; \ldots\Big) \quad (1.71)$$

with $\alpha_L = J_L/J_1$ and $\alpha_2 = J_2/J_1$. The excitation gap is at either $q = 0$ (for $J_2 > 2J_{\rm L}$ in the lowest order, alternating AF chain type spectrum) or $q = \pi$ ($J_2 < 2J_{\rm L}$, ladder type spectrum). For a finite regime in the space of coupling constants an expansion in the dimer-dimer couplings leads to converging expressions for the low-energy frequencies. Expansions have now been carried out up to $14^{\rm th}$ order by the methods of cluster expansion [68, 187, 188] and are convergent even close to the isotropic point.

We note two curiosities: In a small but finite transition regime, the minimum of the dispersion curve changes continuously from $q = 0$ to $q = \pi$ [187,189]; on the Shastry-Sutherland line, $\alpha_L = \alpha_2/2$ the energy of the mode at $q = \pi$ is known exactly, $\omega(q = \pi) = J_1$.

For nearly Heisenberg chains with NNN interaction and small alternation dimer series expansions have been used extensively to investigate further details of the spectra in e.g. $CuGeO_3$ [68]. Bound states for the standard spin ladder have been calculated to high order [190] and used to describe optically observed two-magnon states in $(La,Ca)_{14}Cu_{24}O_{41}$ [191].

The strong coupling approach has also been applied to describe interacting dimer materials such as $KCuCl_3$, $TlCuCl_3$ [192,193] with 3D interactions and $(C_4H_{12}N_2)Cu_2Cl_6$ (= PHCC) [194] with 2D interactions. These interactions are quantitatively important but not strong enough to close the spin gap and to drive the system into the 3D ordered state. The dimer expansions are much more demanding than in 1D, but nevertheless were done successfully up to $6^{\rm th}$ order [195, 196].

Bond Boson Operator Approach

This approach makes use of the representation of spin operators in terms of the so-called *bond bosons* [197]. On each ladder rung, one may introduce four bosonic operators s, t_a ($a \in (x,y,z)$) which correspond to creation of the singlet state $|s\rangle$ and three triplet states $|t_a\rangle$ given by

$$|s\rangle = \frac{1}{\sqrt{2}}\big(|\uparrow\downarrow\rangle - |\downarrow\uparrow\rangle\big), \qquad |t_z\rangle = \frac{1}{\sqrt{2}}\big(|\uparrow\downarrow\rangle + |\downarrow\uparrow\rangle\big), \tag{1.72}$$
$$|t_x\rangle = -\frac{1}{\sqrt{2}}\big(|\uparrow\uparrow\rangle - |\downarrow\downarrow\rangle\big), \qquad |t_y\rangle = \frac{i}{\sqrt{2}}\big(|\uparrow\uparrow\rangle + |\downarrow\downarrow\rangle\big),$$

Then the rung spin-$\frac{1}{2}$ operators $\boldsymbol{S}_{1,2}$ can be expressed through the bond bosons as

$$\boldsymbol{S}_{1,2} = \pm\frac{1}{2}(s^\dagger \boldsymbol{t} + \boldsymbol{t}^\dagger s) - \frac{1}{2}i(\boldsymbol{t}^\dagger \times \boldsymbol{t}). \tag{1.73}$$

One may check that the above representation satisfies all necessary commutation relations, if the following *local* constraint is assumed to hold:

$$s^\dagger s + \boldsymbol{t}^\dagger \cdot \boldsymbol{t} = 1, \tag{1.74}$$

which implies that the bond bosons are 'hardcore' (no two bosons are allowed to occupy one bond), and, moreover, exactly one boson must be present at each bond/rung. The constraint is easy to handle formally (e.g. in the path integral formulation), but practically one can do that only at the mean-field level [198], replacing the local constraint by a global one, i.e., (1.74) is assumed to be true only on average, which introduces rather uncontrollable approximations.

In a slightly different version of the bond boson approach [199], the vacuum state is introduced as corresponding to the state with fully condensed s bosons. Then for spin operators one obtains the formulae of the form (1.73) with s replaced by 1, and instead of the constraint (1.74) one has just a usual hardcore constraint $\boldsymbol{t}^\dagger \cdot \boldsymbol{t} = 0, 1$. This version is most useful in the limit of weakly coupled dimers (e.g., $J_1 \gg J_2, J_L$). Passing to the momentum representation, one obtains on the quadratic level the effective Hamiltonian of the form

$$\mathcal{H}_{eff} = \sum_{ka} A_k t^\dagger_{k,a} t_{k,a} + \frac{1}{2} B_k (t^\dagger_{k,a} t^\dagger_{k,a} + \text{h.c.}), \tag{1.75}$$

where the amplitudes A_k, B_k are given by the expressions

$$B_k = (J_L - J_2/2)\cos(k), \qquad A_k = J_1 + B(k). \tag{1.76}$$

Thus, neglecting the boson interaction, one obtains for the excitation energy

$$\omega(k) = \sqrt{J_1^2 + 2\,J_1\,\left(J_L - \frac{1}{2}J_2\right)\cos k}\,, \tag{1.77}$$

which coincides with the corresponding RPA expression. Upon comparison to the full systematic series of the perturbation theory, one can see that (1.77) contains only the leading contributions at each cosine term $\cos(nk)$ of the complete series and misses the remaining terms starting in the second order [187].

The Hamiltonian (1.75) does not take into account any interaction between the bosons. One may argue that the most important contribution to the interaction comes from the hardcore constraint, which is effectively equivalent to the infinite on-site repulsion U.

The effect of the local hardcore constraint can be handled using the so-called *Brueckner approximation* as proposed by Kotov *et al.* [199]. In this approach, one neglects the contribution of anomalous Green's functions and obtains in the limit $U \to \infty$ the vertex function $\Gamma_{aa',ss'} = \Gamma(k,\omega)(\delta_{as}\delta_{a's'} + \delta_{as'}\delta_{a's})$, where k and $\hbar\omega$ are respectively the total momentum and energy of the incoming particles, with

$$\frac{1}{\Gamma(k,\omega)} = -\frac{1}{N}\sum_q \frac{Z_q Z_{k-q} u_q^2 u_{k-q}^2}{\omega - \Omega_q - \Omega_{k-q}}. \tag{1.78}$$

The corresponding normal self-energy $\Sigma(k,\omega)$ is

$$\Sigma(k,\omega) = (4/N)\sum_q Z_q v_q^2 \Gamma(k+q, \omega - \Omega_q) \tag{1.79}$$

Here Ω_k is the renormalized spectrum, which is found as a pole of the normal Green function

$$G(k,\omega) = \frac{\omega + A_k + \Sigma(-k,-\omega)}{(\omega - \Sigma_-)^2 - (A_k + \Sigma_+)^2 + B_k^2}, \tag{1.80}$$

where $\Sigma_\pm \equiv \frac{1}{2}\big\{\Sigma(k,\omega) \pm \Sigma(-k,-\omega)\big\}$. The quasiparticle contribution to the above Green function is given by

$$G(k,\omega) = \frac{Z_k u_k^2}{\omega - \Omega_k + i\varepsilon} - \frac{Z_k v_k^2}{\omega + \Omega_k - i\varepsilon} \tag{1.81}$$

which defines the renormalization factors Z_k, the Bogoliubov coefficients u_k, v_k and the spectrum Ω_k as follows [131]:

$$\begin{aligned}
&\Omega_k = \Sigma_- + E_k, \quad E_k = \{(A_k + \Sigma_+)^2 - B_k^2\}^{1/2},\\
&u_k^2 = \frac{1}{2}\big\{1 + (A_k + \Sigma_+)/E_k\big\}, \quad v_k^2 = u_k^2 - 1,\\
&\frac{1}{Z_k} = 1 - \frac{\partial\Sigma_-}{\partial\omega} - \frac{(A_k + \Sigma_+)}{E_k}\,\frac{\partial\Sigma_+}{\partial\omega}
\end{aligned} \tag{1.82}$$

where $\Sigma_\pm$ and their derivatives are understood to be taken at $\omega = \Omega_k$. The system of equations (1.78), (1.79), (1.82) has to be solved self-consistently with respect to Z and Σ. This approach is valid as long as the boson density $\rho = \frac{3}{N}\sum_q Z_q v_q^2$ remains small, ensuring that the contribution of anomalous Green's functions is irrelevant [199].

It should be remarked that the original expressions of Kotov *et al.* [199] can be obtained from (1.82) as a particular case, assuming that $\Sigma(k,\omega)$ is almost linear in ω in the frequency interval $(-\Omega_k, \Omega_k)$; however, this latter assumption fails if one is far away from the phase transition, i.e. if the resulting frequency ω is not small comparing to J_1.

The above way of handling the hardcore constraint is quite general and can be used in other problems as well, e.g., one can apply it to improve the results of using the variational soliton-type ansatz (1.56), (1.57) for the $S = 1$ Haldane chain [131].

Bound Domain Wall Approach

The low-lying excited states in spin ladders in the dimer phase can be discussed in a domain wall representation qualitatively rather similar to the antiferromagnetic Ising chain in Sect. 2.3. In the limit of a twofold degenerate ground state (i.e. on the line $J_1 = J_2 = J < \alpha_c^{-1} J_\mathrm{L}$), excitations can be discussed in terms of pairs of domain walls, mediating between these two states [168].

Moving away from this line into the regime $J_1 \neq J_2$ where bond strengths alternate, a pair of domain walls feels a potential energy linear in the distance between them since the two dimer configurations now have different energies. As a consequence, all domain walls become bound with well defined dispersion $\omega(q)$. The frequency is lowest for the state originating from the simplest pair of domain walls, obtained by exciting one dimer leading to a triplet state. Thus one makes connection with the strong coupling limit and establishes that the free domain wall continuum upon binding develops into the sharp triplet excitation ('magnon') of the Haldane type. For a more quantitative description of the transition between bound and unbound limits, several variational formulations have been developed [189, 200, 201]. Of particular interest is the limit of $J_\mathrm{L} \gg J_1$, i.e. weakly coupled gapless chains which can be studied by bosonization techniques [186]. The zigzag structure is responsible for a "twist" interaction which induces incommensurabilities in the spin correlations.

A particular simple example for a system with unbound domain walls is the Majumdar-Ghosh state ($J_1 = J_2 = 2J_\mathrm{L} = J$ in (1.63)); a domain wall here means a transition from dimers on even bonds to dimers on odd bonds or vice versa and implies the existence of a free spin 1/2, justifying the name spinons for these excitations. For each free spin 1/2 the binding energy of half a dimer bond is lost, producing an energy gap $J/2$ which is lowered to a minimum value of $J/4$ at $q = 0$. For a chain with periodic

boundary conditions the excitation spectrum consists of pairs of these spinons which, owing to isotropy, bind into 4 degenerate states, a triplet and a singlet. Because of the degeneracy of the two ground states these spinons can move independently (completely analogous to the domain walls of the Ising chain with small transverse interactions of Sect. 2.3), their energies therefore simply add and lead to an excitation continuum. For a finite range of wave vectors centered around $q = \pi$ bound states with lower energies exist [168, 200]. The excited state with lowest energy, however, remains the triplet/singlet at $q = 0$.

Moving away from the Majumdar-Ghosh point on the line with two degenerate ground states towards the quantum phase transition at $J_{\mathrm{L}} = J\alpha_c$, the energy of the spinons diminishes until they become gapless at the phase transition. Similar in spirit to the approach from the antiferromagnetic Ising phase, this is another way to approach the gapless excitation spectrum of the Heisenberg chain [202]. Since it preserves isotropy in spin space at each stage, it nicely demonstrates the fourfold degeneracy of the spinon spectrum with one triplet and one singlet, originating from the two independent spins 1/2.

1.4.5 Multileg Ladders

A natural generalization of the two-leg AF ladder is a general n-leg $S = \frac{1}{2}$ ladder model with all antiferromagnetic rung and leg couplings. Except being an interesting theoretical concept representing a system "in between" one and two dimensions, this model is realized in strontium copper oxides of the $\mathrm{Sr_{n-1}Cu_{n+1}O_{2n}}$ family [11]. It turns out that the analogy between the regular two-leg $S = \frac{1}{2}$ ladder and the $S = 1$ Haldane chain can be pursued further, and n-leg ladders with odd n are gapless, while ladders with even n exhibit a nonzero spectral gap Δ [203,204]. One may think of this effect as cancellation of the topological terms coming from single $S = \frac{1}{2}$ chains [174, 204–206]. The problem can be mapped to the nonlinear sigma model [206] with the topological angle $\theta = \pi n$ and coupling constant $g \propto n^{-1}$, so that there is a similarity between the n-leg $S = \frac{1}{2}$ ladder and a single chain with $S = n/2$. The gap $\Delta \propto e^{-2\pi/g}$ vanishes exponentially in the limit $n \to \infty$, recovering the proper two-dimensional behavior.

Instructive numerical results are available for systems of up to 6 coupled chains: improving earlier DMRG studies [159], calculations for standard n-leg ladders using loop cluster algorithms [161, 162] clearly show the decrease of the gap for n even (from 0.502 J for $n = 2$ to 0.160 J for $n = 4$ and 0.055 J for $n = 6$). Further detailed results by this method were obtained for correlation lengths and susceptibilities [162, 207].

1.5 Modified Spin Chains and Ladders

Until now, we have considered only models with purely Heisenberg (bilinear) spin exchange. One should remember, however, that the Heisenberg Hamiltonian is only an approximation, and generally for $S > 1/2$ one has also "non-Heisenberg" terms such as $(\boldsymbol{S}_l \cdot \boldsymbol{S}_{l'})^m, m = 2, \ldots, 2S$ whose strength depends on the Hund's rule coupling. For $S = \frac{1}{2}$, exchange terms involving four or more spins emerge in higher orders of the perturbation theory in the Hubbard model. Those non-Heisenberg terms are interesting since they lead to a rather rich behavior, and even small admixture of such interactions may drive the system in the vicinity of a phase transition.

1.5.1 $S = \frac{1}{2}$ Ladders with Four-Spin Interaction

In case of a two-leg spin-$\frac{1}{2}$ ladder the general form of the isotropic translationally invariant spin ladder Hamiltonian with exchange interaction only between spins on plaquettes formed by neighboring rungs reads as

$$\begin{aligned}\mathcal{H} = &\textstyle\sum_i J_R \boldsymbol{S}_{1,i} \cdot \boldsymbol{S}_{2,i} + J_L \boldsymbol{S}_{1,i} \cdot \boldsymbol{S}_{1,i+1} + J'_L \boldsymbol{S}_{2,i} \cdot \boldsymbol{S}_{2,i+1} \\ &+ J_D \boldsymbol{S}_{1,i} \cdot \boldsymbol{S}_{2,i+1} + J'_D \boldsymbol{S}_{2,i} \cdot \boldsymbol{S}_{1,i+1} + V_{LL} (\boldsymbol{S}_{1,i} \cdot \boldsymbol{S}_{1,i+1})(\boldsymbol{S}_{2,i} \cdot \boldsymbol{S}_{2,i+1}) \\ &+ V_{DD} (\boldsymbol{S}_{1,i} \cdot \boldsymbol{S}_{2,i+1})(\boldsymbol{S}_{2,i} \cdot \boldsymbol{S}_{1,i+1}) + V_{RR} (\boldsymbol{S}_{1,i} \cdot \boldsymbol{S}_{2,i})(\boldsymbol{S}_{1,i+1} \cdot \boldsymbol{S}_{2,i+1}),\end{aligned} \tag{1.83}$$

where the indices 1 and 2 distinguish lower and upper legs, and i labels rungs. The model is schematically represented in Fig. 1.15.

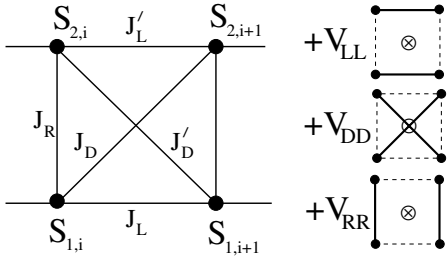

Fig. 1.15. A generalized ladder model with four-spin interactions

There is an obvious symmetry with respect to interchanging $\boldsymbol{S}_1$ and $\boldsymbol{S}_2$ on every other rung and simultaneously interchanging J_L, V_{LL} with J_D, V_{DD}. Less obvious is a symmetry corresponding to the so-called *spin-chirality dual transformation* [208]. This transformation introduces on every rung a pair of new spin-$\frac{1}{2}$ operators $\boldsymbol{\sigma}$, $\boldsymbol{\tau}$, which are connected to the 'old' operators $\boldsymbol{S}_{1,2}$ through

$$\boldsymbol{S}_{1,2} = \frac{1}{2}(\boldsymbol{\sigma} + \boldsymbol{\tau}) \pm (\boldsymbol{\sigma} \times \boldsymbol{\tau}). \tag{1.84}$$

Applying this transformation to the generalized ladder (1.83) generally yields new terms containing mixed products of three neighboring spins; however, in case of a symmetric ladder with $J_{L,D} = J'_{L,D}$ those terms vanish and one obtains the model of the same form (1.83) with new parameters

$$\begin{aligned}
\widetilde{J}_L &= J_L/2 + J_D/2 + V_{LL}/8 - V_{DD}/8 \\
\widetilde{J}_D &= J_L/2 + J_D/2 - V_{LL}/8 + V_{DD}/8 \\
\widetilde{J}_R &= J_R, \qquad \widetilde{V}_{RR} = V_{RR} \\
\widetilde{V}_{LL} &= 2J_L - 2J_D + V_{LL}/2 + V_{DD}/2 \\
\widetilde{V}_{DD} &= -2J_L + 2J_D + V_{LL}/2 + V_{DD}/2
\end{aligned} \tag{1.85}$$

It is an interesting fact that all models having the product of singlet dimers on the rungs as their exact ground state are self-dual with respect to the above transformation, because the necessary condition for having the rung-dimer ground state is [209]

$$J_L - J_D = \frac{1}{4}(V_{LL} - V_{DD}). \tag{1.86}$$

It is worthwhile to remark that there are several families of generalized $S = \frac{1}{2}$ ladder models which allow an exact solution. First Bethe-ansatz solvable ladder models were those including three-spin terms explicitly violating the time reversal and parity symmetries (see the review [210] and references therein). Known solvable models with four-spin interaction include those constructed from the composite spin representation of the $S = 1$ chain [211], models solvable by the matrix product technique [209], and some special models amenable to the Bethe ansatz solution [212–214]. Among the models solvable by the matrix product technique, there exist families which connect smoothly the dimer and AKLT limits [215]. This proves that these limiting cases are in the same phase.

There are several physical mechanisms which may lead to the appearance of the four-spin interaction terms in (1.83). The most important mechanism is the so-called ring (four-spin) exchange. In the standard derivation based on the Hubbard model at half-filling, in the limit of small ratio of hopping t and on-site Coulomb repulsion U, the magnitude of standard (two-spin) Heisenberg exchange is $J \propto t^2/U$. Terms of the fourth order in t/U yield, except bilinear exchange interactions beyond the nearest neighbors, also exchange terms containing a product of four or more spin operators [216–218]. Those higher-order terms were routinely neglected up to recent times, when it was realized that they can be important for a correct description of many physical systems. Four-spin terms of the V_{LL} type can arise due to the spin-lattice interaction [219], but most naturally they appear in the so-called spin-orbital models, where orbital degeneracy is for some reason not lifted [220].

Ring Exchange

Ring exchange was introduced first to describe the magnetic properties of solid ^{3}He [221]. Recently it was suggested that ring exchange is non-negligible in some strongly correlated electron systems like spin ladders [222, 223] and cuprates [224,225]. The analysis of the low-lying excitation spectrum of the p-d-model shows that the Hamiltonian describing CuO_2 planes should contain a finite value of ring exchange [224, 225]. The search for ring exchange in cuprates was additionally motivated by inelastic neutron scattering experiments [226] and NMR experiments [227–229] on $Sr_{14}Cu_{24}O_{41}$ and $Ca_8La_6Cu_{24}O_{41}$. These materials contain spin ladders built of Cu atoms. The attempts to fit the experimental data with standard exchange terms yielded an unnaturally large ratio of $J_L/J_R \approx 2$ which is expected neither from the geometrical structure of the ladder nor from electronic structure calculations [230]. It can be shown that inclusion of other types of interactions, e.g., additional diagonal exchange, does not help to solve this discrepancy [223].

The ring exchange interaction corresponds to a special structure of the four-spin terms in (1.83), namely $V_{LL} = V_{RR} = -V_{DD} = 2J_{\rm ring}$. Except adding the four-spin terms, ring exchange renormalizes the "bare" values of the bilinear exchange constants as well: $J_{L,L'} \to J_{L,L'} + \frac{1}{2}J_{\rm ring}$, $J_{D,D'} \to J_{D,D'} + \frac{1}{2}J_{\rm ring}$, $J_R \to J_R + J_{\rm ring}$. Thus, an interesting and physically motivated special case of (1.83) is that of a regular ladder with rung exchange J_1, leg exchange coupling J_2, and with added ring exchange term, i.e., $J_R = J_1 + J_{\rm ring}$, $J_L = J'_L = J_2 + \frac{1}{2}J_{\rm ring}$, $J_D = J'_D = \frac{1}{2}J_{\rm ring}$, $V_{LL} = V_{RR} = -V_{DD} = 2J_{\rm ring}$.

It turns out that the line $J_{\rm ring} = J_2$ belongs to the general family of models (1.86) with two remarkable properties [209]: (i) on this line the product of singlets on the rungs is the ground state for $J_{\rm ring} < J_1/4$ and (ii) a propagating triplet is an exact excitation which softens at $J_{\rm ring} = J_1/4$ [222]. Thus, on this line there is an exactly known phase transition point and one knows also the exact excitation responsible for the transition. The transition at $J_{\rm ring} = J_2 = J_1/4$ is from the rung-singlet phase (dominant J_1) to the phase with a checkerboard-type long range dimer order along the ladder legs (see Fig. 1.18). In the $(J_{\rm ring}, J_1)$ plane, there is a transition boundary separating the rung singlet and dimerized phase [222, 231], and arguments based on bosonization suggest that in the limit $J_{\rm ring}, J_1 \to 0$ this boundary is a straight line $J_{\rm ring} = {\rm const} \cdot J_1$. In the vicinity of this line, even a small value of $J_{\rm ring}$ can strongly decrease the gap. For higher values of $J_{\rm ring}$, according to recent numerical studies [208, 232], additional phases appear in the phase diagram (see Fig. 1.16): one phase is characterized by the long-range scalar chiral order defined as mixed product of three spins on two neighboring ladder rungs, and another phase has dominating short-range correlations of vector chirality (1.61). Actually, under the dual transformation (1.84) staggered magnetization maps onto vector chirality, and checkerboard-type dimerizations is connected with the scalar chirality, so that the two additional phases may be viewed as duals of the Haldane and dimerized phase.

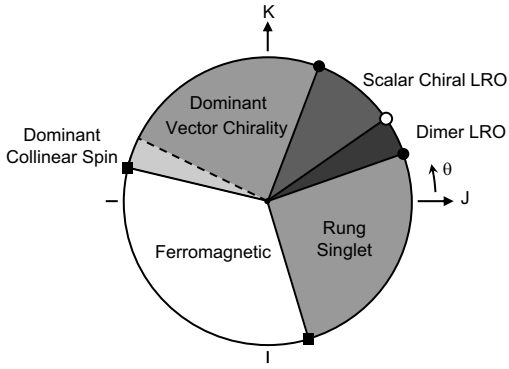

Fig. 1.16. Phase diagram of the $S = \frac{1}{2}$ ladder with equal rung and leg exchange $J_L = J_R = J$ and ring exchange $J_{\rm ring} = K$ (from [232], LRO stands for long range order)

It is now believed [223] that inclusion of ring exchange is necessary for a consistent description of the excitation spectrum in the spin ladder material $La_6Ca_8Cu_{24}O_{41}$. This substance turns out to be close to the transition line to the dimerized phase, and therefore has an unusually small gap. Since the measured value of the energy gap sets the scale for the determination of the exchange parameters, this implies that actual values of these parameters are considerably higher compared to an analysis neglecting ring exchange. This solves the long-standing puzzle of apparently different exchange strength on the Cu-O-Cu bonds in ladders and 2D cuprates. Stimulated by infrared absorption results [233] and neutron scattering results on zone boundary magnons in pure La_2CuO_4 [234], ring exchange is now also believed to be relevant in 2D cuprates with large exchange energy. In the following we shortly discuss this related question:

In 2D magnetic materials with CuO_2-planes the basic plaquette is the same as in the ladder material discussed above. The signature of cyclic exchange in the 2D Heisenberg model which is usually assumed for materials with CuO_2-planes is a nonzero difference in the energies of two elementary excitations at the boundary of the Brillouin zone,

$$\Delta = \omega(q_x = \pi, q_y = 0) - \omega(q_x = \frac{\pi}{2}, q_y = \frac{\pi}{2}).$$

For the 2D Heisenberg antiferromagnet with its LRO, elementary excitations are described to lowest order in the Holstein-Primakoff (HP) spin wave approximation. In this approximation $\Delta \propto J_{\rm ring}$ results, i.e. Δ vanishes for the Heisenberg model with only bilinear exchange. Higher order corrections to the HP result as calculated in [235, 236] lead to $\Delta \approx -1.4 \cdot 10^{-2} J$. This theoretical prediction is in agreement with the experimental result in copper deuteroformate tetradeuterate (CFTD), another 2D Heisenberg magnet, but differs from the value $\Delta \approx +3 \cdot 10^{-2} J$ found from neutron scattering

experiments in pure La_2CuO_4. In this latter material, diagonal, i.e. NNN interactions would have to be ferromagnetic to account for the discrepancy and can therefore be excluded, but a finite amount of ring exchange, $J_{\rm ring} \sim 0.1\ J$, is in agreement with observations.

CFTD and La_2CuO_4 appear to differ in nothing but their energy scale ($J \approx 1400K$ for La_2CuO_4 and $J \approx 70K$ for CFTD) and experimental results would be contradictory when bilinear and biquadratic exchange scale with the same factor. This is, however, not the case: In terms of the basic Hubbard model with hopping amplitude t and on-site Coulomb energy U one has $J \propto |t|^2/U$ and $J_{\rm ring} \propto |t|^4/U^3$. Thus, the relative strength of the ring exchange $J_{\rm ring}/J \propto J/U$ is material-dependent. In two materials with the same ions and therefore identical single-ion Coulomb energies, any differences result from different hopping rates. Thus in materials with high energy scale J such as La_2CuO_4 the relative importance of cyclic exchange is enhanced and it is therefore observable whereas cyclic exchange goes unnoticed in materials with low energy scale such as CFTD.

Spin-Orbital Models

Modified ladder models (1.83) arise also in one-dimensional systems with coupled spin and orbital degrees of freedom which can be described by a two-band orbitally degenerate Hubbard model at quarter filling (Fig. 17). In this case orbital degrees of freedom may be viewed as pseudospin-$\frac{1}{2}$ variables: one of the ladder legs can be interpreted as carrying the real spins $\boldsymbol{S}_{1,i} \equiv \boldsymbol{S}_i$ and the other one corresponds to the pseudospins $\boldsymbol{S}_{2,i} \equiv \boldsymbol{\tau}_i$. The corresponding effective Hamiltonian for the two-band Hubbard model was first derived by Kugel and Khomskii [220]. In addition to the spin exchange J_S and effective orbital exchange J_τ, its characteristic feature is the presence of strong spin-orbital interaction terms of the form $(\boldsymbol{S}_i \cdot \boldsymbol{S}_{i+1})(\boldsymbol{\tau}_i \cdot \boldsymbol{\tau}_{i+1})$, which is equivalent to the four-spin interaction of the V_{LL} type in (1.83).

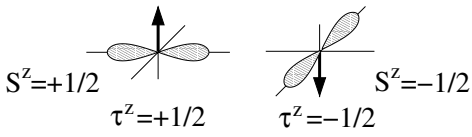

Fig. 1.17. Pseudospin variables $\boldsymbol{\tau}$ describe two degenerate orbital states of the magnetic ion

Generally, the above Hamiltonian has an SU(2) symmetry in the spin sector, but only U(1) or lower symmetry in the orbital sector. Under certain simplifying assumptions (neglecting Hund's rule coupling, nearest neighbor hopping between the same type of orbitals only, and only one Coulomb on-site repulsion constant) one obtains a Hamiltonian of the form

$$\mathcal{H} = \sum_i J_S(\boldsymbol{S}_i \cdot \boldsymbol{S}_{i+1}) + J_\tau(\boldsymbol{\tau}_i \cdot \boldsymbol{\tau}_{i+1}) + K(\boldsymbol{S}_i \cdot \boldsymbol{S}_{i+1})(\boldsymbol{\tau}_i \cdot \boldsymbol{\tau}_{i+1}) \qquad (1.87)$$

with $J_S = J_\tau = J$ and $K = \frac{1}{4}J$, which possesses hidden SU(4) symmetry [212,237]. At this special point, the model is Bethe ansatz solvable [238] and gapless. This high symmetry can be broken in several ways depending on the microscopic details of the interaction, e.g., finite Hund's rule coupling and existence of more than one Coulomb repulsion constant makes the three parameters J_S, J_τ and K independent, reducing the symmetry to SU(2) × SU(2), and further breaking to SU(2) × U(1) is achieved through local crystal fields which can induce considerable anisotropy in the orbital sector.

The phase diagram of the model (1.87) is extensively studied analytically [239–241] as well as numerically [240,242,243]. The SU(4) point lies on the boundary of a critical phase which occupies a finite region of the phase diagram. Moving off the SU(4) point towards larger J_S, J_τ, one runs into the spontaneously dimerized phase with a finite gap and twofold degenerate ground state. The weak coupling region $J_S = J_\tau \gg |K|$ of the dimerized phase is a realization of the so-called *non-Haldane spin liquid* [219] where magnons become incoherent excitations since they are unstable against the decay into soliton-antisoliton pairs. At the special point $J_S = J_\tau = \frac{3}{4}K$ the exact ground state [244] is a checkerboard-type singlet dimer product shown in Fig. 1.18a, which provides a visual interpretation of the dimerized phase for $K > 0$. Solitons can be understood as domain walls connecting two degenerate ground states, see Fig. 1.18b, and magnons may be viewed as soliton-antisoliton bound states, in a close analogy to the situation at the Majumdar-Ghosh point for the frustrated spin-$\frac{1}{2}$ chain [168]. Numerical and variational studies [245] show that solitons remain the dominating low-energy excitations in the finite region around the point $J_S = J_\tau = \frac{3}{4}K$, but as one moves from it towards the SU(4) point, magnon branch separates from the soliton continuum and magnons quickly become the lowest excitations.

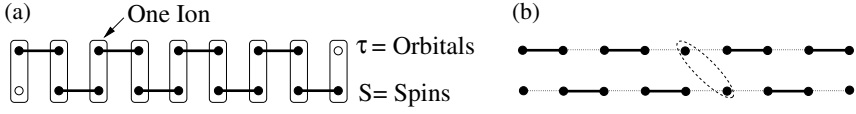

Fig. 1.18. Schematic representation of the spin-orbital model: (a) checkerboard-type dimerized ground state of (1.87) at $J_S = J_\tau = \frac{3}{4}K$; (b) a soliton connecting two equivalent dimerized states

For weak negative K one also expects a spontaneously dimerized phase [219], but now instead of a checkerboard dimer order one has spin and orbital singlets placed on the same links. A representative exactly solvable point inside this phase is $J_S = J_\tau = J = -\frac{1}{4}K$, $K < 0$, which turns out to be equivalent to the 16-state Potts model. At this point, the model has a

large gap of about $0.78J$ and its ground state can be shown to be twofold degenerate [214].

1.5.2 $S = 1$ Bilinear-Biquadratic Chain

The isotropic Heisenberg spin-1 AF chain is a generic example of a system in the Haldane phase. However, the most general isotropic exchange interaction for spin $S = 1$ includes biquadratic terms as well, which naturally leads to the model described by the following Hamiltonian:

$$\mathcal{H} = \sum_n \cos\theta\,(\boldsymbol{S}_n \cdot \boldsymbol{S}_{n+1}) + \sin\theta\,(\boldsymbol{S}_n \cdot \boldsymbol{S}_{n+1})^2. \tag{1.88}$$

The AKLT model considered in Sect. 1.3 is a particular case of the above Hamiltonian with $\tan\theta = \frac{1}{3}$. There are indications [246] that strong biquadratic exchange is present in the quasi-one-dimensional compound $LiVGe_2O_6$. The points $\theta = \pi$ and $\theta = 0$ correspond to the Heisenberg ferro- and antiferromagnet, respectively. The bilinear-biquadratic chain (1.88) has been studied rather extensively, and a number of analytical and numerical results for several particular cases are available (Fig. 19). It is firmly established that the Haldane phase with a finite spectral gap occupies the interval $-\pi/4 < \theta < \pi/4$, and the ferromagnetic state is stable for $\pi/2 < \theta < 5\pi/4$, while $\theta = 5\pi/4$ is an SU(3) symmetric point with highly degenerate ground state [247].

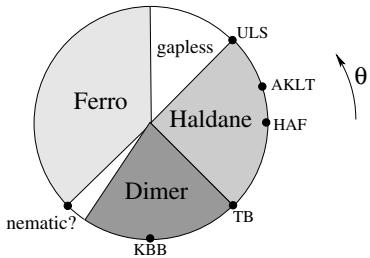

Fig. 1.19. Phase diagram of the $S = 1$ bilinear-biquadratic chain (1.88)

An exact solution is available [238] for the Uimin-Lai-Sutherland (ULS) point $\theta = \pi/4$ which has SU(3) symmetry. The ULS point was shown [248] to mark the Berezinskii-Kosterlitz-Thouless (BKT) transition from the massive Haldane phase into a massless phase occupying the interval $\pi/4 < \theta < \pi/2$ between the Haldane and ferromagnetic phase; this is supported by numerical studies [249].

The properties of the remaining region between the Haldane and ferromagnetic phase are more controversial. The other Haldane phase boundary $\theta = -\pi/4$ corresponds to the exactly solvable Takhtajan-Babujian model [250]; the transition at $\theta = -\pi/4$ is of the Ising type and the ground

state at $\theta < -\pi/4$ is spontaneously dimerized with a finite gap to the lowest excitations [249, 251–256]. The dimerized phase extends at least up to and over the point $\theta = -\pi/2$ which has a twofold degenerate ground state and finite gap [257–259].

Chubukov [260] used the Holstein-Primakoff-type bosonic representation of spin-1 operators [261] based on the quadrupolar ordered "spin nematic" reference state with $\langle \boldsymbol{S} \rangle = 0$, $\langle S^2_{x,y} \rangle = 1$, $\langle S^2_z = 0 \rangle$, and suggested, on the basis of the renormalization group arguments, that the region with $\theta \in [5\pi/4, \theta_c]$, where $\frac{5\pi}{4}\theta_c < \frac{3\pi}{2}$, is a disordered nematic phase. Early numerical studies [262] have apparently ruled out this possibility, forming a common belief [263, 264] that the dimerized phase extends all the way up to the ferromagnetic phase, i.e., that it exists in the entire interval $5\pi/4 < \theta < 7\pi/4$. However, recent numerical results [265, 266] indicate that the dimerized phase ends at certain $\theta_c > 5\pi/4$, casting doubt on the conclusions reached nearly a decade ago.

Using special coherent states for $S = 1$,

$$|\boldsymbol{u}, \boldsymbol{v}\rangle = \sum_j (u_j + iv_j)|t_j\rangle, \qquad |\pm\rangle = \mp\frac{1}{\sqrt{2}}(|t_x\rangle \pm i|t_y\rangle), \quad |0\rangle = |t_z\rangle, \tag{1.89}$$

subject to the normalization condition $\boldsymbol{u}^2 + \boldsymbol{v}^2 = 1$ and gauge-fixing constraint $\boldsymbol{u} \cdot \boldsymbol{v} = 0$, one can show [267] that for θ slightly above $\frac{5\pi}{4}$ the effective low-energy physics of the problem can be described by the nonlinear sigma model of the form (1.47). The topological term is absent and the coupling constant is given by

$$g = (1 - \operatorname{ctg}\theta)^{1/2} \ll 1 \tag{1.90}$$

(note that in this case smallness of g is not connected to the large-S approximation). By the analogy with the Haldane phase, this mapping suggests that for $\theta > 5\pi/4$ the system is in a disordered state with a short-range nematic order and exponentially small gap $\Delta \propto e^{-\pi/g}$. The antiferromagnetism unit vector $\boldsymbol{l}$ gets replaced by the unit *director* $\boldsymbol{u}$ and the opposite vectors $\boldsymbol{u}$ and $-\boldsymbol{u}$ correspond to the same physical state, which makes the model live in the RP^2 space instead of $O(3)$. The main difference from the usual $O(3)$ NLSM is that the RP^2 space is doubly connected, which supports the existence of *disclinations* – excitations with a nontrivial π_1 topological charge. However, the characteristic action of a disclination is of the order of $\sin\theta$ and thus the low-energy physics on the characteristic scale of Δ should not be affected by the disclinations.

1.5.3 Mixed Spin Chains: Ferrimagnet

In the last decade there has been much interest in 'mixed' 1d models involving spins of different magnitude S. The simplest system of this type is actually of a fundamental importance since it represents the generic model of a quantum ferrimagnet described by the Hamiltonian

$$\mathcal{H} = \sum_n (\boldsymbol{S}_n \boldsymbol{\tau}_n + \boldsymbol{\tau}_n \boldsymbol{S}_{n+1}) \tag{1.91}$$

where $\boldsymbol{S}_n$ and $\boldsymbol{\tau}_n$ are respectively spin-1 and spin-$\frac{1}{2}$ operators at the n-th elementary magnetic cell (with S^z eigenstates denoted in the following as $(+,0,-)$ and $(\uparrow,\downarrow)$, respectively). An experimental realization of such a system is the molecular magnet $\mathrm{NiCu(pba)(D_2O)_3 \cdot D_2O}$ [268].

According to the Lieb-Mattis theorem [269], the ground state of the system has the total spin $S_{\mathrm{tot}} = L/2$, where L is the number of unit cells. There are two types of magnons [270, 271]: a gapless "acoustical" branch with $S^z = L/2 - 1$, and a gapped "optical" branch with $S^z = L/2 + 1$. The energy of the "acoustical" branch rises with field, and in strong fields those excitations can be neglected, while the "optical" magnon gap closes at the critical field.

A good quantitative description of the ferrimagnetic chain can be achieved with the help of the variational matrix product states (MPS) approach [34, 181]. The MP approach is especially well suited to this problem since the fluctuations are extremely short-ranged, with the correlation radius smaller than one unit cell length [181,270,271]. The ground state properties, including correlation functions, are within a few percent accuracy described by the MPS $|\Psi_0\rangle = \mathrm{Tr}(g_1 g_2 \cdots g_L)$, where the elementary matrix has the form (1.70) and the variational parameters u, v are determined from the energy minimization. The variational energy per unit cell is $E_{\mathrm{var}} = -1.449$, to be compared with the numerical value $E_{\mathrm{g.s.}} \simeq 1.454$ [139, 181]. According to (1.67), the above matrix has the "hyperspin" quantum numbers $(\frac{1}{2}, \frac{1}{2})$, which in turn ensures that the variational state $|\Psi_0\rangle$ has correct $S_{\mathrm{tot}} = S^z_{\mathrm{tot}} = L/2$.

The MPS approach works also very well for the excited states [34]. The dispersion of optical magnons can be reproduced within a few percent by using the MPS ansatz $|n\rangle = \mathrm{Tr}(g_1 g_2 \cdots g_{n-1} \widetilde{g}_n g_{n+1} \cdots g_L)$ with one of the ground state matrices g_n replaced by the matrix

$$\widetilde{g}_n = \frac{f-1}{\sqrt{2}}\, g_n\, \sigma^{+1} - \frac{f+1}{\sqrt{2}}\, \sigma^{+1}\, g_n + \widetilde{w}\, \sigma^{+1}\, \psi_{\frac{1}{2},\frac{1}{2}}\,, \tag{1.92}$$

which carries the "hyperspin" $(\frac{3}{2}, \frac{3}{2})$ and contains two free parameters f, w . Generally the states $|n\rangle$ are orthogonal to Ψ_0, but are not orthogonal to each other. Since the states with a certain momentum $|k\rangle = \sum_n e^{ikn}|n\rangle$ obviously depend only on $\widetilde{w}$, one parameter in (1.92) is redundant and can be fixed by requiring that one-magnon states $\{|n\rangle\}$ become mutually orthogonal [34]. The resulting variational dispersion for the optical magnon is in excellent agreement with the exact diagonalization data [34]; the variational value for the optical magnon gap is $\Delta_{\mathrm{var}} \simeq 1.754\, J$, to be compared with the numerically exact value $\Delta_{\mathrm{opt}} = 1.759\, J$ [139, 270].

Several other mixed-spin systems were studied, particularly mixed-spin ladders which may exhibit either ferrimagnetic or singlet ground states depending on the ladder type [272, 273].

1.6 Gapped 1D Systems in High Magnetic Field

The presence of an external magnetic field brings in a number of new features. In gapped low-dimensional spin systems, the gap will be closed by a sufficiently strong external magnetic field $H = H_c$, and a finite magnetization will appear above H_c [274]. For a system with high (at least axial) symmetry the high-field phase at $H > H_c$ is critical [275–277] and the low-energy response is dominated by a two-particle continuum [278–280]. When the field is further increased, the system may stay in this critical phase up to the saturation field H_s, above which the system is in a saturated ferromagnetic state. Under certain conditions, however, the excitations in this high-field phase may again acquire a gap, making the magnetization per spin m "locked" in some field range; this phenomenon is known as a *magnetization plateau* and has been receiving much attention from both theoretical and experimental side [122, 203, 281–291]. Other singularities of the $m(H)$ dependence, the so-called *magnetization cusps* [292, 293], may arise in frustrated systems. In anisotropic systems with no axial symmetry the high-field phase has long-range order and the response is of the quasi-particle type [275, 276].

1.6.1 The Critical Phase and Gapped (Plateau) Phase

In a one-dimensional spin chain with the spin S, a necessary condition for the existence of a plateau is given by the generalized Lieb-Schulz-Mattis theorem [122] discussed in Sect. 1.3.2 as the requirement that $lS(1-M)$ is an integer number, where l is the number of spins in the magnetic unit cell, and $M = m/S$ is the magnetization per spin in units of saturation. This condition ensures that the system is allowed to have a spectral gap at finite magnetization, so that one needs to increase the magnetic field by a finite value to overcome the gap and make the magnetization grow. It yields the allowed values of M at which plateaux may exist, but it does not guarantee their existence. For a mixed spin system with ions having different spins S_i the quantity lS in the above condition would be replaced by the sum of spin values over the unit cell $\sum_i S_i$. The number l may differ from that dictated by the Hamiltonian in case of a spontaneous translational symmetry breaking. A trivial plateau at $M = 0$ is obviously possible for any integer-S spin chain, which is just another way to say that the ground state has a finite gap to magnetic excitations.

As an intuitively clear example of a magnetization plateau one can consider the $S = \frac{3}{2}$ chain with large easy-plane single-ion anisotropy described by the Hamiltonian

$$\mathcal{H} = \sum_l J\boldsymbol{S}_l \cdot \boldsymbol{S}_{l+1} + D(S_l^z)^2 - HS_l^z. \tag{1.93}$$

If $D \gg J$, the spins are effectively suppressed to have $S^z = \pm 1/2$, and with increasing field to $H \sim J$ one gets first to the polarized $m = 1/2$ ($M = 1/3$)

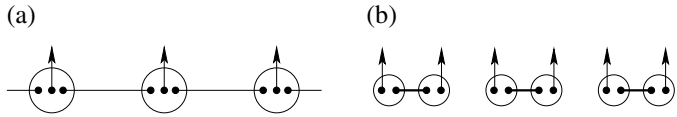

Fig. 1.20. VBS states visualizing (a) $M = 1/3$ plateau in the large-D $S = \frac{3}{2}$ chain (1.93); (b) $M = 1/2$ plateau in the bond-alternated $S = 1$ chain

state (see Fig. 1.20a), and the magnetization remains locked at $m = 1/2$ up to a much larger field $H \sim D$, where it gets finally switched to $m = 3/2$ [122].

An experimentally more relevant example is a $S = 1$ chain with alternating bond strength, where $l = 2$ and a nontrivial plateau at $M = \frac{1}{2}$ is allowed. In the strong alternation regime (weakly coupled $S = 1$ dimers) this plateau can be easily visulaized as the state with all dimers excited to $S = 1$, $S^z = +1$ (see Fig. 1.20b). The $M = 1/2$ plateau was experimentally observed in magnetization measurements up to 70 T in NTENP [294].

Very distinct magnetization plateaux at $M = \frac{1}{4}$ and $M = \frac{3}{4}$ were observed in NH_4CuCl_3 [295], a material which contains weakly coupled $S = \frac{1}{2}$ dimers. The nature of those plateaux is, however, most probably connected to three-dimensional interactions in combination with an additional structural transition which produces three different dimer types [296].

Plateaux and Critical Phase in an Alternated $S = \frac{1}{2}$ Zigzag Chain

Another simple example illustrating the occurrence of a plateau and the physics of a high-field critical phase is a strongly alternating $S = \frac{1}{2}$ zigzag chain, which can be also viewed as a ladder in the regime of weakly coupled dimers, as shown in Fig. 1.21. For a single dimer in the field, the energy of the $S^z = +1$ triplet state $|t_+\rangle$ becomes lower than that of the singlet $|s\rangle$ at $H = J$. If the dimers were completely decoupled, then there would be just one critical field $H_c^{(0)} = J$ and the magnetization M would jump from zero to one at $H = H_c^{(0)}$. A finite weak interdimer coupling will split the point $H = H_c$ into a small but finite field region $[H_c, H_s]$. Assuming that the coupling is small and thus H_c and H_s are close to J, one can neglect for each dimer all states except the two lowest ones, $|s\rangle$ and $|t_+\rangle$ [289,290]. The Hilbert space is reduced to two states per dimer, and one may introduce pseudospin-$\frac{1}{2}$ variables, identifying $|s\rangle$ with $|\widetilde{\downarrow}\rangle$ and $|t_+\rangle$ with $|\widetilde{\uparrow}\rangle$. The effective spin-$\frac{1}{2}$ Hamiltonian in the reduced Hilbert space takes the form

$$\mathcal{H} = \sum_n \widetilde{J}_{xy}(\widetilde{S}_n^x \widetilde{S}_{n+1}^x + \widetilde{S}_n^y \widetilde{S}_{n+1}^y) + \widetilde{J}_z \widetilde{S}_n^z \widetilde{S}_{n+1}^z - \widetilde{h}\widetilde{S}_n^z, \tag{1.94}$$

where the effective coupling constants are given by

$$\widetilde{J}_{xy} = \alpha - \beta/2, \quad \widetilde{J}_z = \alpha/2 + \beta/4, \quad \widetilde{h} = H - J - \alpha/2 - \beta/4. \tag{1.95}$$

At $\widetilde{h} = 0$, depending on the value of the parameter $\varepsilon = \widetilde{J}_z/|\widetilde{J}_{xy}|$, the effective spin-$\frac{1}{2}$ chain can be in three different phases: the Néel ordered, gapped phase for $\varepsilon > 1$, gapless XY phase for $-1 < \varepsilon < 1$, and ferromagnetic phase for $\varepsilon < -1$. Boundaries between the phases are lines $\beta = 6\alpha$ and $\beta = 2\alpha/3$, as shown in Fig. 1.21.

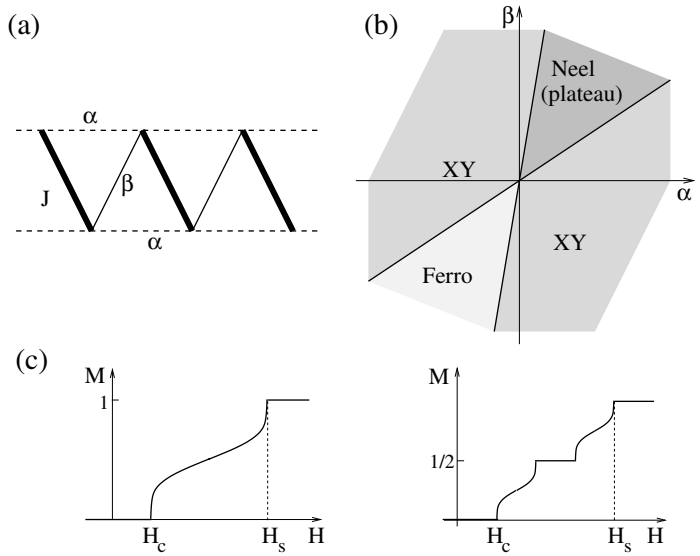

Fig. 1.21. (a) alternating zigzag chain in the strong coupling limit $\alpha, \beta \ll J$; (b) its phase diagram in the high-field regime $\widetilde{h} \simeq 0$ (see (1.95)); (c) the magnetization behavior in the XY and Néel phases

It is easy to understand what the magnetization curve looks like in different phases. In the XY phase the magnetization per spin of the effective chain $\widetilde{m}(\widetilde{h})$ reaches its saturation value $\frac{1}{2}$ at $\widetilde{h} = \pm h_c$, where $h_c = |\widetilde{J}_{xy}| + \widetilde{J}_z$. Point $\widetilde{h} = -h_c$ can be identified with the first critical field $H = H_c$, and $\widetilde{h} = +h_c$ corresponds to the saturation field H_s. The symmetry $\widetilde{h} \mapsto -\widetilde{h}$ corresponds to the symmetry against the middle point $H = (H_c + H_s)/2$. This symmetry is only valid in the first order in the couplings α, β and is a consequence of our reduction of the Hilbert space. The magnetization $M = \widetilde{m} + \frac{1}{2}$ of the original chain has only trivial plateaux at $M = 0$ and $M = 1$, as shown in Fig. 1.21c.

Near the first critical field H_c the magnetization behaves as $(H - H_c)^{1/2}$. This behavior is easy to understand for the purely XY point $\widetilde{J}_z = 0$. At this point the model can be mapped to free fermions with the dispersion $E(k) = \widetilde{J}_{xy} \cos k - \widetilde{h}$ which is quadratic at its bottom. The magnetization M is connected to the Fermi momentum k_F via $M = 1 - k_F/\pi$, which yields the square root behavior. Further, if the fermions are interacting, this interaction

can be neglected in the immediate vicinity of H_c where the particle density is low, so that the square root behavior is universal in one dimension (it can be violated only at special points where the fermion dispersion is not quadratic, or in presence of anisotropy which breaks the axial symmetry).

In the Néel phase there is a finite gap Δ, and $\widetilde{m}$ stays zero up to $\widetilde{h} = \Delta$, so that in the language of the original chain there is a nontrivial plateau at $M = \frac{1}{2}$ whose width is 2Δ (Fig. 1.21c).

A Few Other Examples

A similar mapping to an effective $S = \frac{1}{2}$ chain can be sometimes achieved for systems with no obvious small parameter. An instructive example is the AKLT chain (1.51) in strong magnetic field H [297, 298]. The zero-field gap of the AKLT model is known to be $\Delta \simeq 0.70$ [111], and we are interested in the high-field regime $H > H_c \equiv \Delta$ where the gap closes. One may use the matrix product soliton ansatz (1.56), (1.57) to describe the triplet excitation with $\mu = +1$. States $|\mu, n\rangle$ with different n can be orthogonalized by putting in (1.57) $a/b = 3$ [131]. Further, one may introduce effective spin-$\frac{1}{2}$ states $|\alpha_n\rangle = |\uparrow\rangle, |\downarrow\rangle$ at each site, making the identification

$$|\alpha_1 \alpha_2 \cdots \alpha_L\rangle = \mathrm{Tr}(g_1 g_2 \cdots g_L), \tag{1.96}$$

where the matrix g_n is either the ground state matrix (1.55) if $|\alpha_n\rangle = |\uparrow\rangle$, or the matrix (1.57) corresponding to the lowest $S^z = +1$ triplet if $|\alpha_n\rangle = |\downarrow\rangle$, respectively. Then the desired mapping is achieved by restricting the Hilbert space to the states of the above form (1.96). The resulting effective $S = \frac{1}{2}$ chain is described by the Hamiltonian

$$\mathcal{H}_{S=1/2} = \sum_n \widetilde{J}_{xy}\big(\widetilde{S}^x_n \widetilde{S}^x_{n+1} + \widetilde{S}^y_n \widetilde{S}^y_{n+1}\big) - \widetilde{h}\widetilde{S}^z_n + \sum_{n,m} V_m \widetilde{S}^z_n \widetilde{S}^z_{n+m}, \tag{1.97}$$

where $\widetilde{J}_{xy} = \frac{10}{9}$, $\widetilde{h} \simeq (H - 1.796)$, and the interaction constants V_m are exponentially decaying with m and always very small, $V_1 = -0.017$, $V_2 = -0.047$, $V_3 = 0.013$, $V_4 = -0.0046$, etc. [297, 298] Thus, if one neglects the small interaction V_m, then in the vicinity of H_c the AKLT chain is effectively described by the XY model, i.e. by noninteracting hardcore bosons.

The critical phase appears also in a ferrimagnet (1.91): in an applied field the ferromagnetic magnon branch acquires a gap which increases with the field, while the optical branch goes down and its gap closes at $H = \Delta_{\mathrm{opt}} \simeq 1.76\, J$. A mapping to a $S = \frac{1}{2}$ chain can be performed can be performed [34] in a way very similar to the one described above for the AKLT model, using the MP ansatz with the elementary matrices (1.70) and (1.92). Restricting all effective interactions to nearest neighbors only, one obtains the effective Hamiltonian of the form (1.94), where $\widetilde{J}_{xy} \simeq 0.52$, $\widetilde{J}_z \simeq 0.12$, $h_e \simeq (H - 2.44)$ are determined by the numerical values of the optimal variational parameters

in the matrices (1.70) and (1.92) [34]. Similarly to (1.97), the complete effective Hamiltonian contains exchange interactions exponentially decaying with distance, but this decay is very rapid, e.g., the next-nearest neigbor exchange constants $\widetilde{J}_{xy}^{(2)} \simeq 0.04$, $\widetilde{J}_{z}^{(2)} \simeq 0.02$, so that one may safely use the reduced nearest-neighbor Hamiltonian.

For both the ladder and the ferrimagnet, in the critical phase the temperature dependence of the low-temperature part of the specific heat C exhibits a rather peculiar behavior [34, 299, 300]. With the increase of the field H, a single well-pronounced low-T peak pops up when H is in the middle between H_c and H_s. When H is shifted towards H_c or H_s, the peak becomes flat and develops a shoulder with another weakly pronounced peak at very low temperature. This phenomenon can be fully explained within the effective $S = \frac{1}{2}$ chain model [34] and results from unequal bandwidth of particle-type and hole-type excitations in the effective spin-$\frac{1}{2}$ chain [301]: In zero field the contributions into the specific heat from particles and holes are equal; with increasing field, the hole bandwidth grows up, while the particle bandwidth decreases, and the average band energies do not coincide. This leads to the presence of two peaks in $C(T)$: holes yield a strong, round peak moving towards higher temperatures with increasing the field, and the other peak (due to the particles) is weak, sharp, and moves to zero when $\widetilde{h}$ tends to $\pm h_c$.

1.6.2 Magnetization Cusp Singularities

Cusp singularities were first discovered in integrable models of spin chains [302], but later were found to be a generic feature of frustrated spin systems where the dispersion of elementary excitations has a minimum at an incommensurate value of the wave vector [292,293]. The physics of this phenomenon can be most easily understood on the example of a frustrated $S = \frac{1}{2}$ chain described by the isotropic version of (1.60) with $\Delta = 1$ and $j > \frac{1}{4}$. Assume we are above the saturation field, so that the ground state is fully polarized. The magnon dispersion

$$\varepsilon(k) = H - 1 - j + \cos k + j\cos(2k)$$

has a minimum at $k = k_0 = \pi \pm \arccos(1/4j)$. The gap at $k = k_0$ closes if the field H is reduced below the saturation value $H_s = 1 + 2j + 1/(8j)$. If one treats magnons as hardcore bosons, they are in one dimension equivalent to fermions, and in the vicinity of H_s, when the density of those fermions is low, they can be treated as free particles. If $H_{\rm cusp} < H < H_s$, where $H_{\rm cusp} = 2$ corresponds to the point where $\varepsilon(k = \pi) = 0$, there are *two* Fermi seas (four Fermi points), and if H is reduced below $H_{\rm cusp}$ they join into a single Fermi sea. It is easy to show that the magnetization m behaves as

$$m(H) - m(H_{\rm cusp}) \propto \begin{cases} (H - H_{\rm cusp})^{1/2} & , \quad H > H_{\rm cusp} \\ H - H_{\rm cusp} & , \quad H < H_{\rm cusp} \end{cases},$$

so that there is indeed a cusp at $H = H_{\rm cusp}$, see Fig. 1.22.

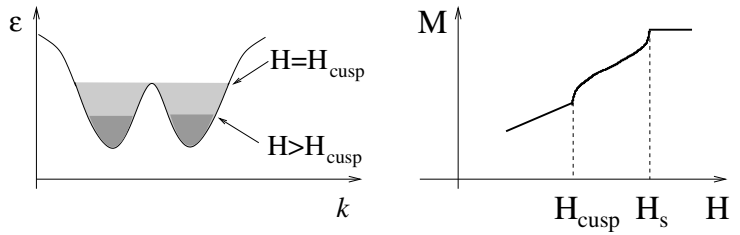

Fig. 1.22. Schematic explanation of cusp singularities: two Fermi seas join at $H = H_{\rm cusp}$ (left) leading to a cusp in the magnetization curve (*right*)

1.6.3 Response Functions in the High-Field Phase

The description of the critical phase in terms of an effective $S = \frac{1}{2}$ chain is equivalent to neglecting certain high-energy degrees of freedom, e.g., two of the three rung triplet states in case of the strongly coupled spin ladder. Those neglected states, however, form excitation branches which contribute to the response functions at higher energies, and this contribution is generally easier to see experimentally than the highly dispersed low-energy continuum of the particle-hole ("spinon") excitations coming from the effective $S = \frac{1}{2}$ chain. In case of an axially anisotropic system, the continuum will collapse into a delta-function, and weights of low- and high-energy branches will be approximately equal. Those high-energy branches were found to exhibit interesting behavior in electron spin resonance (ESR) and inelastic neutron scattering (INS) experiments in two quasi-one-dimensional materials, $Ni(C_2H_8N_2)_2Ni(CN)_4$ (known as NENC) [303] and $Ni(C_5H_{14}N_2)_2N_3(PF_6)$ (abbreviated NDMAP) [304].

As mentioned before, the physics of the high-field phase depends strongly on whether the field is applied along a symmetry axis or not.

Response in an Axially Symmetric Model

Let us consider the main features of the response in the critical phase of the axially symmetric system using the example of the strongly coupled ladder addressed in the previous subsection. In order to include the neglected $|t_-\rangle$ and $|t_0\rangle$ states, it is convenient to use the hardcore boson language. One may argue [298,305] that the most important part of interaction between the bosons is incorporated in the hardcore constraint. Neglecting all interactions except the constraint, one arrives at the simplified effective model of the type

$$\mathcal{H}_{\rm eff} = \sum_{n\mu} \varepsilon_\mu b^\dagger_{n,\mu} b_{n,\mu} + t(b^\dagger_{n,\mu} b_{n+1,\mu} + \text{h.c.}), \tag{1.98}$$

where $\mu = 0, \pm 1$ numbers three boson species (triplet components with $S^z = \mu$), $t = \alpha - \beta/2$ is the hopping amplitude which is equal for all species, and $\varepsilon_\mu = J - \mu H$.

The ground state at $H > H_c$ contains a "condensate" (Fermi sea) of b_{+1} bosons. Thus, at low temperatures for calculating the response it suffices to take into account only processes involving states with at most one b_0 or b_{-1} particle: (A) creation/annihilation of a low-energy b_{+1} boson; (B) creation/annihilation of one high-energy (b_{-1} or b_0) particle, and (C) transformation of a b_{+1} particle into b_0 one.

The processes of the type (A) can be considered completely within the model of an effective $S = \frac{1}{2}$ chain, for which analytical results are available [306–308]. For example, the transversal dynamical susceptibility $\chi^{xx}(q,\omega) = \chi^{yy}(q,\omega)$ for q close to the antiferromagnetic wave number π is given by the expression

$$\chi^{xx}(\pi + k, \omega) = A_x(H) \frac{\sin(\frac{\pi\eta}{2}) \Gamma^2(1 - \frac{\eta}{2}) u^{1-\eta}}{(2\pi T)^{2-\eta}} \times \frac{\Gamma\left(\frac{\eta}{4} - i\frac{\omega - vk}{4\pi T}\right) \Gamma\left(\frac{\eta}{4} - i\frac{\omega + vk}{4\pi T}\right)}{\Gamma\left(1 - \frac{\eta}{4} - i\frac{\omega - vk}{4\pi T}\right) \Gamma\left(1 - \frac{\eta}{4} - i\frac{\omega + vk}{4\pi T}\right)} . \tag{1.99}$$

Here $A_x(H)$ is the non-universal amplitude which is known numerically [309], v is the Fermi velocity, and $\eta = 1 - \frac{1}{\pi} \arccos(\widetilde{J}_z / \widetilde{J}_{xy})$ (neglecting interaction between b_{+1} bosons corresponds to $\widetilde{J}_z = 0$). This contribution describes a low-energy "spinon" continuum, and the response function has an edge singularity at its lower boundary. A similar expression is available for the longitudinal susceptibility [306]; for the longitudinal DSF of the XY chain in case of zero temperature a closed exact expression is available as well [49], and for $T \neq 0$ the exact longitudinal DSF can be calculated numerically [56]. Applying the well-known relation $S^{\alpha\alpha}(q,\omega) = \frac{1}{\pi} \frac{1}{1 - e^{-\omega/T}} \mathrm{Im}\chi^{\alpha\alpha}(q,\omega)$, one obtains in this way the contribution $I^A(q,\omega)$ of the (A) processes to the dynamic structure factor. The processes of (B) and (C) types, which correspond to excitations with higher energies, cannot be analyzed in the language of the $S = \frac{1}{2}$ chain.

Consider first the zero temperature case for (B)-type processes. The model (1.98) with just one high-energy particle present is equivalent to the problem of a single mobile impurity in the hardcore boson system. The hopping amplitudes for the impurity and for particles are equal, and in this case the model can be solved exactly [310]. Creation of the impurity leads to the orthogonality catastrophe [311] and to the corresponding edge-type singularity in the response.

In absence of the impurity, the eigenstates of the hardcore boson Hamiltonian (1.98) can be represented in the form of a Slater determinant constructed of the free plane waves $\psi_i(x) = \frac{1}{\sqrt{L}} e^{ik_i x}$ (L is the system length), with an additional antisymmetric sign factor attached to the determinant, which ensures symmetry of the wave function under permutations of k_i (this construction points to the equivalence between fermions and hardcore bosons which is a peculiarity of dimension one).

Let us assume for definiteness that the total number of b_{+1} particles in the ground state N is even. The allowed values of momenta k_i are then given by

$$k_i = \pi + (2\pi/L)I_i, \quad i = 1, \ldots, N \tag{1.100}$$

where the numbers I_i should be all different and half-integer. The ground state $|\text{g.s.}\rangle$ is given by the Fermi sea configuration with the momenta filling the $[k_F, 2\pi - k_F]$ interval, the Fermi momentum being defined as

$$k_F = \pi(1 - N/L). \tag{1.101}$$

The energy of is $E = \sum_{i=1}^{N}(\varepsilon_{+1} + 2t\cos k_i)$, and the total momentum $P = \sum_i k_i$ of the ground state is zero (mod2π).

Since the hopping amplitudes for "particles" and "impurities" are equal, it is easy to realize that the above picture of the distribution of wave vectors remains true when some of the particles are replaced by the impurities: they form a single "large" Fermi sea.

The excited configuration $|(\mu,\lambda)_{k'_1\ldots k'_N}\rangle$ with a single impurity boson b_μ having the momentum λ can be also exactly represented in the determinantal form [310] with determinants containing wave functions $\varphi_i(x)$ which become asymptotically equivalent to the free scattering states $\frac{1}{\sqrt{L}}e^{i(k'_i x+\delta_i)}$ in the thermodynamic limit; for noninteracting hardcore particles the phase shifts $\delta_i = -\pi/2$. The total momentum of the excited state is $P' = \sum_{i=1}^{N} k'_i + \lambda$, and its energy is given by $E' = \sum_{i=1}^{N}(\varepsilon_{+1} + 2t\cos k'_i) + \varepsilon_\mu + 2t\cos\lambda$. Here the allowed wave vectors k'_i and λ are determined by the same formula (1.100), but since the total number of particles has changed by one, the numbers I_i are now integer.

The matrix element $\langle(\mu,\lambda)_{k'_1\ldots k'_N}|b^\dagger_\mu(q)|\text{g.s.}\rangle$, which determines the contribution to the response from the (B)-type processes, is nonzero only if the selection rules $\lambda = q$, $P' = P + q$ are satisfied [298], and is proportional to the determinant $M_{fi} = \det\{\langle\varphi_i|\psi_j\rangle\}$ of the overlap matrix. Due to the orthogonality catastrophe (OC), the overlap determinant is generally algebraically vanishing in the thermodynamic limit, $|M_{fi}|^2 \propto L^{-\beta}$. The response is, however, nonzero and even singular because there is a macroscopic number of "shake-up" configurations with nearly the same energy.

The OC exponent β can be calculated using the results of boundary conformal field theory (BCFT) [312]. For this purpose it is necessary to calculate the energy difference ΔE_f between the ground state and the excited state $|f\rangle$, including the $1/L$ corrections. Then in case of *open boundary conditions* the OC exponent β, according to BCFT, can be obtained as

$$\beta = \frac{2L\widetilde{\Delta E_f}}{\pi v_F} \equiv \frac{\widetilde{2\Delta E_f}}{\Delta E_{\min}}. \tag{1.102}$$

Here $v_F = 2t\sin k_F$ is the Fermi velocity, so that $\Delta E_{\min} = \pi v_F/L$ is the lowest possible excitation energy, and $\widetilde{\Delta E_f}$ is the $O(1/L)$ part of ΔE_f (i.e., with the bulk contribution subtracted). In this last form this formula should be also valid for the *periodic boundary conditions*, then $\Delta E_{\min}$ should be

replaced by $2\pi v_F/L$. For noninteracting hardcore bosons one obtains $\beta = \frac{1}{2}$. It is worthwhile to note that this value for the OC exponent coincides with the one obtained earlier for the regime of weak coupling [313] by means of the bosonization technique.

The value of the OC exponent is connected to another exponent $\alpha = 1-\beta$ which determines the character of the singularity in the response,

$$S^B(q,\omega) \propto \frac{1}{(\omega - \omega_\mu(q))^\alpha}, \tag{1.103}$$

where $\omega_\mu(q)$ is the minimum energy difference between the ground state and the excited configuration. For example, at $q = \pi$, where the strongest response is expected, the lowest energy excited configuration is symmetric about $k = \pi$ and is given by $\lambda = \pi$, $k'_j = \pi \pm \frac{2\pi}{L} j$, $j = 1, \ldots, N/2$, so that

$$\omega_\mu(q = \pi) = \varepsilon_\mu + 2t \cos k_F = (1 - \mu)H. \tag{1.104}$$

Note that the quantity $\omega_\mu(\pi)$, which determines the position of the peak in the response, and in an inelastic neutron scattering experiment would be interpreted as the energy of the corresponding mode with $S^z = \mu$, has a counter-intuitive dependence on the magnetic field: one would rather expect that it behaves as $-\mu H$. The resulting picture of modes which should be seen e.g. in the INS experiment is schematically shown in Fig. 1.23.

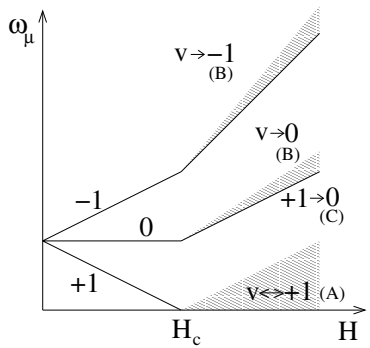

Fig. 1.23. The schematic dependence of "resonance" lines (peaks in the dynamic structure factor at $q = \pi$, shown as solid lines) on the magnetic field in an axially symmetric system. The dashed areas represent continua. The processes responsible for the transitions are indicated near the corresponding lines, e.g. $\mathrm{v} \to -1$ denotes the (B)-type process of creating one boson with $S^z = -1$ from the vacuum, etc.

As q moves further from π, λ must follow q, and in order to satisfy the selection rules one has to create an additional particle-hole pair to compensate the unwanted change of momentum. Away from $q = \pi$ this configuration does not necessarily have the lowest energy, and there are other configurations with generally large number of umklapp-type of particle-hole pairs, whose energy may be lower, but, as discussed in [305], their contribution to the response can be neglected because the corresponding OC exponent is larger than 1 for this type of configurations.

At finite temperature $T \neq 0$ the singularity gets damped. The contribution of B-type processes to the dynamical susceptibility $\chi(q,\omega)$ is proportional to the following integral:

$$\chi(q,\omega) \propto \int_0^\infty dt e^{i\Omega t} \Big(\frac{\pi T}{\sinh \pi T t}\Big)^\beta ,$$

where $\Omega \equiv \omega - \omega_\mu(q)$ is the deviation from the edge. Then for the dynamical structure factor $S(q,\omega)$ one obtains

$$S^B(q,\omega) \propto \frac{\cos(\pi\beta/2)}{1-e^{-\omega/T}} \sinh\left(\frac{\Omega}{2T}\right) T^{\beta-1} \Big|\Gamma\Big(\frac{\beta}{2} + i\frac{\Omega}{2\pi T}\Big)\Big|^2 . \tag{1.105}$$

From (1.105) one recovers the edge singularity behavior (1.103) at $T = 0$.

For $H > H_c$ there will be also a contribution from C-type transitions corresponding to the transformation of b_{+1} bosons into b_0 ones. Those processes do not change the total number of particles and thus do not disturb the allowed values of the wave vector, so that there is no OC in this case. The problem of calculating the response is equivalent to that for the 1D Fermi gas, with the only difference that we have to take into account the additional change in energy $\varepsilon_0 - \varepsilon_{+1}$ which takes place in the transition. The well-known formula for the susceptibility of a Fermi gas yields the contribution of C-type processes into the response:

$$\begin{aligned} S^C(q,\omega) = {} & \frac{1}{1-e^{-\omega/T}} \frac{\pi - k_F}{2\pi^2} \\ & \times \int dk \, \big[n_{+1}(k) - n_0(k+q)\big] \delta\big(\omega - \varepsilon_0(k+q) + \varepsilon_{+1}(k)\big), \end{aligned} \tag{1.106}$$

where $\varepsilon_\mu(k) = \varepsilon_\mu + 2t\cos k$, and $n_\mu = (e^{\varepsilon_\mu/T} + 1)^{-1}$ is the Fermi distribution function. This contribution contains a square-root singularity, whose edge is located at

$$\omega = \varepsilon_0 - \varepsilon_{+1} + 2t\sqrt{2(1-\cos q)} \tag{1.107}$$

and which survives even for a finite temperature.

Role of Weak 3D Coupling in the Axially Symmetric Case: Bose-Einstein Condensation of Magnons

In the axially symmetric case, the high-field phase is gapless and thus is extremely sensitive to even a small 3D interaction. If one views the process of formation of the high-field phase as an accumulation of hardcore bosonic particles (magnons) in the ground state, then the most important effect is that in a 3D system those bosons can undergo the Bose-Einstein Condensation (BEC) transition. In one dimension there is no difference between hardcore bosons and fermions, and instead of BEC one obtains, as we have seen, a Fermi sea.

In 3D coupled system, increasing the field beyond H_c leads to the formation of the Bose-Einstein condensate of magnons. The U(1) symmetry gets spontaneously broken, and the condensate wave function picks a certain phase which is physically equivalent to the transverse (with respect to the field) staggered magnetization.

The idea of field-induced BEC was discussed theoretically several times [275, 278, 280], but only recently such a transition was observed [314] in $TlCuCl_3$, which can be viewed as a system of weakly coupled $S = \frac{1}{2}$ dimers. The observed behavior of magnon density (longitudinal magnetization) n as a function of temperature T was in a qualitative agreement with the predictions of the BEC theory: with increasing T from zero to the critical temperature T_c the magnetization decreases, and then starts to increase, so that the minimum of n occurs at $T = T_c$. There was, however, some discrepancy between the predicted and observed field dependence of the critical temperature: according to the BEC theory, $T_c \propto (H - H_c)^{\phi}$ with $\phi = 2/3$, while the experiment yields rather $\phi \approx 1/2$ [314, 315]. The reason for this discrepancy seems to be clarified in the recent work [316]: since in $TlCuCl_3$ experiments the critical temperature T_c becomes comparable with the magnon gap Δ, one has to take into account the "relativistic" nature of the magnon dispersion $\varepsilon(q) = \sqrt{\Delta^2 + v^2 k^2}$, which modifies the theoretical $T_c(H)$ curves and brings them in a good agreement with the experiment. The BEC exponent $\phi = 2/3$ is recovered only in a very narrow interval of fields close to H_c [317].

Due to the spontaneous symmetry breaking the elementary excitations in the ordered (BEC) phase become of a quasiparticle type, i.e., edge-type singularities characteristic for the purely 1D axially symmetric system (with unbroken symmetry) are replaced by delta functions. The response in the 3D-ordered (BEC) phase of $TlCuCl_3$ was measured in INS experiments of Rüegg et al. [318, 319] and was successfully described within the bond-boson mean-field theory [320]. The observed field dependence of gaps resembles the 1D picture of Fig. 1.23, with a characteristic change of slope at $H = H_c$ where the long-range 3D order appears.

To understand the main features of the dynamics in the 3D ordered high-field phase of a weakly coupled dimer system, it is instructive to consider an

effective dimer field theory which is in fact a continuum version of the very successful bond boson calculation of [320]. The theory can be constructed using dimer coherent states [321]

$$|\boldsymbol{A},\boldsymbol{B}\rangle = (1-A^2-B^2)^{1/2}|s\rangle + \sum_j (A_j + iB_j)|t_j\rangle, \tag{1.108}$$

where the singlet state $|s\rangle$ and three triplet states $|t_j\rangle$, $j=(x,y,z)$ are given by (1.72), and $\boldsymbol{A}$, $\boldsymbol{B}$ are real vectors which are in a simple manner connected with the magnetization $\boldsymbol{M}=\langle \boldsymbol{S}_1+\boldsymbol{S}_2\rangle$, sublattice magnetization $\boldsymbol{L}=\langle \boldsymbol{S}_1-\boldsymbol{S}_2\rangle$, and vector chirality $\boldsymbol{\kappa}=(\boldsymbol{S}_1\times\boldsymbol{S}_2)$ of the spin dimer:

$$\boldsymbol{M}=2(\boldsymbol{A}\times\boldsymbol{B})\,,\quad \boldsymbol{L}=2\boldsymbol{A}\sqrt{1-A^2-B^2}\,,\quad \boldsymbol{\kappa}=2\boldsymbol{B}\sqrt{1-A^2-B^2}. \tag{1.109}$$

We will assume that we are not too far above the critical field, so that the magnitude of the triplet components is small, $A,B\ll 1$. Assuming further that all exchange interactions are isotropic, one gets the following effective Lagrangian density in the continuum limit:

$$\begin{aligned}\mathcal{L} = {} & \hbar(\boldsymbol{A}\cdot\partial_t\boldsymbol{B}-\boldsymbol{B}\cdot\partial_t\boldsymbol{A}) - \frac{1}{2}\beta a^2(\nabla\boldsymbol{A})^2 - (m\boldsymbol{A}^2+\widetilde{m}\boldsymbol{B}^2)\\ & + 2\boldsymbol{H}\cdot(\boldsymbol{A}\times\boldsymbol{B}) - \lambda_0(\boldsymbol{A}^2)^2 - \lambda_1(\boldsymbol{A}^2\boldsymbol{B}^2) - \lambda_2(\boldsymbol{A}\cdot\boldsymbol{B})^2.\end{aligned} \tag{1.110}$$

Here a plays the role of the lattice constant, $(\nabla\boldsymbol{A})^2\equiv(\partial_k\boldsymbol{A})(\partial_k\boldsymbol{A})$, and the energy constants β, m, $\widetilde{m}$, $\lambda_{0,1,2}$ depend on the details of interaction between the dimers. For example, in case of purely bilinear exchange only between neighboring dimers of the type shown in Fig. 1.15, they are given by

$$\begin{aligned}&\alpha = J_L + J_L' + J_D + J_D', \quad \beta = |J_L + J_L' + J_D + J_D'|\\ &\widetilde{m} = J, \quad m = \widetilde{m} - \beta Z/2,\\ &\lambda_0 = \beta Z, \quad \lambda_1 = (\alpha+\beta)Z/2, \quad \lambda_2 = -\alpha Z/2\end{aligned} \tag{1.111}$$

The spatial derivatives of $\boldsymbol{B}$ are omitted in (1.110) because they appear only in terms which are of the fourth order in $\boldsymbol{A}$, $\boldsymbol{B}$. Generally, we can assume that spatial derivatives are small (small wave vectors), but we shall not assume that the time derivatives (frequencies) are small since we are going to describe high-frequency modes as well.

The vector $\boldsymbol{B}$ can be integrated out, and under the assumption $A\ll 1$ it can be expressed through $\boldsymbol{A}$ as follows:

$$\begin{aligned}&\boldsymbol{B} = \widehat{Q}\boldsymbol{F}, \quad \boldsymbol{F} = -\hbar\partial_t\boldsymbol{A} + (\boldsymbol{H}\times\boldsymbol{A})\\ &Q_{ij} = (1/\widetilde{m})\,\delta_{ij} - (\lambda_2/\widetilde{m}^2)A_iA_j.\end{aligned} \tag{1.112}$$

After substituting this expression back into (1.110) one obtains the effective Lagrangian depending on $\boldsymbol{A}$ only:

$$\mathcal{L} = \frac{\hbar^2}{\widetilde{m}}\big\{(\partial_t \boldsymbol{A})^2 - v^2(\nabla \boldsymbol{A})^2\big\} - \frac{2\hbar}{\widetilde{m}}(\boldsymbol{H}\times\boldsymbol{A})\cdot\partial_t\boldsymbol{A} - U_2 - U_4, \quad (1.113)$$

where v is the magnon velocity, $v^2 = \frac{1}{2}(\beta\widetilde{m}a^2/\hbar^2)$, and the quadratic and quartic parts of the potential are given by

$$U_2(\boldsymbol{A}) = m\boldsymbol{A}^2 - \frac{1}{\widetilde{m}}(\boldsymbol{H}\times\boldsymbol{A})^2, \quad (1.114)$$

$$U_4(\boldsymbol{A}, \partial_t\boldsymbol{A}) = \lambda_0(\boldsymbol{A}^2)^2 + \frac{\lambda_1}{\widetilde{m}^2}\boldsymbol{A}^2\boldsymbol{F}^2 + \frac{\lambda_2}{\widetilde{m}^2}(\boldsymbol{A}\cdot\boldsymbol{F})^2$$

Note that the cubic in $\boldsymbol{A}$ term in (1.112) must be kept since it contributes to the U_4 potential.

Now it is easy to calculate the excitation spectrum in the whole range of the applied field $\boldsymbol{H}$ which we assume do be directed along the z axis. At zero field, there is a triplet of magnons with the gap $\Delta = \sqrt{m\widetilde{m}}$, which gets trivially split by fields below the critical field $H_c = \Delta$, so that there are three distinct modes with the energies $E_\mu = \Delta + \mu H$, $\mu = S^z = 0, \pm 1$. For $H > H_c$ the potential energy minimum is achieved at a finite $\boldsymbol{A} = \boldsymbol{A}_0$,

$$A_0^2 = \frac{(H^2 - \Delta^2)\widetilde{m}}{2(\lambda\widetilde{m}^2 + \lambda_1 H^2)}.$$

All orientations of $\boldsymbol{A}_0$ in the plane perpendicular to $\boldsymbol{H}$ are degenerate. This U(1) symmetry is spontaneously broken, so that $\boldsymbol{A}_0$ chooses a certain direction, let us say $\boldsymbol{A}_0 \parallel x$. Then above H_c the Bose-condensed ground state is to leading order a product of single-dimer wavefunctions of the type (1.108), which mix *three* states: a singlet $|s\rangle$ and two triplets $|\uparrow\uparrow\rangle$, $|\downarrow\downarrow\rangle$. From this, it is clear that this BEC transition cannot be correctly described within an approach based on the reduced Hilbert space with only *two* states $|s\rangle$, $|\uparrow\uparrow\rangle$ per dimer.

The spectrum at $H > H_c$ can be obtained in a straightforward way. One of the modes always remains gapless (the Goldstone boson), while the two other modes have finite gaps given by

$$\Delta_z^2 = (1-\gamma_1)^{-1}\big\{\Delta^2 + 2\gamma_0\widetilde{m}^2 + \gamma_1 H^2\big\} \quad (1.115)$$

$$\Delta_{xy}^2 = [(1-\gamma_1-\gamma_2)(1-\gamma_1)]^{-1}\big\{2(H^2-\Delta^2) + 4H^2(1-2\gamma_1)^2, \big\}$$

where the coefficients $\gamma_\nu \equiv \lambda_\nu(H^2 - \Delta^2)/[2(\lambda_0\widetilde{m}^2 + \lambda_1 H^2)]$. In the limit of a simplified interaction with $\lambda_{1,2} = 0$ the gaps do not depend on the interaction parameters and acquire the compact form $\Delta_z = H$, $\Delta_{xy} = \sqrt{6H^2 - \Delta^2}$, which compares rather well with the INS data [318, 319] on $TlCuCl_3$. It is worthwhile to note a certain similarity in the field dependence of the spectra in 3D and 1D case: the quasiparticle modes in the 3D case behave roughly in the same way as the edges of continua in the 1D case.

Response in an Anisotropic System

Typically, quasi-one-dimensional materials are not completely isotropic. For example, up to our knowledge there is no experimental realization of the isotropic $S = 1$ Haldane chain, and in real materials like NENP or NDMAP the single-ion anisotropy leads to splitting of the Haldane triplet into three distinctive components. When the axial symmetry is *explicitly* broken, the system behavior changes drastically: the high-field phase is no more critical and acquires a long-range order even in the purely 1D case.

We will illustrate the general features of the behavior of a gapped anisotropic 1D system in magnetic field by using the example of the strongly alternated anisotropic $S = \frac{1}{2}$ chain described by the Hamiltonian

$$\mathcal{H} = \sum_{n\alpha} J_\alpha S^\alpha_{2n-1} S^\alpha_{2n} + \sum_n \{J'(\boldsymbol{S}_{2n} \cdot \boldsymbol{S}_{2n+1}) - \boldsymbol{H} \cdot \boldsymbol{S}_n\}, \qquad J' \ll J. \tag{1.116}$$

Since this system consists of weakly coupled anisotropic dimers, one may again use a mapping to the dimer field theory as considered above for 3D coupling. One again obtains a Lagrangian of the form similar to (1.110), but the quadratic part of the potential energy gets distorted by the anisotropy: instead of $(m\boldsymbol{A}^2 + \widetilde{m}\boldsymbol{B}^2)$ one now has $\sum_j \{m_j A_j^2 + \widetilde{m}_j B_j^2\}$. For the alternated chain (1.116) the Lagrangian parameters are given by $m_i = \widetilde{m}_i - J'$, $\widetilde{m}_i = \frac{1}{4}\sum_{jn} |\epsilon_{ijn}|(J_j + J_n)$, $\lambda_0 = J'$, $\lambda_1 = 2J'$, $\lambda_2 = -J'$, $\beta = J'$. Due to this "distortion", the effective Lagrangian obtained after integrating out $\boldsymbol{B}$ takes a somewhat more complicated form

$$\mathcal{L} = \frac{\hbar^2}{\widetilde{m}_i}\Big\{(\partial_t A_i)^2 - v_i^2(\partial_x A_i)^2\Big\} - 2\frac{\hbar}{\widetilde{m}_i}(\boldsymbol{H} \times \boldsymbol{A})_i \partial_t A_i - U_2 - U_4, \tag{1.117}$$

where $v_i^2 = \frac{1}{2}J'\widetilde{m}_i a^2/\hbar^2$, and

$$\begin{aligned} U_2(\boldsymbol{A}) &= m_i A_i^2 - \frac{1}{\widetilde{m}_i}(\boldsymbol{H} \times \boldsymbol{A})_i^2, \\ U_4(\boldsymbol{A}, \frac{\partial \boldsymbol{A}}{\partial t}) &= \lambda(\boldsymbol{A}^2)^2 + \lambda_1 \boldsymbol{A}^2 \frac{1}{\widetilde{m}_i^2} F_i^2 + \lambda_2 \frac{A_i A_j}{\widetilde{m}_i \widetilde{m}_j} F_i F_j, \end{aligned} \tag{1.118}$$

with $\boldsymbol{F}$ defined in (1.112).

Having in mind that the alternated $S = \frac{1}{2}$ chain, the Haldane chain, and $S = \frac{1}{2}$ ladder belong to the same universality class, one may now conjecture that in the form (1.117-1.118) the above theory can be also applied to a variety of other anisotropic gapped 1D systems, with the velocities v_i and interaction constants m_i, $\widetilde{m}_i$, λ_i treated as phenomenological parameters.

Several phenomenological field-theoretical description of the strong-field regime in the anisotropic case were proposed in the early 90s [275, 276, 322]. One can show that the Lagrangian (1.117) contains theories of Affleck [275]

and Mitra and Halperin [322] as particular cases: after restricting the interaction to the simplified form with $\lambda_{1,2} = 0$ and assuming isotropic velocities $v_i = v$, Affleck's Lagrangian corresponds to the isotropic $\boldsymbol{B}$-stiffness $\widetilde{m}_i = \widetilde{m}$, while another choice $\widetilde{m}_i = m_i$ yields the theory of Mitra and Halperin.

For illustration, let us assume that $\boldsymbol{H} \parallel \widehat{\boldsymbol{z}}$. Then the quadratic part of the potential takes the form

$$U_2 = (m_x - \frac{H^2}{\widetilde{m}_y})A_x^2 + (m_y - \frac{H^2}{\widetilde{m}_x})A_y^2 + m_z A_z^2, \tag{1.119}$$

and the critical field is obviously $H_c = \min\{(m_x\widetilde{m}_y)^{1/2}, (m_y\widetilde{m}_x)^{1/2}\}$. At zero field the three triplet gaps are given by $\Delta_i = (m_i\widetilde{m}_i)^{1/2}$. Below H_c the energy gap for the mode polarized along the field stays constant $E_z = \Delta_z$, while the gaps for the other two modes are given by

$$(E_{xy}^{\pm})^2 = \frac{1}{2}(\Delta_x^2 + \Delta_y^2) + H^2 \pm \left[(\Delta_x^2 - \Delta_y^2)^2 + H^2(m_x + m_y)(\widetilde{m}_x + \widetilde{m}_y)\right]^{1/2}. \tag{1.120}$$

Below H_c the mode energies do not depend on the interaction constants λ_i, while the behavior of gaps at $H > H_c$ is sensitive to the details of the interaction potential.

It is easy to see that in the special case $m_i = \widetilde{m}_i$, the above expression transforms into

$$E_{xy}^{\pm} = \frac{1}{2}(\Delta_x + \Delta_y) \pm \left[\frac{1}{4}(\Delta_x - \Delta_y)^2 + H^2\right]^{1/2}, \tag{1.121}$$

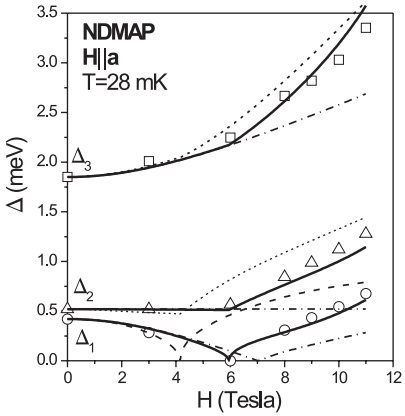

Fig. 1.24. Measured field dependence of the gap energies in NDMAP at $T = 30$ mK and H applied along the crystallographic a axis (open symbols). Dashed and dash-dot lines are predictions of the theoretical models proposed in [275] and [276], respectively. The solid lines are the best fit to the data using the alternative model (1.117). (From [304])

which exactly coincides with the formulas obtained in the approach of Tsvelik [276], as well as with the perturbative formulas of [323, 324] and with the results of modified bosonic theory of Mitra and Halperin [322] who postulated a bosonic Lagrangian to match Tsvelik's results for the field dependence of the gaps below H_c.

The present approach was applied to the description of the INS [304] and ESR [325] experiments on the $S = 1$ Haldane material NDMAP and yielded a very good agreement with the experimental data, see Fig. 1.24. It turns out that for a satisfactory quantitative description the inclusion of $\lambda_{1,2}$ is important, as well as having unequal stiffness constants $m_i \neq \widetilde{m}_i$.

References

1. W. Lenz: Z. Physik **21**, 613 (1920); E. Ising: Z. Physik **31**, 253 (1925)
2. H. Bethe: Z. Physik **71**, 205 (1931)
3. W. Heisenberg: Z. Physik **49**, 619 (1928)
4. T. D. Schulz, D. C. Mattis, E. H. Lieb: Rev. Mod. Phys. **36**, 856 (1964)
5. R. J. Baxter: Phys. Rev. Lett. **26**, 834 (1971); Ann. Phys. (N.Y.) **70**, 323 (1971)
6. N.D. Mermin, H. Wagner: Phys. Rev. Lett. **17**, 1133 (1966)
7. S. Coleman: Commun. Math. Phys. **31**, 259 (1973)
8. M. T. Hutchings, G. Shirane, R. J. Birgeneau, S. L. Holt: Phys. Rev. B **5**, 1999 (1972)
9. L.D. Faddeev, L.A. Takhtajan: Phys. Lett. **85A**, 375 (1981)
10. F. D. M. Haldane: Phys. Lett. A **93**, 464 (1983); Phys. Rev. Lett. **50**, 1153 (1983)
11. E. Dagotto and T. M. Rice: Science **271**, 618 (1996)
12. E. Fradkin: *Field Theories of Condensed Matter Systems* (Addison-Wesley, Reading, 1991)
13. A.M. Tsvelik: *Quantum Field Theory in Condensed Matter Physics* (Cambridge University Press, 1995); A.O. Gogolin, A.A. Nersesyan, A.M. Tsvelik: *Bosonization and Strongly Correlated Systems* (Cambridge University Press, 1999)
14. A. Auerbach: *Interacting Electrons and Quantum Magnetism* (Springer-Verlag, 1994)
15. I.U. Heilmann, G. Shirane, Y. Endoh, R.J. Birgeneau, S.L. Holt: Phys. Rev. B **18**, 3530 (1978)
16. M. Hase, I. Terasaki, K. Uchinokura: Phys. Rev. Lett. **70**, 3651 (1993)
17. M. Steiner, J. Villain, C.G. Windsor: Adv. Phys. **25**, 87 (1976)
18. H.-J. Mikeska and M. Steiner: Adv. Phys. **40**, 191 (1991)
19. D.C. Mattis: *The Theory of Magnetism I*, Springer Series in Solid State Sciences, vol. 17 (1981)
20. F.C. Alcaraz, S.R. Salinas, W.F. Wreszinski: Phys. Rev. Lett. **75**, 930 (1995)
21. T. Koma, B. Nachtergaele: Lett. Math. Phys. **40**, 1 (1996)
22. R. Coldea, D.A. Tennant. A.M. Tsvelik, Z. Tylczynski: Phys. Rev. Lett. **86**, 1335 (2001)
23. N. Ishimura, H. Shiba: Progr. Theor. Phys. **63**, 743 (1980)

24. J. Villain: Physica B **79**, 1 (1975)
25. P. Jordan, E. Wigner: Z. Phys. **47**, 631 (1928)
26. E. Lieb, T. D. Schultz, D. C. Mattis: Ann. Phys. (NY) **16**, 407 (1961)
27. B. M. McCoy: Phys. Rev. **173**, 531 (1968)
28. T. Tonegawa: Solid State Comm. **40**, 983 (1981)
29. H.-J. Mikeska, W. Pesch: Z. Phys. B **26**, 351 (1977)
30. B. McCoy, J. H. H. Perk, R. E. Shrock: Nucl. Phys. **220**, 35 (1983); Nucl. Phys. **220**, 269 (1983)
31. F. Colomo, A. G. Izergin, V. E. Korepin, V. Tognetti: Theor. Mat. Phys. **94**, 11 (1993); A. R. Its, A. G. Izergin, V. E. Korepin, N. A. Slavnov, Phys. Rev. Lett. **70**, 1704 (1993)
32. A. Luther, I. Peschel: Phys. Rev. B **9**, 2911 (1974); Phys. Rev. B **12**, 3908 (1975)
33. S. Tomonaga: Prog. Theor. Phys. **5**, 544 (1950); J. M. Luttinger: J. Math. Phys. **4**, 1154 (1963); F. D. M. Haldane: J. Phys. C **14**, 2585 (1981)
34. A. K. Kolezhuk, H.-J. Mikeska, K. Maisinger, U. Schollwöck: Phys. Rev. B **59** (1999), 13565
35. I. Affleck: J. Phys. A: Math. Gen. **31**, 4573 (1998)
36. I. Affleck, D. Gepner, H.J. Schulz, T. Ziman: J. Phys. A: Math. Gen. **22**, 511 (1989)
37. R. P. Singh, M. E. Fisher, R. Shankar: Phys. Rev. B **39**, 2562 (1989)
38. S. Eggert, I. Affleck, M. Takahashi: Phys. Rev. Lett. **73**, 332 (1994)
39. N. Motoyama, H. Eisaki, S. Uchida: Phys. Rev. Lett. **76**, 3212 (1996)
40. J. des Cloizaux, J.J. Pearson: Phys. Rev. **128**, 2131 (1962)
41. S. Lukyanov, A. Zamolodchikov: Nucl. Phys. B **493**, 571 (1997)
42. S. Lukyanov, V. Terras: Nucl. Phys. B **654**, 323 (2003)
43. H.-J. Mikeska, S. Miyashita, G. Ristow: J. Phys.: Condens. Matter **3**, 2985 (1991)
44. J.D. Johnson, S. Krinsky, B.M. McCoy, Phys. Rev. A **8**, 2526 (1973)
45. A.H. Bougourzi, M. Karbach, G. Müller, Phys. Rev. B **57**, 11429 (1998)
46. S. Brehmer: PhD thesis, Universität Hannover (1998)
47. H. J. Schulz: Phys. Rev. B **34**, 6372 (1986)
48. Th. Niemeier: Physica **36**, 377 (1967)
49. G. Müller, H. Thomas, H. Beck, J. C. Bonner: Phys. Rev. B **24**, 1429 (1981)
50. H.-J. Mikeska: Phys. Rev. B **12**, 2794 (1975); H.-J. Mikeska, W. Pesch: J. Phys. C **12**, L37 (1979)
51. H.-J. Mikeska, E. Patzak: Z. Phys. B **26**, 253 (1977)
52. G. Müller, H. Beck, J. C. Bonner: Phys. Rev. Lett. **43**, 75 (1979)
53. M. Karbach, G. Müller, A.H. Bougourzi, A. Fledderjohann, K.-H. Mütter: Phys. Rev. B **55**, 12510 (1997)
54. D.A. Tennant, T.G. Perring, R.A. Cowley, S.E. Nagler: Phys. Rev. Lett. **70**, 4003 (1993); D.A. Tennant, R.A. Cowley, S.E. Nagler, A.M. Tsvelik: Phys. Rev. B **52**, 13368 (1995);
55. M. Arai, M. Fujita, M. Motokawa, J. Akimitsu, S.M. Bennington: Phys. Rev. Lett. **77**, 3649 (1996)
56. O. Derzhko, T. Krokhmalskii, J. Stolze: J. Phys. A: Math. Gen. **33**, 3063 (2000)
57. K. Fabricius, U. Löw, J. Stolze: Phys. Rev. B **55**, 5833 (1997)
58. F.D.M. Haldane: Phys. Rev. Lett. **60**, 635 (1988); B.S. Shastry: Phys. Rev. Lett. **60**, 639 (1988)

59. F.D.M. Haldane, M.R. Zirnbauer: Phys. Rev. Lett. **71**, 4055 (1993)
60. H. Yoshizawa, K. Hirakawa, S.K. Satija, G. Shirane: Phys. Rev. B **23**, 2298 (1981)
61. S.E. Nagler, W.J.L. Buyers, R.L. Armstrong, B. Briat: Phys. Rev. B **27**, 1784 (1983)
62. J.P. Goff, D.A. Tennant, S.E. Nagler: Phys. Rev. B **52**, 15992 (1995)
63. F. Matsubara, S. Inawashiro: Phys. Rev. B **43**, 796 (1991)
64. F.D.M. Haldane: Phys. Rev. B **25**, 4925 (1982)
65. K. Okamoto, K. Nomura: Phys. Lett. A **169**, 433 (1992).
66. C.K. Majumdar, D.K. Ghosh: J. Math. Phys. **10**, 1399 (1969)
67. M. C. Cross, D. S. Fisher: Phys. Rev. B **19**, 402 (1979); M. C. Cross: Phys. Rev. B **20**, 4606 (1979)
68. G. Uhrig: Phys. Rev. B **57**, R14004 (1998)
69. A. Weiße, G. Wellein, H. Fehske: Phys. Rev. B **60**, 6566 (1999)
70. R.J. Bursill, R.H. McKenzie, C.J. Hamer: Phys. Rev. Lett. **83**, 408 (1999)
71. K. Uchinokura: J. Phys.: Condens. Matter **14**, R195 (2002)
72. A. Koga, K. Okunishi, N. Kawakami: Phys. Rev. B **62**, 5558 (2000)
73. N.B. Ivanov, J. Richter: Phys. Lett. **232A**, 308 (1997); J. Richter, N.B. Ivanov, J. Schulenburg: J. Phys.: Condens. Matter **10**, 3635 (1998)
74. D.S. Fisher: Phys. Rev. B **50**, 3799 (1994)
75. K. Hida: J. Phys. Soc. Jpn **66**, 3237 (1997)
76. E. Westerberg, A. Furusaki, M. Sigrist, P. A. Lee: Phys. Rev. Lett. **75**, 4302 (1995)
77. K. Hida: J. Phys. Soc. Jpn. **66**, 330 (1997); Phys. Rev. Lett. **79**, 1750 (1999)
78. C. N. Yang, C. P. Yang: Phys. Rev. **150**, 321, 327 (1966); Phys. Rev. **151**, 258 (1966)
79. T. Sakai, M. Takahashi: Prog. Theor. Phys. Suppl. No. **145**, 125 (2002)
80. D. C. Dender, P. R. Hammar, D. H. Reich, C. Broholm, G. Aeppli: Phys. Rev. Lett. **79**, 1750 (1997)
81. M. Karbach, G. Müller, Phys. Rev. B **60**, 14871 (2000)
82. J. Kurmann, H. Thomas, G. Müller: Physica A **112**, 235 (1982)
83. R. Feyerherm, S. Abens, D. Günther, T. Ishida, M. Meißner, M. Meschke, T. Nogami, M. Steiner: J. Phys.: Condens. Matter **12**, 8495 (2000).
84. R. Helfrich, M. Köppen, M. Lang, F. Steglich, A. Ochiai: J. Magn. Magn. Mater. **177-181**, 309 (1998); M. Köppen et al.: Phys. Rev. Lett. **82**, 4548 (1999)
85. M. Oshikawa, I. Affleck: Phys. Rev. Lett. **79**, 2833 (1997)
86. I. Affleck, M. Oshikawa: Phys. Rev. B **60**, 1038 (1999); *ibid.* **62**, 9200 (2000)
87. T. Asano, H. Nojiri, Y. Inagaki, J. P. Boucher, T. Sakon, Y. Ajiro, M. Motokawa: Phys. Rev. Lett. **84**, 5880 (2000)
88. F. H. L. Essler, A. M. Tsvelik: Phys. Rev. B **57**, 10592 (1998).
89. F. H. L. Essler, A. Furusaki, T. Hikihara: Phys. Rev. B **68**, 064410 (2003)
90. P. Pfeuty: Ann. Phys. (*N.Y.*) **57**, 79 (1970); J. Phys. C: Solid State Phys. **9**, 3993 (1976)
91. S. Sachdev: *Quantum Phase Transitions* (Cambridge University Press, 1999).
92. D. V. Dmitriev, V. Ya. Krivnov, A. A. Ovchinnikov: Phys. Rev. B **65**, 172409 (2002); D. V. Dmitriev, V. Ya. Krivnov, A. A. Ovchinnikov, A. Langari: JETP **95**, 538 (2002)
93. J.-S. Caux, F.H.L. Essler and U. Löw: Phys. Rev. B **68**, 134431 (2003)

94. C. J. Mukherjee, R. Coldea, D. A. Tennant, K. Habicht, P. Smeibidl, M. Koza, M. Enderle, Z. Tylczynski: contribution to ICM2003 (Rome, 2003);
95. D. J. Scalapino, Y. Imry, P. Pincus: Phys. Rev. B **11**, 2042 (1975)
96. H.J. Schulz: Phys. Rev. Lett. **77**, 2790 (1996)
97. F. H. L. Essler, A. M. Tsvelik, G. Delfino: Phys. Rev. B **56**, 11001 (1997)
98. A. Zheludev, S. Raymond, L.-P. Regnault, F. H. L. Essler, K. Kakurai, T. Masuda, K. Uchinokura: Phys. Rev. B **67**, 134406 (2003)
99. B. Lake, D. A. Tennant, S. E. Nagler: Phys. Rev. Lett. **85**, 832 (2000)
100. A. Zheludev, K. Kakurai, T. Masuda, K. Uchinokura, K. Nakajima: Phys. Rev. Lett. **89**, 197205 (2002)
101. M. P. Nightingale, H. W. J. Blöte: Phys. Rev. B **33**, 659 (1986)
102. S. R. White: Phys. Rev. Lett. **69**, 2863 (1992)
103. S. Yamamoto, S. Miyashita: Phys. Lett. A **235**, 545 (1997)
104. S. R. White, D. A. Huse: Phys. Rev. B **48**, 3844 (1993)
105. M. Yamanaka, Y. Hatsugai, M. Kohmoto: Phys. Rev. B**48**, 9555 (1993)
106. M. den Nijs, K. Rommelse: Phys. Rev. B **40**, 4709 (1989)
107. S.M. Girvin, D.P. Arovas: Physica Scripta T **27**, 156 (1989)
108. T. Kennedy, H. Tasaki: Phys. Rev. B**45**, 304 (1992); Commun. Math. Phys. **147**, 431 (1992)
109. G. Gómez-Santos: Phys. Rev. Lett. **63**, 790 (1989)
110. H.-J. Mikeska: Europhys. Lett. **19**, 39 (1992)
111. G. Fáth, J. Sólyom: J. Phys.: Condens. Matter **5**, 8983 (1993)
112. N. Elstner, H.-J. Mikeska: Phys. Rev. B **50**, 3907 (1994)
113. G.E. Granroth, M.W. Meisel, M. Chaparala, Th. Jolicoeur, B.H. Ward, D.R. Talham: Phys. Rev. Lett. **77**, 1616 (1996)
114. H. Kadowaki, K. Ubukoshi, K. Hirakawa: J. Phys. Soc. Jpn. **56**, 751 (1987)
115. W. Chen, K. Hida, B. C. Sanctuary: Phys. Rev. B **67**, 104401 (2003)
116. U. Schollwöck, T. Jolicoeur: Europhys. Lett. **30**, 493 (1995); U. Schollwöck, O. Golinelli, T. Jolicoeur: Phys. Rev. B **54**, 4038 (1996)
117. I. Affleck: J. Phys.: Cond. Matter **1**, 3047 (1989)
118. A. M. Polyakov: Phys. Lett. B **59**, 87 (1975)
119. E. Brézin, J. Zinn-Justin: Phys. Rev. B **14**, 3110 (1976)
120. A. A. Belavin, A. M. Polyakov: JETP Lett. **22**, 245 (1975)
121. I. Affleck, E. H. Lieb: Lett. Math. Phys. **12**, 57 (1986)
122. M. Oshikawa, M. Yamanaka , I. Affleck: Phys. Rev. Lett. **78**, 1984 (1997)
123. I. Affleck, T. Kennedy, E.H. Lieb, H. Tasaki: Phys. Rev. Lett. **59**, 799 (1987); Commun. Math. Phys. **115**, 477 (1988)
124. T. Kennedy: J. Phys.: Condens. Matter **2**, 5737 (1990)
125. M. Fannes, B. Nachtergaele, R. F. Werner: Europhys. Lett. **10**, 633 (1989); Commun. Math. Phys. **144**, 443 (1992)
126. A. Klümper, A. Schadschneider, J. Zittartz: J. Phys. A **24**, L955 (1991); Z. Phys. B **87**, 281 (1992); Europhys. Lett. **24**, 293 (1993)
127. K. Totsuka, M. Suzuki: J. Phys.: Condens. Matter **7**, 1639 (1995)
128. S. Miyashita, S. Yamamoto: Phys. Rev. B **48**, 913 (1993)
129. U. Schollwöck, Th. Jolicoeur, Th. Garel: Phys. Rev. B **53**, 3304 (1996)
130. M. Hagiwara, K. Katsumata, I. Affleck, B. I. Halperin, J. P. Renard: Phys. Rev. Lett. **65**, 3181 (1990)
131. A. K. Kolezhuk, U. Schollwöck: Phys. Rev. B **65**, 100401(R) (2002)
132. D. P. Arovas, A. Auerbach, F. D. M. Haldane: Phys. Rev. Lett. **60**, 531 (1988)

133. U. Neugebauer, H.-J. Mikeska: Z. Phys. B **99**, 151 (1996).
134. S. Yamamoto: Phys. Lett. A **225**, 157 (1997)
135. I. Affleck: Nucl. Phys. B **257**, 397 (1985); **265**, 409 (1986)
136. R.R.P. Singh, M. Gelfand: Phys. Rev. Lett. **61**, 2133 (1988); M. Yajima, M. Takahashi: J. Phys. Soc. Jpn. **65**, 39 (1996); M. Yamanaka, M. Oshikawa, S. Miyashita: J. Phys. Soc. Jpn. **65**, 1652 (1996); S. Yamamoto: Phys. Rev. B **55**, 3603 (1997)
137. Y. Narumi, M. Hagiwara, M. Kohno, K. Kindo: Phys. Rev. Lett. **86**, 324 (2001)
138. S. Pati, R. Chitra, D. Sen, H. R. Krishnamurthy, S. Ramasesha: Europhys. Lett. **33**, 707 (1996)
139. S. Pati, R. Chitra, D. Sen, S. Ramasesha, H. R. Krishnamurthy: J. Phys.: Condens. Matter, **9**, 219 (1997)
140. A. K. Kolezhuk, R. Roth, U. Schollwöck: Phys. Rev. Lett. **77**, 5142 (1996); Phys. Rev. B **55**, 8928 (1997)
141. S. Todo, M. Matsumoto, C. Yasuda, H. Takayama: Phys. Rev. B **64**, 224412 (2001)
142. A. A. Nersesyan, A. O. Gogolin, F. H. L. Essler: Phys. Rev. Lett. **81**, 910 (1998)
143. A. A. Aligia, C. D. Batista, F. H. L. Eßler: Phys. Rev. B **62**, 6259 (2000)
144. D. Allen, D. Sénéchal: Phys. Rev. B **61**, 12134 (2000)
145. M. Kaburagi, H. Kawamura, T. Hikihara: J. Phys. Soc. Jpn. **68**, 3185 (1999)
146. T. Hikihara, M. Kaburagi, H. Kawamura, T. Tonegawa: J. Phys. Soc. Jpn. **69**, 259 (2000)
147. A. K. Kolezhuk: Phys. Rev. B **62**, R6057 (2000)
148. S. Rao, D. Sen: Nucl. Phys. B **424**, 547 (1994)
149. D. Allen and D. Sénéchal: Phys. Rev. B **51**, 6394 (1995)
150. T. Hikihara, M. Kaburagi, H. Kawamura: Phys. Rev. B **63**, 174430 (2001)
151. J. Villain: Ann. Isr. Phys. Soc. **2**, 565 (1978)
152. A. K. Kolezhuk: Prog. Theor. Phys. Suppl. **145**, 29 (2002)
153. Y. Nishiyama: Eur. Phys. J. B **17**, 295 (2000)
154. P. Lecheminant, T. Jolicoeur, P. Azaria: Phys. Rev. B **63**, 174426 (2001)
155. M. Affronte, A. Caneschi, C. Cucci, D. Gatteschi, J. C. Lasjaunias, C. Paulsen, M. G. Pini, A. Rettori, R. Sessoli: Phys. Rev. B **59**, 6282 (1999)
156. E. Dagotto, J. Riera, D.J. Scalapino: Phys. Rev. B **45**, 5744 (1992)
157. E. Dagotto: Rep. Prog. Phys. **62**, 1525 (1999)
158. M. Uehara, T. Nagatta, J. Akimitsu, H. Takahashi, N. Mori, K. Kinoshita: J. Phys. Soc. Japan **65**, 2764 (1996)
159. S. R. White, R. M. Noack, D. J. Scalapino: Phys. Rev. Lett. **73**, 886 (1994)
160. T. Barnes, J. Riera: Phys. Rev. B **50**, 6817 (1994)
161. N. Hatano, Y. Nishiyama: J. Phys. A **28**, 3911 (1995)
162. M. Greven, R. J. Birgeneau, U.-J. Wiese: Phys. Rev. Lett. **77**, 1865 (1996)
163. K. Hida: J. Phys. Soc. Jpn. **60**, 1347 (1991); J. Magn. Magn. Mater. **104**, 783 (1992)
164. S. P. Strong, A. J. Millis: Phys. Rev. B **50**, 9911 (1994)
165. A. K. Kolezhuk, H.-J. Mikeska: Phys. Rev. B **53**, R8848 (1996)
166. T. Vekua, G.I. Japaridze, H.J. Mikeska: Phys. Rev. B **67**, 064419 (2003)
167. M. Roji, S. Miyashita: J. Phys. Soc. Japan **65**, 883 (1996)
168. B. S. Shastry, B. Sutherland: Phys. Rev. Lett. **47**, 964 (1981)

169. S. R. White: Phys. Rev. B **53**, 52 (1996)
170. S. Brehmer, H.-J. Mikeska, U. Neugebauer: J. Phys.: Condens. Matter **8**, 7161 (1996)
171. H. Yokoyama, S. Watanabe: J. Phys. Soc. Japan **68**, 2073 (1999)
172. S. Takada, H. Watanabe: J. Phys. Soc. Japan **61**, 39 (1992)
173. Y. Nishiyama, N. Hatano, M. Suzuki: J. Phys. Soc. Japan **64**, 1967 (1995)
174. D. G. Shelton, A. A. Nersesyan, A. M. Tsvelik: Phys. Rev. B **53**, 8521 (1996)
175. E.H. Kim, J. Sólyom: Phys. Rev. B**60**, 15230 (1999); E.H. Kim, G. Fáth, J. Sólyom, D.J. Scalapino: Phys. Rev. B **62**, 14965 (2000)
176. C. Itoi, S. Qin: Phys. Rev. B**63**, 224423 (2001)
177. S.R. White, I. Affleck: Phys. Rev. B**54**, 9862 (1996)
178. T. Tonegawa, I. Harada: J. Phys. Soc. Japan **56**, 2153 (1987)
179. R. Chitra, S. Pati, H. R. Krishnamurthy, D. Sen, S. Ramasesha: Phys. Rev. B **52**, 6581 (1995)
180. D.V. Dmitriev, Y.Ya. Krivnov, A.A. Ovchinnikov: Z. Phys. B **103**, 193 (1997)
181. A. K. Kolezhuk, H.-J. Mikeska, S. Yamamoto: Phys. Rev. B **55**, R3336 (1997).
182. S. Ostlund, S. Rommer: Phys. Rev. Lett. **75**, 3537 (1995)
183. M. A. Martin-Delgado, G. Sierra: Int. J. Mod. Phys. A **11**, 3145 (1996)
184. J. Dukelsky, M. A. Martin-Delgado, T. Nishino, G. Sierra: Europhys. Lett. **43**, 457 (1998)
185. J. M. Roman, G. Sierra, J. Dukelsky, M. A. Martin-Delgado: J. Phys. A **31**, 9729 (1998)
186. D. Allen, F. H. L. Essler, A. A. Nersesyan: Phys. Rev. B **61**, 8871 (2000)
187. M. Müller, H.-J. Mikeska: J. Phys.: Condens. Matter **12**, 7633 (2000)
188. Zheng Weihong, V. Kotov, J. Oitmaa: Phys. Rev. B **57**, 11439 (1998)
189. S. Brehmer, A. K. Kolezhuk, H.-J. Mikeska, U. Neugebauer: J. Phys.: Condens. Matter **10**, 1103 (1998)
190. C. Knetter, K. P. Schmidt, M. Grüninger, G. S. Uhrig: Phys. Rev. Lett. **87**, 167204 (2001).
191. M. Windt, M. Grüninger, T. Nunner, C. Knetter, K. P. Schmidt, G. S. Uhrig, T. Kopp, A. Freimuth, U. Ammerahl, B. Büchner, A. Revcolevschi: Phys. Rev. Lett. **87**, 127002 (2001).
192. T. Kato, K. Takatsu, H. Tanaka, W. Shiramura, M. Mori, K. Nakajima, K. Kakurai: J. Phys. Soc. Japan **67**, 752 (1996)
193. N. Cavadini, G. Heigold, W. Henggeler, A. Furrer H.-U. Güdel, K. Krämer, M. Mutka: Phys. Rev. B **63**, 17414 (2001)
194. M. B. Stone, I. Zaliznyak, D. H. Reich, C. Broholm: Phys. Rev. B **64**, 144405 (2001)
195. H.-J. Mikeska, M. Müller: Appl. Phys. A **74** [Suppl], S580 (2003)
196. A. Oosawa, T. Kato, H. Tanaka, K. Kakurai, M. Müller, H.-J. Mikeska: Phys. Rev. B **65**, 094426 (2003)
197. S. Sachdev, R. N. Bhatt: Phys. Rev. B **41**, 9323 (1990)
198. T. Gopalan, T.M. Rice, M. Sigrist: Phys. Rev. B **49**, 8901 (1999)
199. V. N. Kotov, O. Sushkov, Zheng Weihong, J. Oitmaa: Phys. Rev. Lett. **80**, 5790 (1998)
200. I. Affleck: in Proc. of NATO ASI Workshop on Dynamical Properties of Unconventional Magnetic Systems, Geilo, Norway, 1997 (Plenum, New York, 1997)
201. G. Bouzerar, A. P. Kampf, F. Schönfeld: preprint cond-mat/9701176 (unpublished).

202. B. Lake, R.A. Cowley, D.A. Tennant: J. Phys.: Condens. Matter **9**, 10951 (1997)
203. A. A. Zvyagin: Sov. Phys. Sol. St. **32**, 181 (1990); Sov. J. Low Temp. Phys. **18**, 558 (1992)
204. D. V. Khveshchenko: Phys. Rev. B **50**, 380 (1994)
205. D. Sénéchal: Phys. Rev. B **52**, 15319 (1995)
206. G. Sierra: J. Phys. A **29**, 3299 (1996)
207. B. Frischmuth, B. Ammon, M. Troyer: Phys. Rev. B **54**, R3714 (1996)
208. T. Hikihara, T. Momoi, X. Hu: Phys. Rev. Lett. **90**, 087204 (2003)
209. A. K. Kolezhuk, H.-J. Mikeska: Int. J. Mod. Phys. B **5**, 2305 (1998)
210. A. A. Zvyagin: J. Phys.: A **34**, R21 (2001) and references therein.
211. Ö. Legeza, G. Fáth, J. Sólyom: Phys. Rev. B **55**, 291 (1997)
212. Y. Q. Li, M. Ma, D. N. Shi, F. C. Zhang: Phys. Rev. Lett. **81**, 3527 (1998)
213. Yupeng Wang: Phys. Rev. B **60**, 9326 (1999)
214. M. J. Martins, B. Nienhuis: Phys. Rev. Lett. **85**, 4956 (2000)
215. A. K. Kolezhuk, H.-J. Mikeska: Phys. Rev. B **56**, R11380 (1997)
216. A. H. MacDonald, S. M. Girvin, D. Yoshioka: Phys. Rev. B, **37**, 9753 (1988)
217. A. H. MacDonald, S. M. Girvin, D. Yoshioka: Phys. Rev. B **41**, 2565 (1990)
218. M. Takahashi: J. Phys. C **10**, 1289 (1977)
219. A. A. Nersesyan, A. M. Tsvelik: Phys. Rev. Lett. **78**, 3939 (1997)
220. I. Kugel, D. I. Khomskii: Sov. Phys. JETP **37**, 725 (1973); Sov. Phys. Usp. **25**, 231 (1982)
221. M. Roger, J. H. Hetherington, J. M. Delrieu: Rev. Mod. Phys. **55**, 1 (1983)
222. S. Brehmer, H.-J. Mikeska, M. Müller, N. Nagaosa, S. Uchida: Phys. Rev. B **60**, 329 (1999)
223. M. Matsuda, K. Katsumata, R. S. Eccleston, S. Brehmer, H.-J. Mikeska: J. Appl. Phys. **87**, 6271 (2000); Phys. Rev. B **62**, 8903 (2000)
224. H. J. Schmidt, Y. Kuramoto: Physica C **167**, 263 (1990)
225. Y. Honda, Y. Kuramoto, T. Watanabe: Phys. Rev. B **47**, 11329 (1993)
226. R. S. Eccleston, M. Uehara, J. Akimitsu, H. Eisaki, N. Motoyama, S. Uchida: Phys. Rev. Lett. **81**, 1702 (1998)
227. M. Takigawa, N. Motoyama, H. Eisaki, S. Uchida: Phys. Rev. B **57**, 1124 (1998)
228. K. Magishi, S. Matsumoto, Y. Kitaoka, K. Ishida, K. Asayama, M. Uehara, T. Nagata, J. Akimitsu: Phys. Rev. B**57**, 11533 (1998)
229. T. Imai, K. R. Thurber, K. M. Shen, A. W. Hunt, F. C. Chou: Phys. Rev. Lett. **81**, 220 (1998)
230. T. F. A. Müller, V. Anisimov, T. M. Rice, I. Dasgupta, T. Saha-Dasgupta: Phys. Rev. B **57**, 665 (1998)
231. M. Müller, T. Vekua, H.-J. Mikeska: Phys. Rev. B **66**, 134423 (2002)
232. A. Läuchli, G. Schmid, M. Troyer: Phys. Rev. B **67**, 100409 (2003)
233. J. Lorenzana, J. Eroles, S. Sorella: Phys. Rev. Lett. **83**, 5122 (1999)
234. R. Coldea, S. M. Hayden, G. Aeppli, T. G. Perring, C. D. Frost, T. E. Mason, S.-W. Cheong, Z. Fisk: Phys. Rev. Lett. **86**, 5377 (2001)
235. O. Syljuåsen, H.M. Rønnow: J. Phys.: Condens. Matter **12**, L405 (2000)
236. H. M. Rønnow, D.F. McMorrow, R. Coldea, A. Harrison, I. D. Youngson, T. G. Perring, G. Aeppli, O. Syljuåsen, K. Lefmann, C. Rischel: Phys. Rev. Lett. **89**, 079702 (2002)
237. Y. Yamashita, N. Shibata, K. Ueda: Phys. Rev. B **58**, 9114 (1998)

238. G. V. Uimin: JETP Lett. **12**, 225 (1970); C. K. Lai: J. Math. Phys. **15**, 1675 (1974); B. Sutherland: Phys. Rev. B **12**, 3795 (1975)
239. P. Azaria, A. O. Gogolin, P. Lecheminant, A. A. Nersesyan: Phys. Rev. Lett. **83**, 624 (1999); P. Azaria, E. Boulat, P. Lecheminant: Phys. Rev. B **61**, 12112 (2000)
240. C. Itoi, S. Qin and I. Affleck: Phys. Rev. B **61**, 6747 (2000)
241. Yu-Li Lee, Yu-Wen Lee: Phys. Rev. B **61**, 6765 (2000)
242. S.K. Pati, R.R.P. Singh, D.I. Khomskii: Phys. Rev. Lett. **81**, 5406 (1998)
243. Y. Yamashita, N. Shibata, K. Ueda: J. Phys. Soc. Jpn. **69**, 242 (2000)
244. A. K. Kolezhuk, H.-J. Mikeska: Phys. Rev. Lett. **80**, 2709 (1998)
245. A. K. Kolezhuk, H.-J. Mikeska, U. Schollwöck: Phys. Rev. B **63**, 064418 (2001)
246. P. Millet, F. Mila, F. C. Zhang, M. Mambrini, A. B. Van Oosten, V. A. Pashchenko, A. Sulpice, A. Stepanov: Phys. Rev. Lett. **83**, 4176 (1999)
247. C. D. Batista, G. Ortiz, J. E. Gubernatis: Phys. Rev. B **65**, 180402(R) (2002)
248. C. Itoi, M.-H. Kato: Phys. Rev. B **55**, 8295 (1997)
249. G. Fáth, J. Sólyom: Phys. Rev. B **47**, 872 (1993)
250. L. A. Takhtajan: Phys. Lett. A **87**, 479 (1982); H. M. Babujian: Phys. Lett. A **90**, 479 (1982); Nucl. Phys. B **215**, 317 (1983); P. Kulish, N. Reshetikhin, E. Sklyanin: Lett. Math. Phys. **5**, 393 (1981)
251. I. Affleck: Nucl. Phys. B **265**[FS15], 409 (1986); I. Affleck, F. D. M. Haldane: Phys. Rev. B **36**, 5291 (1987)
252. H.W.J. Blöte, H.W. Capel: Physica A **139**, 387 (1986)
253. J. Oitmaa, J. B. Parkinson. J. C. Bonner: J. Phys. C **19**, L595 (1986)
254. J. Sólyom: Phys. Rev. B **36**, 8642 (1987)
255. R.R.P. Singh, M.P. Gelfand: Phys. Rev. Lett. **61**, 2133 (1988)
256. K. Chang, I. Affleck, G.W. Hayden, Z.G. Soos: J. Phys.: Condens. Matter **1**, 153 (1989)
257. J.B. Parkinson: J. Phys. C **21**, 3793 (1988)
258. A. Klümper: Europhys. Lett. **9**, 815 (1989); J. Phys. A **23**, 809 (1990); Int. J. Mod. Phys. B **4**, 871 (1990)
259. M.N. Barber, M.T. Batchelor: Phys. Rev. B **40**, 4621 (1989)
260. A.V. Chubukov: J. Phys.: Condens. Matter **2**, 1593 (1990); Phys. Rev. B **43**, 3337 (1991)
261. N. Papanicolaou: Nucl. Phys. B **305** [FS23], 367 (1988)
262. G. Fáth, J. Sólyom: Phys. Rev. B **51**, 3620 (1995)
263. A. Schadschneider, J. Zittartz: Ann. Physik **4**, 157 (1995)
264. K. Katsumata: J. Mag. Magn. Mater. **140-144**, 1595 (1995) and references therein
265. N. Kawashima: Prog. Theor. Phys. Suppl. **145**, 138 (2002)
266. A. Läuchli, G. Schmid, and S. Trebst, preprint cond-mat/0311082.
267. B. A. Ivanov, A. K. Kolezhuk: Phys. Rev. B **68**, 052401 (2003)
268. M. Hagiwara, K. Minami, Y. Narumi, K. Tatani, K. Kindo: J. Phys. Soc. Jpn. **67**, 2209 (1998).
269. E. Lieb, D. Mattis: J. Math. Phys. **3**, 749 (1962)
270. S. Brehmer, H.-J. Mikeska, S. Yamamoto: J. Phys.: Condens. Matter **9**, 3921 (1997)
271. S. K. Pati, S. Ramasesha, D. Sen: Phys. Rev. B **55**, 8894 (1997); J. Phys.: Condens. Matter **9**, 8707 (1997)
272. T. Fukui, N. Kawakami: Phys. Rev. B **57**, 398 (1998)

273. A. E. Trumper, C. Gazza: Phys. Rev. B 64, 134408 (2001)
274. K. Katsumata, H. Hori, T. Takeuchi, M. Date, A. Yamagishi, J. P. Renard: Phys. Rev Lett. **63**, 86 (1989)
275. I. Affleck: Phys. Rev. B **41**, 6697 (1990); Phys. Rev. B **43**, 3215 (1991)
276. A. Tsvelik: Phys. Rev. B **42**, 10499 (1990)
277. T. Sakai, M. Takahashi: Phys. Rev. B **43**, 13383 (1991)
278. S. Sachdev, T. Senthil, R. Shankar: Phys. Rev. B **50**, 258 (1994)
279. R. Chitra, T. Giamarchi: Phys. Rev. B **55**, 5816 (1997)
280. T. Giamarchi, A. M. Tsvelik: Phys. Rev. B **59**, 11398 (1999).
281. K. Hida: J. Phys. Soc. Jpn. **63**, 2359 (1994)
282. K. Okamoto: Solid State Commun. **98**, 245 (1996)
283. T. Tonegawa, T. Nakao, M. Kaburagi: J. Phys. Soc. Jpn. **65**, 3317 (1996)
284. K. Totsuka: Phys. Lett. A **228**, 103 (1997)
285. D. C. Cabra, A. Honecker, P. Pujol, Phys. Rev. Lett. **79**, 5126 (1997)
286. D. C. Cabra, A. Honecker, P. Pujol, Phys. Rev. B **58**, 6241 (1998)
287. T. Tonegawa, T. Nishida, M. Kaburagi: Physica B **246& 247**, 368 (1998)
288. Y. Narumi, M. Hagiwara, R. Sato, K. Kindo, H. Nakano, M. Takahashi: Physica B **246&247**, 509 (1998)
289. K. Totsuka: Phys. Rev. B **57**, 3454 (1998); Eur. Phys. J. B **5**, 705 (1998)
290. F. Mila: Eur. Phys. J B **6**, 201 (1998)
291. H. Nakano, M. Takahashi: J. Phys. Soc. Jpn. **67**, 1126 (1998); T. Sakai, M. Takahashi: Phys. Rev. B **57**, R3201 (1998)
292. K. Okunishi, Y. Hieida, Y. Akutsu: Phys. Rev. B **60**, R6953 (1999)
293. K. Okunishi: Prog. Theor. Phys. Suppl. **145**, 119 (2002) and references therein
294. Y. Narumi: PhD Thesis, Osaka University (2001)
295. W. Shiramura, K. Takatsu, B. Kurniawan, H. Tanaka, H. Uekusa, Y. Ohashi, K. Takizawa, H. Mitamura, T. Goto: J. Phys. Soc. Jpn. **67**, 1548 (1998)
296. M. Matsumoto: Phys. Rev. B **68**, 180403(R) (2003)
297. M. Krohn, Diploma thesis, Universität Hannover (2000)
298. A. K. Kolezhuk, H.-J. Mikeska: Prog. Theor. Phys. Suppl. **145**, 85 (2002)
299. K. Maisinger, U. Schollwöck, S. Brehmer, H.-J. Mikeska, S. Yamamoto: Phys. Rev. B **58**, 5908 (1998)
300. X. Wang, Lu Yu: Phys. Rev. Lett. **84**, 5399 (2000)
301. A. Klümper: Z. Phys. B **91**, 507 (1993); Euro. Phys. J. B **5**, 677, (1998)
302. J. B. Parkinson: J. Phys.: Condens. Matter **1**, 6709 (1989)
303. M. Orendáč, S. Zvyagin, A. Orendáčová, M. Seiling, B. Lüthi, A. Feher, M. W. Meisel: Phys. Rev. B **60**, 4170 (1999)
304. A. Zheludev, Z. Honda, C. Broholm, K. Katsumata, S. M. Shapiro, A. Kolezhuk, S. Park, Y. Qiu: Phys. Rev. B **68**, 134438 (2003)
305. A. K. Kolezhuk, H.-J. Mikeska: Phys. Rev. B **65**, 014413 (2002)
306. M. Bocquet, F. H. L. Essler, A. M. Tsvelik, A. O. Gogolin: Phys. Rev. B **64**, 094425 (2001)
307. H.J. Schulz, C. Bourbonnais: Phys. Rev. B **27**, 5856 (1983); H.J. Schulz: Phys. Rev. B **34**, 6372 (1986)
308. V. Barzykin: Phys. Rev. B **63**, 140412(R) (2001)
309. T. Hikihara, A. Furusaki: Phys. Rev. B **63**, 134438 (2001)
310. H. Castella, X. Zotos: Phys. Rev. B **47**, 16186 (1993)
311. P. W. Anderson: Phys. Rev. Lett. **18**, 1049 (1967); Phys. Rev. **164**, 352 (1967)
312. I. Affleck, A.W.W. Ludwig: J. Phys. A **27**, 5375 (1994); A. M. Zagoskin, I. Affleck: ibid., **30**, 5743 (1997)

313. A. Furusaki and S.-C. Zhang: Phys. Rev. B **60**, 1175 (1999)
314. T. Nikuni, M. Oshikawa, A. Oosawa, H. Tanaka: Phys. Rev. Lett. **84**, 5868 (2000)
315. H. Tanaka, A. Oosawa, T. Kato, H. Uekusa, Y. Ohashi, K. Kakurai, A. Hoser: J. Phys. Soc. Jpn. **70**, 939 (2001)
316. E.Ya. Sherman, P. Lemmens, B. Busse, A. Oosawa, H. Tanaka: Phys. Rev. Lett. **91**, 057201 (2003)
317. O. Nohadani, S. Wessel, B. Normand, S. Haas: preprint cond-mat/0307126.
318. Ch. Rüegg, N. Cavadini, A. Furrer, H.-U. Güdel, P. Vorderwisch and H. Mutka: Appl. Phys. A **74**, S840 (2002)
319. Ch. Rüegg, N. Cavadini, A. Furrer, H.-U. Güdel, K. Krämer, H. Mutka, A. Wildes, K. Habicht, P. Vorderwisch: Nature **423**, 62 (2003)
320. M. Matsumoto, B. Normand, T. M. Rice, M. Sigrist: Phys. Rev. Lett. **89**, 077203 (2002); see also preprint cond-mat/0309440
321. A. K. Kolezhuk: Phys. Rev. B **53**, 318 (1996)
322. P. P. Mitra, B. I. Halperin: Phys. Rev. Lett. **72**, 912 (1994)
323. O. Golinelli, Th. Jolicoeur, R. Lacaze: Phys. Rev. B **45**, 9798 (1992); J. Phys.: Condens. Matter **5**, 7847 (1993).
324. L.-P. Regnault, I. A. Zaliznyak, S. V. Meshkov: J. Phys: Condens. Matter **5**, L677 (1993)
325. M. Hagiwara, Z. Honda, K. Katsumata, A. K. Kolezhuk, H.-J. Mikeska: Phys. Rev. Lett. **9**1, 177601 (2003)